72

GUIDELINES FOR THE EVALUATION OF THE DIELECTRIC STRENGTH OF EXTERNAL INSULATION

Working Group 07
(Dielectric strength of external insulation under transient voltage)
of
Study Committee 33
(Overvoltages and Insulation Coordination)

1992

GUIDELINES FOR THE EVALUATION OF THE DIELECTRIC STRENGTH OF EXTERNAL INSULATION

Working Group 07* (Dielectric strength of external insulation under transient voltage)

of

Study Committee 33 (Overvoltages and Insulation Coordination)

* At the time of the preparation of this document, WG 33.07 had the following Membership :

L. Thione (Convener), A. Pigini (Secretary), N.L. Allen, M. Aro, A.C. Baker, G. Baldo, J. Beran, A.C. Britten, R. Enache, J.R. Fonseca, E. Garbagnati, H. Geldenhuys, B. Hutzler, T. Kawamura, E. Lemke, V. Martins, C. Menemenlis, M. Moreno, K. Naito, P. Nikolopoulos, F. Rizk, K.J. Sadurski, H.M. Said, H. Studinger, J. Van Name, J.C. Zheng.

GUIDELINES FOR THE EVALUATION OF THE DIELECTRIC STRENGTH OF EXTERNAL INSULATION

Table of contents

GUIDELINES FOR THE EVALUATION OF THE DIELECTRIC STRENGTH OF EXTERNAL INSULATION

by W.G. 33.07

1 INTRODUCTION

The Guideline, prepared within WG 33.07, deals with the dielectric strength of external insulation, namely air gaps and insulators, with special reference to transient overvoltages. The aim of the Guideline is to illustrate the general trends in the dielectric strength as a function of the most important influencing parameters and to give methods and criteria for the evaluation of the strength.

The Guideline is composed of different chapters, compiled by "ad hoc Groups" set up within the WG. A summary of the content of the Guideline is given in this chapter (chapter 1).

Chapter 2 deals with general aspects, such as definitions of the various stresses considered and of the parameters defining the strength.

Chapter 3 gives basic information on the discharge mechanisms and illustrates the main existing models of the discharge. This information may help in understanding and rationalizing the influence of the various stress and geometry parameters.

Chapter 4 to 6 deal with the strength under the various overvoltages under standard atmospheric conditions and under wet conditions.

Chapter 7 and 8 deal with the influence on the dielectric strength of air density and air humidity respectively. The chapter about influence of air density includes the influence of altitude.

Chapter 9 deals specifically with the performance of insulators when contaminated. The analysis is made with special reference to transient overvoltage. The performance under continuous service voltage, which may in many conditions determine the strength under contamination, is out of the scope of WG 33.07 and thus is not dealt with in the Guide.

Chapter 10 and 11 deal with very special conditions: the dielectric performance in connection with ice/snow and fires.

Finally chapter 12 deals with conclusions and future research needs.

2 GENERALITIES AND DEFINITIONS

by W.G. 33.07

2.1 GENERAL

In the following, general aspects and definitions will be considered, making reference for these last, as far as possible to IEC documents.

2.2 CONFIGURATIONS CONSIDERED

The guideline will consider the strength of "External Insulation" only. This is defined as: "The *distances in atmosphere*, and the *surfaces in contact with open air* of solid insulation of the equipment which are subject to dielectric stresses and to the effects of atmospheric and other external conditions, such as pollution, humidity, vermin, etc.." [IEV 604-03-02]

In particular, typical air gap configurations for EHV/UHV lines and substations will be considered. Special attention will be paid to the strength of phase-to-earth configurations. Consideration will be given also to the strength of phase-to-phase configurations, when considered of practical interest.

The influence of the presence of insulators in the gap on the strength will be analyzed deeply, considering two main insulator families: line insulators (mainly cap and pin) and substation insulators.

The strength will be examined:

- in standard atmospheric conditions, as defined by IEC 60, i.e.:

  Temperature: 20 °C
  Pressure: 101.3 kPa (1013 mbar)
  Absolute humidity: 11 g/m³

- in dry and wet conditions, making reference to the test procedure described in IEC 60.

- in non standard conditions, as low air density, high relative humidity, contamination, ice and snow, high temperatures and presence of combustion particles.

2.3 STRESSES CONSIDERED AND THEIR SIMULATION IN LABORATORY

Dielectric strengths under the following voltages will be examined:

Fast-front overvoltages: Transient overvoltages, usually unidirectional, with time to peak 0.1 $\mu s \leq T_1 \leq 20$ μs, and tail duration $T_2 < 300$ μs. The overvoltages are usually simulated in laboratory by standard and non standard lightning impulses. The first one is double exponential with a time to crest of 1.2 μs and a time to half value of 50 μs.

Slow-front overvoltages: Transient overvoltages, usually unidirectional with time to peak 20 $\mu s \leq T_1 \leq$ 5000 μs, and time to half-value $T_2 \leq 20$ ms.

The overvoltages are simulated in laboratory by standard switching impulses (oscillating or double exponential type) with a time to peak of 250 μs and a time to half value of 2500 μs and non standard switching impulses.

Temporary overvoltages: An oscillatory overvoltage (at power frequency) at a given location, of relatively long duration and which is undamped or weakly damped. [IEV 604-03-12]

The overvoltage is usually simulated by a power frequency voltage of short duration. The standardized duration is 60 seconds.

Combined overvoltages: Combined overvoltages consist of two voltage components applied simultaneously between each of the two phase terminals of a phase-to-phase or longitudinal insulation and earth.

Each component can be simulated in laboratory by any of the voltages mentioned above.

Composite overvoltages: Composite overvoltages consist of the superposition of two of the voltages mentioned above. In this report, only those applied between one insulation terminal and earth are considered.

The strength under DC voltage will be also examined, under wet and dry conditions.

2.4 ASSESSMENT OF THE STRENGTH

In the assessment of the insulation strength it should be taken into account the fact that the physical processes that determine a disruptive discharge in the insulation are of a random nature. Consequently, the application of the same test voltage sometimes results in a disruptive discharge and sometimes in a withstand. A statistical procedure, therefore, should be applied to the study of the phenomenon, associating at each test voltage a probability P to produce a disruptive discharge in the insulation. Changing the test voltage P changes, and *only physical reasons* govern the dependence of P on the test voltage.

As an example Figure 1 shows the results of impulse tests on an air gap [2.6]. Impulses of equal peak value were applied at each voltage level. The corresponding probability has been estimated by dividing the number of discharges obtained by the number of impulses applied. To obtain information about the low probability range, a very large mumber of impulses were applied in total.
To estimate the probability function P(U), the points should be fitted by means of a function assumed to represent the corresponding physical law.
It has been common use to assume functions corresponding to one of the various statistical laws (as an example the Gaussian function or the Weibull function). These assumptions, however, have no other basis than the fact that they fit reasonably well the test results in the range usually investigated ($0.02 < P < 0.98$).

From the best fitting function the voltages corresponding to any assigned probability may be determined: e.g., the voltage which has a probability of 50% $U_{50}=U(0.50)$, the voltage which has a probability of 10% $U_{10}=U(0.10)$ (U_{10} is the statistical withstand voltage adopted for self-restoring insulation). Making reference to the Gaussian function the discharge probability function may be fully described by two parameters, namely U_{50} and the conventional deviation z. Once

this parameters are known the voltages having different disruptive discharge probabilities may be easily determined. As an example:

$$U_{10} = U_{50} - 1.28\ z$$

In several cases for a given type of overvoltage the conventional deviation (in per unit of U_{50}) is known and practically independent of the insulation configuration and dimensions (e.g. for lightning impulses, $z/U_{50} \approx 0.03$). It may be sufficient, therefore, to determine only one voltage (usually U_{50}) of a given configuration and dimension, to obtain an estimate of its discharge probability function.

However, since the function assumed has no physical basis, and the estimates are affected by statistical uncertainties (mainly owing to the limited number of tests possible), no estimates of P are justified outside the range 0.02 to 0.98 approximately.

This is the case when very low discharge probability voltage is desired. The limited number of tests possible does not allow even the direct laboratory determination of the voltages corresponding to these probabilities. Physical considerations, supported by some laboratory evidence, indicate that the statistical distribution is truncated at $U_{50} - n\ z$ with n ranging from 3 to 5.

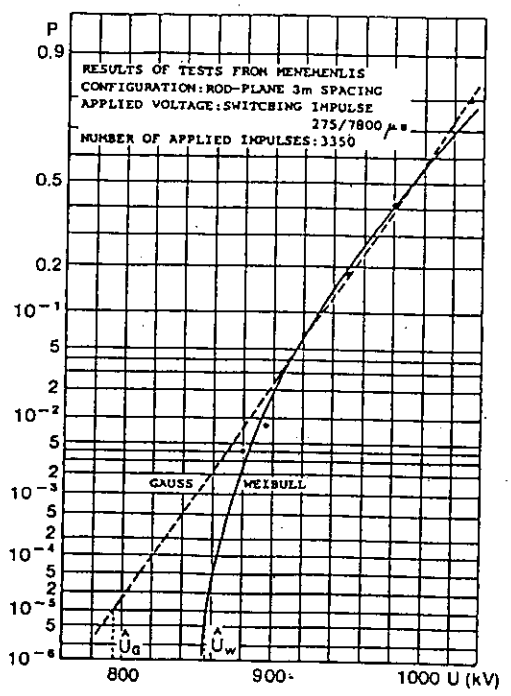

Figure 1: Example of interpolation of test results with two statistical functions.

2.5 REFERENCES

[2.1] IEC Insulation coordination. Part 1: Terms, definition, principles and rules. Pub. 71-1, 1976 (under revision).

[2.2] G. Carrara, W. Hauschild, "Statistical evaluation of dielectric test results. Electra, December 1990, Numb. 133.

[2.3] CIGRE Technical Brochures 1992 W.G. 15.01, S. Yakov, "Statistical analysis of dielectric test results"

[2.4] R. Brambilla, E. Garbagnati, A. Bertazzi, F. Gallucci, A. Pigini, "Switching impulse tests at very low probability levels", 8th Conference on Gas Discharges and their Applications. Oxford 16-20 Sept. 1985.

[2.5] G. Carrara, F. Gallucci, S. Manganaro, A. Pigini, "Practical problems of impulse breakdown requering a physical approach", 3rd International Conference on Gas Dielectrics. Knoxville, March 1982.

[2.6] C. Menemenlis, G. Harbec, "Coeficient of variation of the positive impulse breakdown of long air gaps", IEEE Trans. on PAS, Vol. 93, 1974.

3 FUNDAMENTALS OF THE DISCHARGE MECHANISMS AND DESCRIPTION OF THE PHENOMENA BY PHYSICAL-MATHEMATICAL MODELS

by G.BALDO, B.HUTZLER, A.PIGINI, F.RIZK

3.1 INTRODUCTION

The behaviour of insulation in air depends on various factors, such as the type and polarity of the applied voltage, electric field distribution, gap length and gas conditions.

In HV and EHV systems major attention has to be paid to transient stresses, due to both lightning and switching operations, which in general determine the external insulation design. Due to their high values large clearances are needed so that field distributions, which depend on electrode geometry and gap length, are almost always nonuniform. It is possible to have geometries with a high electric field either near one electrode only, rod-plane gap type, or near both electrodes, rod-rod gap type, the behaviour of the insulation being different. Furthermore as many processes are different if the highly stressed electrode is positive or negative, differences can be expected if the polarity of the applied voltage is changed. Finally the influence of the gas conditions on the basic processes during discharge formation have to be mentioned; in the case of HV air insulation, air density and humidity are of primary importance.

As is well-known, the basic process in gas discharge development is the formation of free charges of opposite sign mainly due to ionization of molecules by collisions with free electrons accelerated by the electric field. Due to both the different mobilities of electrons and of positive ions and to the high value of air density at atmospheric pressure, charge concentrations can be created, which change the electric field distribution and allow the propagation of ionization phenomena also in parts of the gap were the field due to the applied voltage alone would be too low. This causes the propagation of ionization processes along channels which are partially ionized and can cross the whole gap causing breakdown.

The breakdown phenomenon develops in successive phases which can be either well distinguished or partially superimposed, according to the type of applied voltage and to the type of electrode geometry.

The first phase is the first corona, which develops, in the region of high electric field in the proximity of the electrodes, in the form of thin filaments, called streamers, propagating, generally, only for one part of the gap.

The second phase is the leader phase, characterized by the formation and elongation of a channel, more highly ionized than a streamer, which propagates with leader corona developing from its tip. According to the value and shape of the applied voltage and to the gap length, the leader can either stop or reach the opposite electrode.

Once either first corona streamers or leader corona streamers have reached the opposite electrode the third phase develops. The leader channel elongates at increasing velocity bridging the whole gap. At this point the channel becomes highly ionized and the electrodes are short-circuited.

In the case of rod-rod geometry, the phenomenon develops from both electrodes and the last phase occurs when filaments of opposite polarity meet inside the gap.

The first corona phase and mainly leader phase have quite different characteristics according to the polarity of the applied voltage, thus causing a difference in breakdown voltage with the polarity. In almost all

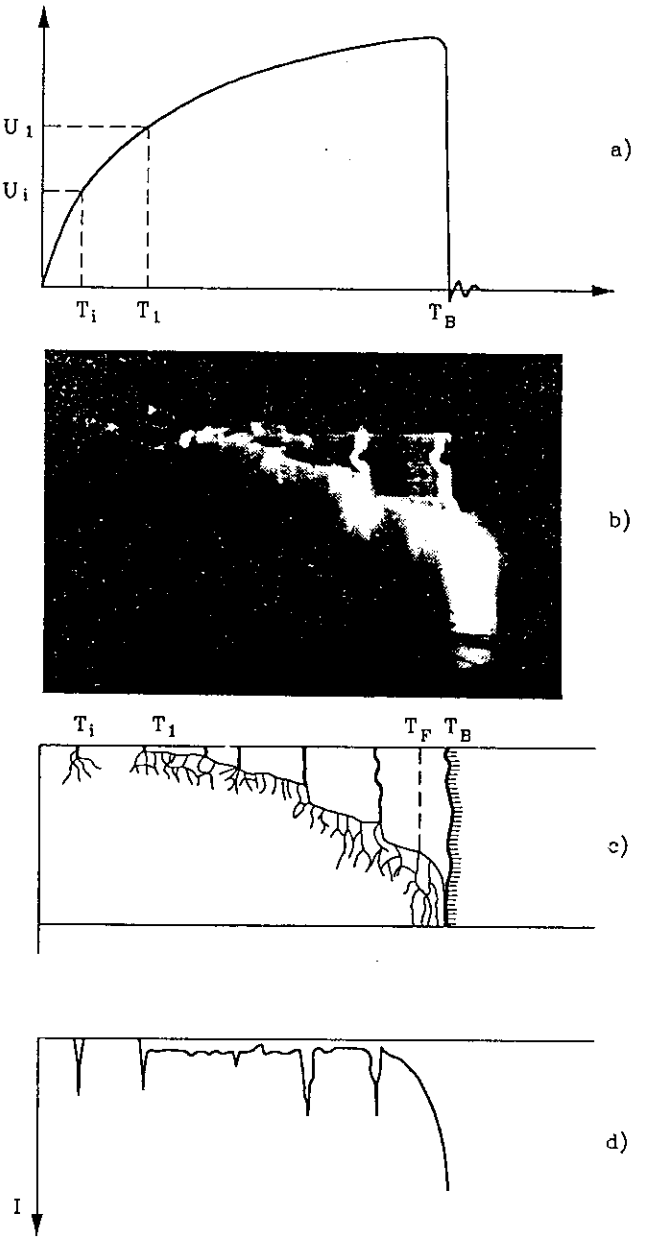

Figure 3.1 Long spark development.
a) applied voltage
b) streak photograph
c) schematic representation
d) current

the geometries of practical use, the breakdown voltage with positive polarity is lower than with negative polarity and the minimum breakdown voltage, with the same gap length and impulse shape, belongs to the case of rod-plane gap, i.e. a geometry in which only one region of the gap is highly stressed.

To examine the discharge development, rod-plane gap geometry will be first considered.

3.2 DISCHARGE WITH POSITIVE POLARITY

The discharge development in a rod-plane gap under positive voltage is described in Figure3.1 which refers to a 10 m rod-plane gap and a switching voltage [3.1]. This type of stress has been choosen because the various phases of discharge development are well distinguished. First corona occurs at instant T_i and leader channel propagation starts at time T_1. When the streamers of the leader corona reach the plane at time T_r, the last phase, usually called "final jump", occurs. Breakdown is completed at time T_s.

3.2.1 First Corona

When the impulse voltage applied to the gap reaches a suitable value U_i, the electric field strength in a region near the rod electrode has values high enough to cause the formation of a certain number of filamentary discharges propagating into the gap with velocity exceeding 10^8 cm/s.

The phenomenon is explained by the streamer theory. A free electron present in the right position is accelerated by the field towards the electrode and ionizes neutral gas molecules creating new free electrons at a rate of α per unit length of path; electrons, however, can attach to molecules at a rate of η per unit length of path, creating negative ions. An electron avalanche is so formed which at its arrival at the electrode has at its head a number of electrons given by

$$n = e^{\int_{r_1}^{r_2} (\alpha-\eta)\,dx} \qquad (3.1)$$

where:

r_1 and r_2 are the starting and arrival points;
$(\alpha-\eta)$ is the net ionization coefficient.

The same number of positive ions is left in the gap.

Both α and η depend on the energy W, gained by electrons between two collisions, and on the number of collisions per unit length of path, i.e. on gas density. The energy gained by an electron in a path l in the field direction, between two collisions, is

$$W = E\, q_e\, l \qquad (3.2)$$

where E is the electric field and q_e the electron charge. As l is inversely proportional to the gas density and pressure, at a given temperature:

$$\alpha = p\, f_1\left(\frac{E}{p}\right) \qquad (3.3)$$

$$\eta = p\, f_2\left(\frac{E}{p}\right) \qquad (3.4)$$

Charge multiplication occurs only when $(\alpha - \eta) \geq 0$ and in air at atmospheric pressure this occurs for field values higher than about 26 kV/cm.

If the electric field is high enough, the avalanche arriving at the anode can reach a critical size which allows for a streamer to be formed by the effect of positive space charge left inside the gap. As schematically shown in Figure 3.2 the streamer formation is promoted by secondary avalanches initiated by electrons which are mainly produced by photoionization [3.2].

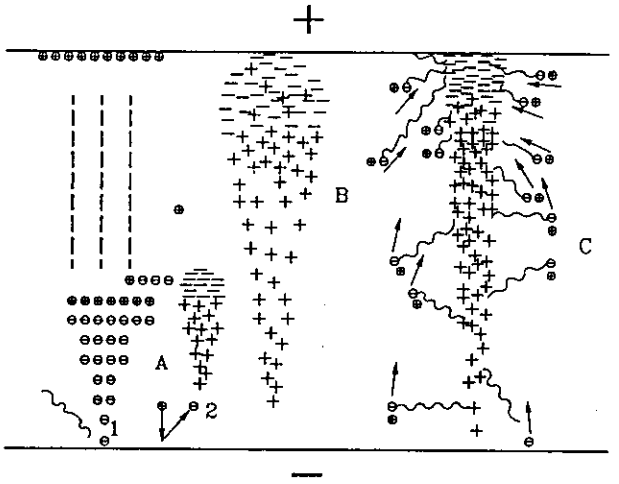

Figure 3.2 a Positive streamer formation
A) the primary avalanche is launched.
B) the primary avalanche reaches the anode.
C) positive space charge initiates a streamer.

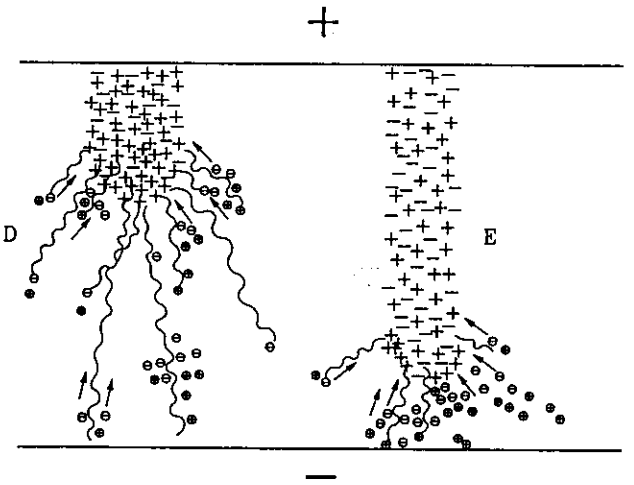

Figure 3.2 b Positive streamer propagation.

The criterion for streamer formation is usually given by:

$$e^{\int_{r_1}^{r_2} (\alpha-\eta)\,dx} = k \qquad (3.5)$$

where k is of the order of 10^8.

Under the action of the total field, the sum of the geometric field and space charge field, the successive avalanches reach the positive space charge, neutralize it and leave a new positive charge in a more advanced position from the electrode. With such a mechanism a positive charge moves step by step into the gap leaving behind it a partially ionized filament. This propagation occurs at a velocity which is very much higher

than the drift velocity of the positive ions. Depending on the size of positive space charge and on statistics, a streamer can branch out as shown in Figure 3.3.

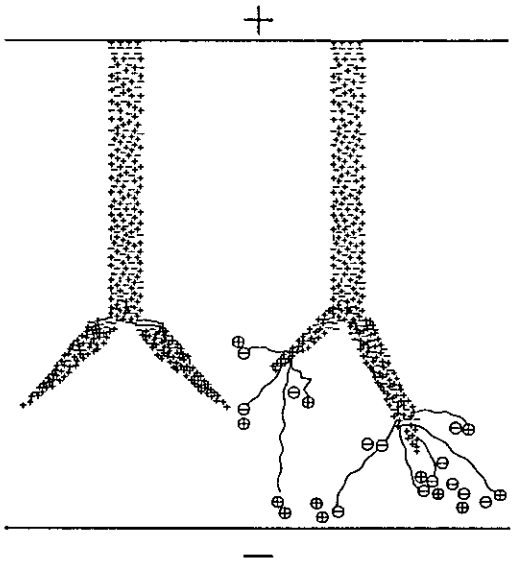

Figure 3.3 Ramification of a positive streamer.

In case of uniform field, due to the high geometric field, a streamer, once formed, propagates to the opposite electrode causing breakdown. In case of nonuniform field, on the contrary, a streamer generally propagates along a part of the gap and it stops due both to the reduction of the geometric field and to the loss of energy of the space charge at its tip. At atmospheric pressure a streamer has a stable propagation in a constant field of 4.5 to 5 kV/cm, which represents also the field along the filament.

Expressions (3.3) and (3.4) show that both α and η depend on air density. The net ionization coefficient $(\alpha-\eta)$ increases when air density decreases so that streamer formation occurs at lower electric fields as air density is reduced.

Water vapour content has an effect, even if less pronounced: an increase of humidity increases the electric field required for an avalanche to reach a critical size.

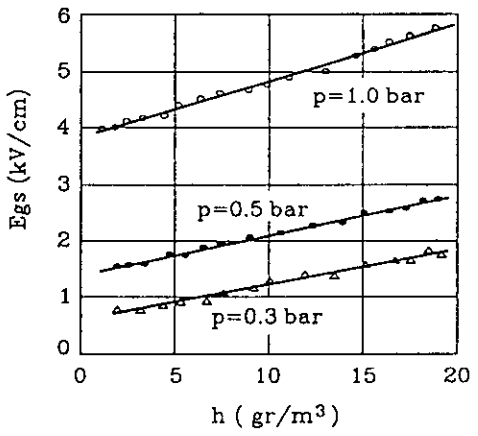

Figure 3.4 Measured variation of the stability field versus absolute humidity h for three values of pressure.

Due to these effects, also the minimum electric field required for a stable streamer propagation increases with the increase of both air density and humidity. Experimental results are shown in Figure 3.4 [3.3].

As the corona inception depends on electric field distribution the minimum corona inception voltage $U_{i,min}$ depends on the electrode type and geometry.

For a constant experimental condition, the corona inception voltage is not constant from one voltage application to another, but is distributed in a range of voltage values. This aspect depends on the fact that for corona occurrence it is not sufficient that the voltage reaches the minimum inception value; it is also necessary that a free electron is present to initiate a primary avalanche of critical size. At minimum inception voltage, there is only one point P_o (Figure 3.5) from which a free electron can success-

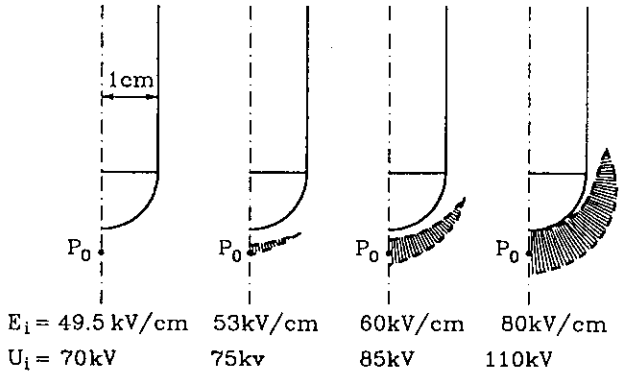

Figure 3.5 Critical volume for different applied voltage, 30 cm gap. E_i is the field at the electrode.

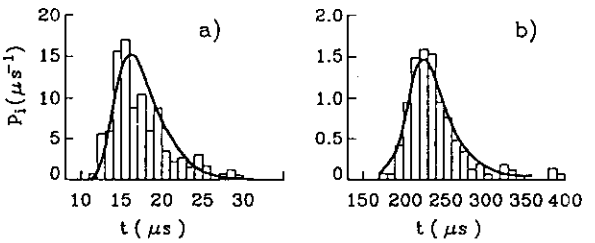

Figure 3.6 Experimental and computed distribution of inception probability.
a) 10 m gap, cone tip 1 cm curvature radius, 500/10000 μs impulse, U_p=1780 kV.
b) 2 m gap, hemispherical tip 30 cm radius, 350/10000 μs impulse, U_p=1000 kV.

fully initiate such an avalanche [3.4]. As voltage increases, the region with sufficiently high field is extended so that a volume can be defined from any point of which an electron can now successfully start such an avalanche. For a given electrode geometry, this critical volume V is a function of applied voltage and time and it can be computed. By combining the production rate of free electrons and the increase of the volume V, the probability of corona inception can be computed as a function of time. Figure 3.6 [3.4] shows a comparison between experimental and computed data. Due to this type of mechanism, if the front

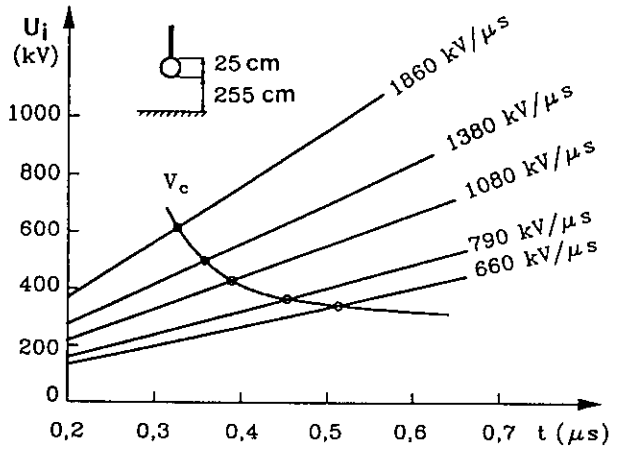

Figure 3.7 Mean corona inception voltage as a function of the rate of rise of the applied voltage.

duration of the impulse voltage is reduced, i.e. if the steepness of the voltage is increased,the mean value of U_i increases, as shown in Figure 3.7 [3.5].

In geometries commonly employed, with increasing voltages, impulse corona develops with a great number of streamers with many branches, starting from a more luminous and ionized element near the electrode, which is called the "stem". A certain amount of negative charge created by ionization processes flows along the streamers into the electrode, so in the region covered by streamers a net positive space charge is left which modifies the previous field distribution; the field intensity is reduced near the electrode and increased out of the corona zone, as schematically shown in Figure 3.8. If the applied voltage is not increased any more, ionization processes stop.

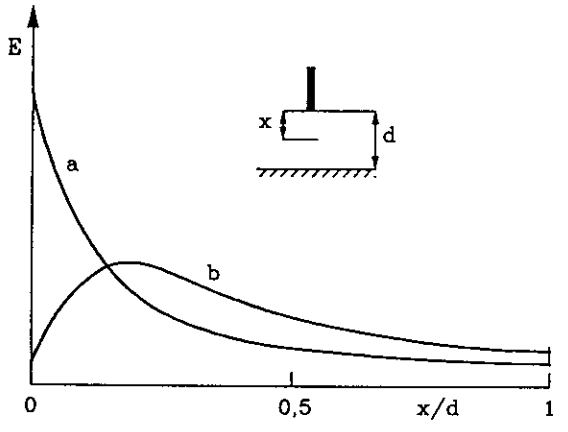

Figure 3.8 Sketch of field distribution along the axis in a rod-plane gap before corona (a) and after corona (b).

3.2.2 Leader phase

As previously stated, after the first corona, ionization phenomena restart and a leader channel usually develops from the corona stem. This fact, which indicates an increase of the electric field previously reduced by corona space charge, can be related to three different effects: increase of the applied voltage, reduction of the choking effect of the space charge due to its diffusion and drift, change in the characteristics of the stem. These three causes will generally act simultaneously but their weight, which is different according to experimental conditions, may hardly be quantitatively assessed.

The first model for the streamer to leader transition has been proposed by Aleksandrov [3.6]. All the electrons flowing in the corona streamers converge in the stem, where they release their energy by elastic and inelastic collisions. If the assumption is made that the gas is heated to a sufficiently high temperature, the ionization degree in the stem may rapidly increase because of thermoionization; by this process the first leader section is formed. The increase of conductivity enhances the electric field around the stem tip and a second corona can therefore be launched which may elongate the leader section through the same mechanism. So a channel is formed which propagates due to subsequent coronas emanating from its tip. Due to the choking effect of space charge left by previous corona, the channel tends to change continuously its direction of propagation. Figure 3.9 gives a sketch

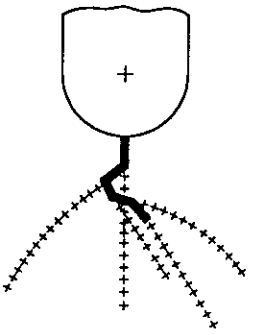

Figure 3.9 Sketch of leader advancement.

of this propagation. However, spectroscopic measurements have shown that temperatures high enough for thermoinization are not reached in the stem; as a consequence, the mechanism which enhances the stem conductivity cannot be thermoinization of the gas molecules.

More recently it has been shown [3.7] that most of the energy imput due to the current flow, is stored as vibrational energy of the gas molecules and then relaxed into thermal energy with a time constant which depends on gas temperature and absolute humidity. This delayed increase of temperature causes thermal detachment of negative ions in the streamers, with consequent increase of the stem conductivity. Furthermore, the free electrons released in the stem flow to the positive electrode in a short time, so the net positive space charge in the stem is rapidly increased. The enhancement of both conductivity and net positive charge in the stem, leads to a sharp increase of the electric field around the stem, which may cause the restart of the ionization phenomena, the inception of a second corona and the leader formation. The time scale for a convenient increase of temperature ranges from about 100 ns to 10 μs, depending on the experimental conditions and mainly on the corona current values.

It has to be mentioned, however, that new ionization phenomena do not coincide necessarily with the starting of a leader propagation. Experimental results have shown that, with electrodes of small radius of curvature, leader starting is delayed with respect to secondary corona and it occurs when the applied voltage has reached a convenient high value.

Once the leader is formed, the leader may propagate or stop if the applied voltage is not sufficient for propagation.

During the continuous propagation stage, the leader elongates with almost constant velocity, of the order of 1.5 - 2 cm/μs, along a tortuous path, 10 to 30 % longer than the straight line corresponding to the gap minimum clearance. The current flowing in the circuit is almost constant; this implies a charge per unit length of leader channel which is almost constant of the order of some tens of μC/m. During the first stage the leader channel is almost dark and it is preceded by a bright corona emanating from its tip. This leader corona is extending more and more into the gap as the leader advances. The presence of the channel can be clearly seen only when in some cases a sudden reillumination occurs.

The situation existing in the leader channel has been studied on the basis of the thermodynamic and hydrodynamic processes produced by the energy input due to the current flow. Assuming a non local thermodynamic equilibrium, it has been possible to build up a model for the determination of the characteristics of a section of the channel as a function of its position with respect to the leader tip, that is as a function of its "age". Figure 3.10 gives the values of channel

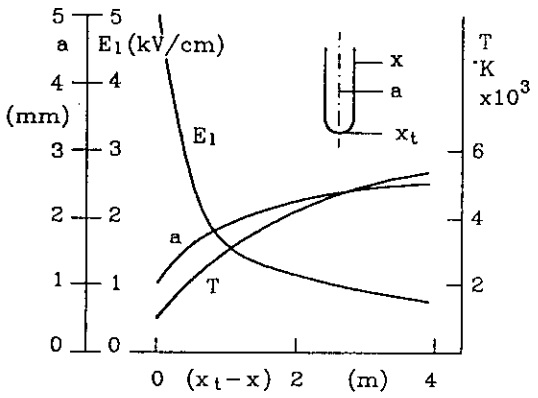

Figure 3.10 Computed leader characteristics Initial conditions: T=1000 °K, a=1 mm.

radius, gas temperature and voltage gradient as a function of x_t-x, where x is the linear coordinate along the real leader path and x_t the real length at time t [3.8]. It can be seen that temperature, radius and conductivity of a section of the leader increase with time. In long gaps, the voltage drop along the "oldest" sections of the leader can fall down to 0.5 kV/cm.

On the basis of this model, if a constant velocity is assumed for leader propagation, the leader tip potential can be calculated as a function of time once the time dependence of the applied voltage is known. Figure 3.11 shows, for a 10 m gap, the potential of the leader tip as a function of time, for three different impulse voltages[3.8]. It may be noted that in the case of impulse voltage with critical time to crest, which is responsable of minimum breakdown voltage, the tip potential remains almost constant. On the other hand, as the field distribution in the region near the leader tip, due to its small radial dimension, depends mainly on the tip potential, leader propagation occurs with almost constant field in front of it; this is consistent with constant velocity and indicates that optimum equilibrium conditions are reached between leader advancement and voltage rate of rise.

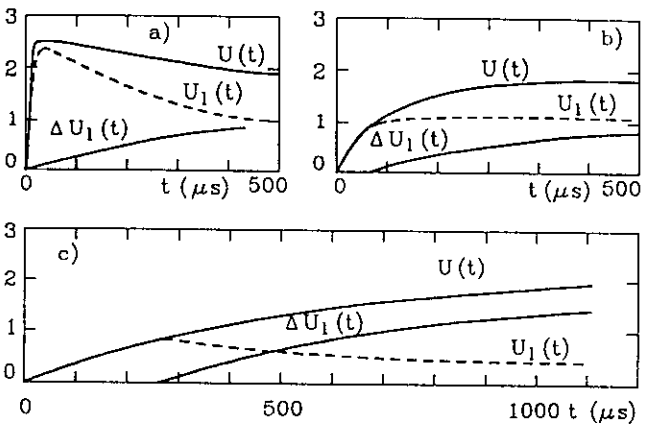

Figure 3.11 Computed voltage at the leader tip, U_l, and voltage drop on the leader ΔU_l, for short (a), critical (b) and long (c) times to crest.

3.2.3 Final Jump

When the leader corona filaments reach the opposite electrode the final jump stage starts: leader velocity and current increase almost exponentially until the leader has covered the total gap length. At the beginning of the final jump the situation in the gap can be represented, in a schematic way, as shown in Figure 3.12. The applied voltage can be expressed as:

$$U = E_l \, l_l + E_s \, l_s \qquad (3.6)$$

where E_l and E_s are the mean gradients along the leader channel and in the streamer zone. In these conditions the current regime is due to leader and streamer conductivity. No completely satisfactory models exist for the description of this phase. However, if only the breakdown voltage is considered, it is sufficient to determine the moment and the voltage at which the final jump starts; then the leader cannot stop any more and the duration of this phase is quite

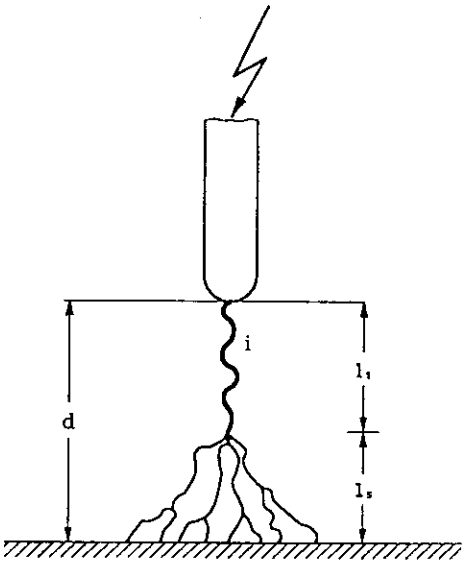

Figure 3.12 Schematic representation of the discharge at the inception of final jump.

short in comparison with the previous stage of continuous leader propagation; thus the voltage at the final jump almost coincides with breakdown voltage.

3.2.4 Influence of impulse shape

The various stages of breakdown formation which have been briefly described, that is first corona, continuous leader and final jump, are clearly defined and easily detectable in the case of impulse voltages of conveniently long duration of front. By reducing the time to crest some overlapping of the various phases can occur, and some phases can be absent.

In the case of lightning impulses, because of the fast decrease of the applied voltage during the tail, the leader cannot develop as in the case of switching impulses. To reach breakdown, the voltage has to be increased very much, causing a different behaviour of the process. Due to the very high rate of rise of the voltage during the front, first corona is almost immediately followed by a succession of pulses which launch streamers farther and farther into the gap. Before a leader has time to develop significantly the streamers reach the opposite electrode, causing a condition in the gap similar to that occurring at the final jump. In this case the phase of continuous leader propagation disappears. Breakdown voltage corresponds to the average field along the streamer zone multiplied by the gap length.

It has to be noted that in the case of short front applied impulse voltage the influence of tail duration is very important, and care has to be taken in comparing results obtained with different front and tail durations. As an example, a 10 m rod-plane gap has a 50% breakdown voltage (U_{50}) of 2610 kV and 4670 kV with impulse voltage shape 22/1500 μs and 7/120 μs respectively. In the first case, due to the length of the tail, a continuous leader propagation was possible and a time to breakdown of 350 μs was observed. In the second case breakdown occurred in 37 μs, indicating only a phase of final jump type. In this second case the average field in the gap at breakdown voltage is approximately 4.7 kV/cm, indicating that streamers have covered the total gap length before a leader elongated appreciably.

3.3 BREAKDOWN WITH NEGATIVE POLARITY

Breakdown of long gaps with negative polarity has been less studied because it has both higher breakdown voltage and greater complexity. However, it is of physical and engineering interest, especially if lightning and rod-rod gap breakdown are to be studied. Even if the negative discharge is much more complex, three main phases may be identified as in the case of positive polarity: impulse corona, leader propagation and final jump. Figure 3.13 shows an image converter picture and a simplified sketch of discharge development [3.9].

3.3.1 First corona

When the applied voltage reaches a convenient value U_i, the first corona occurs as a burst of streamers developing from the electrode toward the anode.

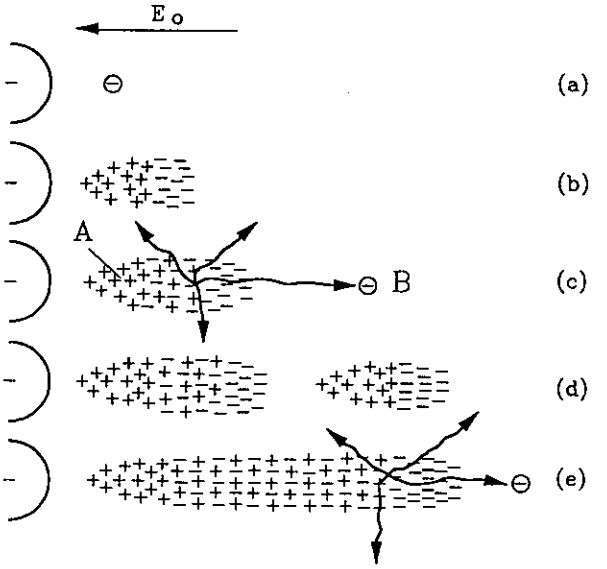

Figure 3.14 Schematic representation of the negative streamer processes.

The mechanism of streamer formation with negative polarity in non uniform field is sketched in Figure 3.14. A free electron near the cathode is accelerated in the anode direction creating an electron avalanche. Due to charge separation the electric field is increased both near the tail and near the head of the ava-

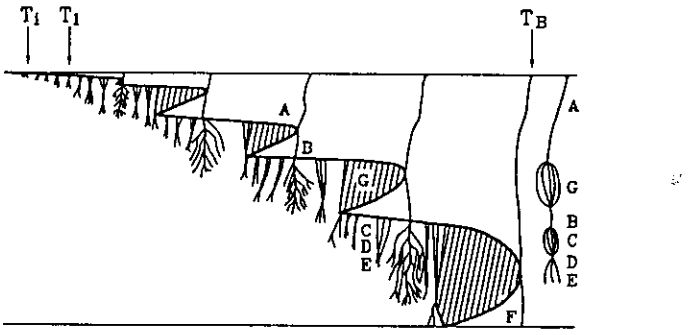

Figure 3.13 Image converter record and simplified sketch showing the typical features of the discharge development; T_{cr}=60 μs, D=7 m hemisphere.

A: negative leader zone
B: space leader zone
C: positive streamers
D: space stem
E: negative streamers
F: positive leader
G: positive streamer zone

lanche. When this primary avalanche has reached a convenient size, from point A a positive streamer develops toward the cathode. In the same time a photoelectron produced in B generates a secondary avalanche; when this secondary avalanche has reached a convenient size a positive streamer develops from its tail toward the head of primary avalanche. The phenomenon can repeat itself through successive secondary avalanches and a negative streamer elongates toward the anode.

Also in this case, due to space charge at its tip, the streamer can propagate in regions where the applied field is reduced, leaving a filament partially ionized with an excess of negative charge. In fact the movement of negative ions, produced by electron attachment, along the filament, tends to leave an excess of positive charge near the cathode which causes an increase of the field in that region. Due to photoionization and ion bombardment, electrons are emitted from the cathode. The arrival of positive ions at the cathode and the emission of electrons cause the excess of negative charge in the filament.

In the case of negative streamers, photoelectrons originating secondary avalanches are produced, in average, at a certain distance from the tip of the streamer and are accelerated in regions where the field due to space charge is rapidly decreasing. The applied field has in this case a greater influence on propagation, so that negative streamers develop more near the field lines, have less ramifications and, with the same applied voltage, a shorter length in comparison with positive streamers. Furthermore it has to be mentioned that the increase of electron attachment in the region of reduced field, reduces the possibility of collisional ionization just in the final part of avalanche development.

This difference in the possibility of propagation of ionization phenomena mainly accounts for the difference of breakdown voltage in non uniform fields when polarity is changed.

3.3.2 Leader phase

The first corona is followed at time T_1 (Figure 3.13) by the formation of a negative leader which appears similar to the positive one previously described. The direction of propagation is largely random and reillumination with large instantaneous elongations occur. For this reason it is difficult to define an average velocity as representative for the advancement of the discharge in the gap. In the continuous phases, between reilluminations, the velocity is approximately 1 cm/μs with an associated current in the range of 0.5÷1 A.

The ionized zone which precedes the leader channel has a more complex structure than in the case of positive polarity. Three different parts may be identified: a luminous nucleus, called the "space stem", at a certain distance ahead of the negative leader tip, and positive and negative streamers propagating from it in opposite directions. This leader-corona system repeats itself regularly in a more advanced position with an equivalent displacement velocity toward the plane of approximately 10 cm/μs.

The mechanism leading to the formation of a space stem is not so clear. It has been proposed [3.9] that in the region where negative streamers stop, a sort of plasma is formed, as sketched in Figure 3.15. The space stem, consequently, would be a dipole where the charge separation is supposed to be a consequence of the field E_o in which the dipole is immersed. With the field distribution shown in Figure 3.15 streamers of opposite polarity can develop in opposite directions. As a consequence of these streamers, a new phenomenon

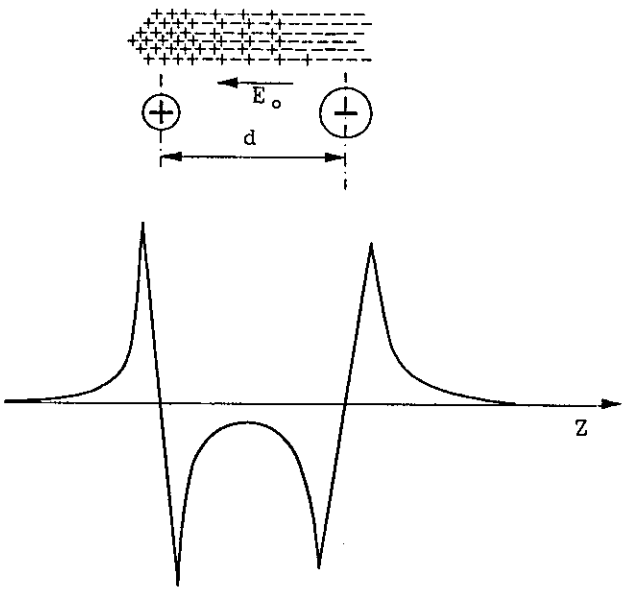

Figure 3.15 Schematic representation of the space stem.

may appear; starting from the space stem, a "space leader" forms which elongates in opposite directions. The region between the upper tip of the space leader and the negative leader is covered by a glow-like corona. When this region is bridged, the negative leader, which suddenly lengthens, is strongly illuminated and a large corona forms from its new tip. This phenomenon causes the above mentioned difficulty of defining an average leader velocity.

Apart from the complexity of development mechanism, once formed the negative leader may be physically described as a positive one.

3.3.3 Final jump

When the negative streamers, starting from the space stem, reach the plane, a positive leader channel develops from it, propagating toward the tip of the downward negative leader. Both channels accelerate and meet together to complete breakdown (Figure 3.16). The formation of a positive leader may be facilitated by the presence of protrusions on the plane, which create local field increase and cause an earlier formation of a positive leader. Figure 3.17 shows the great

Figure 3.16 Arrival of negative streamers at the plane and starting of negative leader.

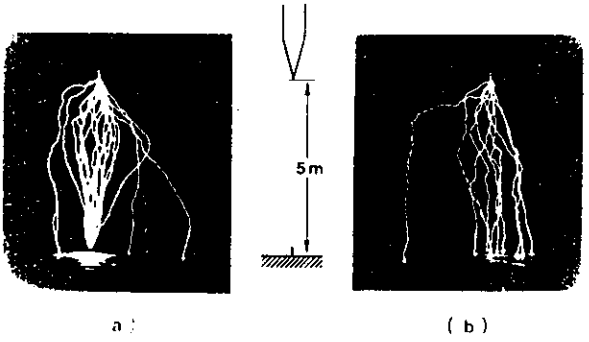

Figure 3.17 Still photographs of discharges in a 5 m gap with 18 cm earthed rod (a) and without rod (b); 60/3000 μs.

influence on discharge paths of a small earthed rod in a rod-plane gap.

3.4 DISCHARGE WITH BOTH ELECTRODES STRESSED

Electrode geometries encountered in HV applications are quite far from simple rod-plane gaps in which only one electrode is highly stressed. Usually both electrodes are stressed, even if in a different way, and the geometries are more similar to rod-rod gaps.In this case two discharge processes, with positive and negative characteristics, develop from the electrodes one toward the other. If the applied voltage is high enough, the two leaders meet inside the gap and breakdown is completed as shown in Figure 3.18.

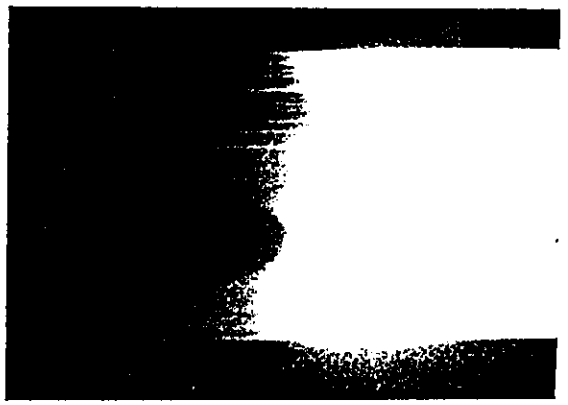

Figure 3.18 6 m rod-rod gap. Positive and negative leaders meeting inside the gap.

As shown before, with the same distribution and values of the electric field, the development of a negative discharge is reduced in comparison with a positive one. Therefore the dependence of breakdown voltage on the polarity of the voltage increases as the field distribution moves away from symmetry.

Furthermore, as the field distribution in the gap strongly depends on the position of the ground, the breakdown voltage can vary even if the gap length and the electrodes shape are the same. Figure 3.19, which refers to rod-rod gaps, gives a general view of the influence of the geometry on breakdown voltages.

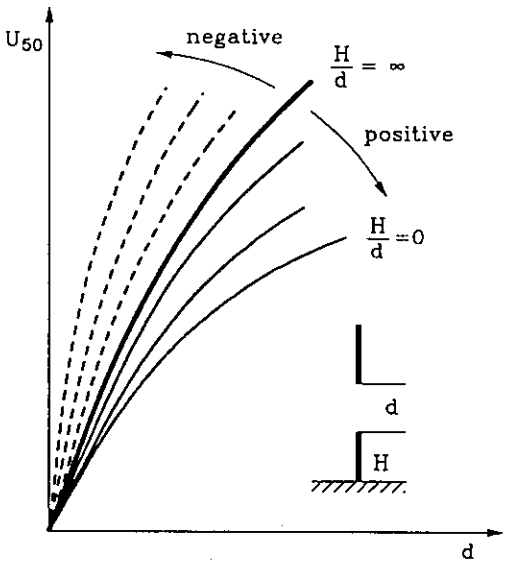

Figure 3.19 Breakdown voltage versus gap length in rod-rod gap with various electrode geometries.

3.5 MODELS

The knowledge gained during the last thirty years on the mechanism of discharge in air allowed the improvement of engineering models for the prediction of gap strength. These models do not enter into detail in physical aspects of the phenomenon but, usually, they utilize the large amount of information, both qualitative and quantitative, gained on the characteristics of various phases of the discharge mechanism. As the weight of these phases is different, according to electrodes geometry and voltage impulse shape, the best modelling of the dominant phase is of primary importance.

Figure 3.20 shows corona inception voltage and breakdown voltage as a function of gap length in a sphere-plane gap when stressed by impulse of positive polarity.

At short gap lengths (d_1), the breakdown voltage coincides with the voltage which causes streamers forma-

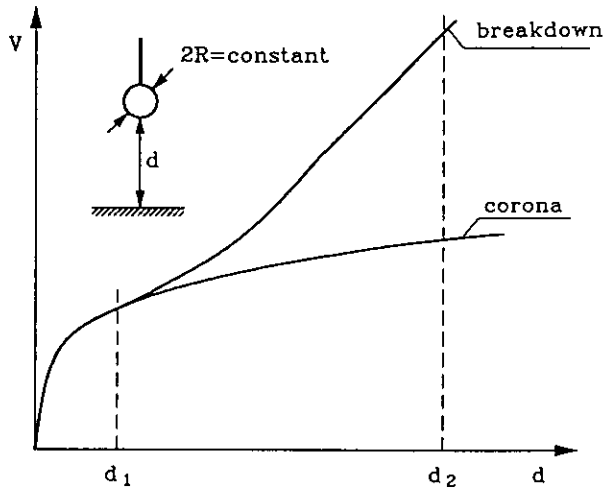

Figure 3.20 Corona inception and breakdown voltage as a function of gap length in a sphere plane gap.

tion, that is corona inception. The field distribution is only slightly ununiform, the average field in the gap is much higher than the average field along a streamer and corona formation causes unavoidably breakdown of the gap. In this case the breakdown voltage can be computed as shown in paragraph 3.2.1 for corona inception.

At long gap lengths (d_1), corona inception has minor importance, especially when the ratio d/R is large. In this case, in fact, the streamer phase is followed by leader propagation, which takes place in different conditions depending on the shape and value of the applied voltage. The leader can develop for a part of the gap and stop without breakdown of the gap. With lightning impulses (LI) the streamer phase reaches the opposite electrode and the leader propagates with increasing velocity in a gap which has been already bridged by partially conducting filaments. The basic condition for breakdown is to have the gap bridged by streamers and modelling has to be based on final jump phase (see paragraph 3.5.1). With switching impulses (SI), on the contrary, the leader, once formed, progresses in virgin air with leader corona in front of it. Its velocity is almost constant, indicating a constant electrical situation at its tip, until streamers reach the opposite electrode; after this moment leader progression is similar to that observed with LI. In this case the modelling of breakdown has to be based on the description of the leader propagation (see paragraph 3.5.2).

3.5.1 LI strength models

The various proposed approaches for the prediction of the dielectric strength of air gaps under lightning overvoltages usually allow the calculation of both the minimum breakdown voltage and the time to breakdown. They can be grouped in two main categories:

a) integration methods
b) physical approaches

The approaches of the second type seem to be a step forward in modelling this type of discharge as they try to take into account the physical processes involved in spark formation.

3.5.1.1 Integration method

In the integration methods the dielectric strength of insulations is described as

$$\int_{T_0}^{T_s} (U - U_0)^n \, dt = D \qquad (3.7)$$

where T_s is the time to breakdown and T_0 is the time after which the applied voltage is higher than a reference voltage U_0. In the case of n=1 the method represents the well known "equal area" criterion.

Different proposals exist for the values of U_0, n and D but each proposal refers to a particular set of results and it cannot be easily generalized. Furthermore it has to be observed that these methods can be applied only to the prospective shape of the impulse voltage, whereas the impulse shape can change even drastically with the applied voltage depending on the characteristics of the generating circuit.

3.5.1.2 Physical approaches

These methods [3.11] consider the different phases of discharge development and their dependence on applied voltage; they compute the time to breakdown as the time which is necessary, once the applied voltage is known, for the completion of all phases of the discharge process, namely:

- corona inception (T_i)
- streamer propagation (T_s)
- leader propagation (T_l)

The time to breakdown T_s is given by:

$$T_s = T_i + T_s + T_l \qquad (3.8)$$

Corona inception

Corona inception occurs at time T_i when the applied voltage has reached a convenient value U_i, which depends on electrode geometry, gap distance and rate of rise of applied voltage (see paragraph 3.2.1). U_i can be computed and T_i derived if the impulse shape of the voltage is known. In the case of gaps with greatly non uniform field distribution, inception voltage is far below breakdown voltage; therefore, due to the high rate of rise of the voltage, T_i can be often disregarded.

Streamer propagation

The streamer phase initiates at corona inception and is completed when the gap is fully crossed by streamers. T_s depends on applied voltage and the minimum value necessary for streamers to cover the whole gap is not far from the U_{50} value when standard lightning impulses are considered. At this voltage T_s has its maximum value and it decreases as voltage is raised. Experimental results have shown that T_s is almost independent of voltage polarity, electrode configuration and gap clearance. Its value, on the contrary, is strongly dependent on the ratio E/E_{50} where E is the average field in the gap at the applied voltage U and E_{50} is the average field at U_{50} (Figure 3.21).

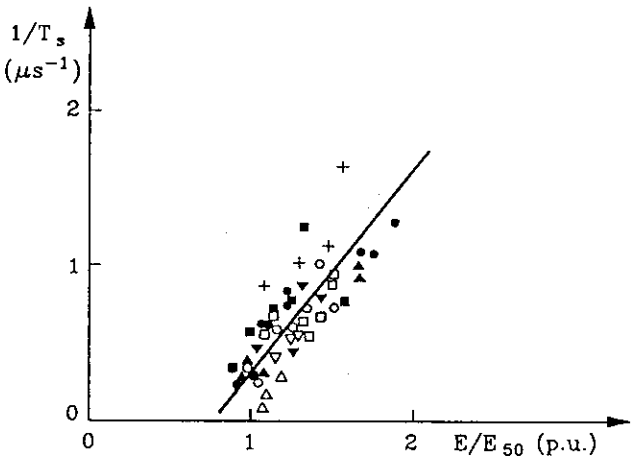

Figure 3.21 $1/T_s$, for various geometries and gap clearences, as a function of the gap, when given in p.u. of the value at 50% level.

In almost all the proposed models, however, it is assumed that the streamer phase is completed when the applied voltage has reached a value which gives an average field in the gap corresponding to E_{50}. Taking into account that T_s is only a part of T_s, this approximation gives acceptable accuracy. It has to be men-

tioned that with this procedure the time $(T_l + T_s)$ is in fact obtained.

Leader propagation

As has been said, the length of the leader at the end of T_s is a small percentage of the total gap length; for this reason it is always assumed that the leader covers the total gap length after the streamers have crossed the gap.

The propagation of the leader is described in terms of the instantaneous values of its velocity. Various formulas have been proposed to relate leader velocity and other parameters, generally applied voltage and position of leader tip in the gap. These formulas are fundamentally of two types:

$$v = K\, d \left(\frac{U}{x} - E_0\right) \tag{3.9}$$

$$v = K_1\, d \left(\frac{d}{x} - 1\right) e^{\left(K_2 \frac{U}{d}\right)} \tag{3.10}$$

where d is the gap length, x is the part of the gap not yet covered by the leader, U is the instantaneous value of the applied voltage, E_0 is reference field value and K_1 and K_2 are suitable constants.

Recently, on the basis of results obtained in a large test program, a combination of the two previous expressions has been proposed:

$$v = K_1\, d \left(\frac{U}{x} - E_0\right) e^{\left(K_2 \frac{U}{x}\right)} \tag{3.11}$$

By integration, the leader development can be described. According to the time dependence of U the leader can either reach the opposite electrode causing breakdown or stop, when velocity tends to become negative. In case of breakdown T_s is also computed.

In all the proposed formulas the value U(t) has to be the actual voltage applied to the gap; due to the voltage drop caused by current flowing during leader propagation, this voltage does not correspond to the theoretical one; this difference is larger the higher is the overvoltage, i.e. the shorter is the time to breakdown. The actual applied voltage can be determined when both generating circuit characteristics and current flowing during leader propagation are known.

Mainly due to difficulties in synchronization, the relationship between current and leader velocity is not so easy to be determined. A linear relationship, however, seems to be acceptable:

$$i = q\, v \tag{3.12}$$

with values of q in the range of 300-400 μC/m.

Generally the computed breakdown voltages are in good agreement with experimental results; larger discrepancies are experienced when insulator strings are present.

3.5.2 SI strength models

In the case of breakdown under SI, leader inception and propagation ending with the threshold of the final jump are the most important phases for assessment of the gap strength. In fact first corona has little bearing on the gap strength even if it constitutes a pre-requisite to leader inception; at the same time, if the final jump phase is reached, in practice breakdown cannot be avoided.

Several models have been put forward to account for leader inception and breakdown of long air gaps under positive SI. They calculate the critical strength of simple configurations of practical interest and they mostly constitute an engineering-physical approach to the problem. In the following the best-known models will be reviewed and the review will progress chronologically from the early to the most recent models.

The bulk of the work deals with impulses having critical time-to-crest, which yield the lowest withstand strength. Furthermore most of the models deal with rod-plane and conductor-plane gaps, which were more thoroughly investigated experimentally.

Few models extends to other configurations such as rod-rod, conductor-rod and conductor-tower leg and among them the most recent permits to take into accounts also the influence of air density .

In the previous chapter dealing with fundamentals of discharges, the stages of first corona, leader inception and continuous propagation and final jump were thoroughly described.

Successful modelling of the first corona stage has been undertaken by Les Renardieres Group [3.12]. While first corona constitutes a pre-requisite to leader inception, first corona models have little bearing on the gap strength and will therefore not be dealt with here. While conditions at the inception of the final jump are important for the determination of the strength of the gap, little is known about the final jump mechanism and no model yet addresses that stage in detail.

This leaves the phase comprising leader inception and propagation ending with the threshold of the final jump as the most important for assessment of the gap strength and it will therefore be dealt with here extensively. This review however will only deal with engineering models, having direct impact on the prediction of the gap strength, rather than detailed physical modelling of one aspect or the other of the discharge mechanism.

The review will progress chronologically from the early to the most recent models but the similarities or contradictions among them will be brought up at the appropriate time. Finally, as far as possible, the same symbol will be used to describe any physical parameter if it occurs in different models, although this may be different from the symbol used in the original publication.

Lemke Model [3.13], [3.14]

This model can be described with reference to Figure 3.22, which refers to a rod-plane gap, under a criti-

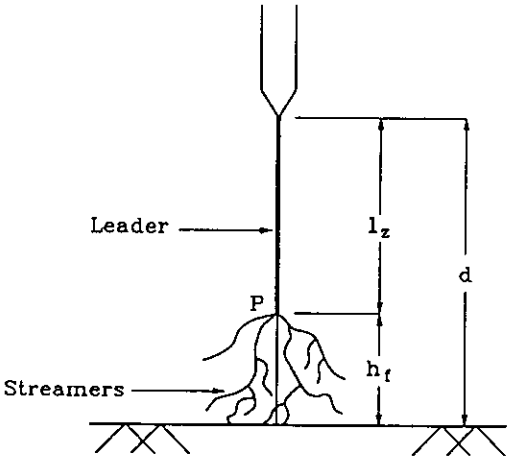

Figure 3.22 Schematic representation of a rod-plane gap at the final jump.

cal switching impulse at the threshold of the final jump. The instant illustrated corresponds to the crest of the impulse. The leader length along the gap axis is l_s and the final jump h_f.

The crest voltage U is then given by the sum of the leader voltage drop ΔU_l and the streamer voltage drop U_s:

$$U = \Delta U_l + U_s \tag{3.13}$$

$$U_s = h_f E_s \tag{3.14}$$

where E_s is the mean streamer gradient taken as 4.5 kV/cm. From measurements, an empirical formula for the length of the final jump is given as:

$$h_f = a_o \left[1 + \ln\left(\frac{d}{a_o}\right)\right] \tag{3.15}$$

Where a_o is an unknown constant.

The leader gradient E_l is more complex, being dependent on position (life time). Lemke used Toepler's theorem, which states that the resistance per unit length of the spark channel is inversely proportional to the charge that flowed through it. Noting that $l_s = d - h_f$, the resulting expression for ΔU_l reads:

$$\Delta U_l = E_{lo}\, a_o \ln\left[\frac{d}{a_o} - \ln\left(\frac{d}{a_o}\right)\right] \tag{3.16}$$

where E_{lo} is taken as 1.5 kV/cm.

Substituting from (3.14), (3.15), (3.16) into (3.13), the 50% breakdown voltage of the gap becomes:

$$U_{50} = a_o E_s \left[1+\ln\left(\frac{d}{a_o}\right)\right] + a_o E_{lo} \ln\left[\frac{d}{a_o} - \ln\left(\frac{d}{a_o}\right)\right] \tag{3.17}$$

Lemke found that to fit experimental results, expression (3.17) has to adopt different values of a_o for different electrode configurations and different voltage forms. For a rod-plane gap Lemke took a_o = 1 m, while for a bundle conductor-plane gap a_o = 1.5 m and for a bundle conductor-tower a_o = 1.3 m. Lemke even found that for a positive switching impulse superimposed on a direct voltage of positive polarity, a_o for a rod-plane configuration must vary in the range 0.9 - 1.25 m to account for the experimental results. The physical reason for the variation of a_o was not given nor a method to uprear determine that parameter.

Aleksandrov Model [3.15], [3.16]

The basic assumption underlying this model is that a critical charge Q_{cr} formed at and near the positive high voltage electrode is a prerequisite for continuous leader development. Such critical charge is a characteristic of the electrode but does not depend on the gap length.

The 50% sparkover voltage of the gap is then related to the critical charge by:

$$U_{50} = \frac{Q_{cr}}{C} \tag{3.18}$$

$$Q_{cr} = Q_{con} + Q_o \tag{3.19}$$

where

- Q_{con} is the electrode charge at corona onset voltage;
- Q_o is the space charge at leader inception;
- C is the capacitance of the electrode taking into account the space charge formed immediately before the continuous leader stage.

For a conductor-plane gap of length d, (3.18) takes the form:

$$U_{50} = \left(\frac{q_{cr}}{2\pi\varepsilon_o}\right) \ln\left(\frac{2\,d}{r_e}\right) \tag{3.20}$$

where

- q_{cr} is the critical charge per unit conductor length
- r_e is the equivalent radius used to determine the capacitance C, including space charge effect.

In expression (3.20) both q_{cr} and r_e are unknown. To avoid the problem of determining both quantities, Aleksandrov applied expression (3.20) to two gaps d_1 and d_2 for which the 50% sparkover voltages are determined experimentally:

$$U_{50}(d_1) = \left(\frac{q_{cr}}{2\pi\varepsilon_o}\right) \ln\left(\frac{2\,d_1}{r_e}\right). \tag{3.21}$$

$$U_{50}(d_2) = \left(\frac{q_{cr}}{2\pi\varepsilon_o}\right) \ln\left(\frac{2\,d_2}{r_e}\right) \tag{3.22}$$

From (3.21), (3.22)

$$U_{50}(d_2) - U_{50}(d_1) = \Delta U_{12} = \left(\frac{q_{cr}}{2\pi\varepsilon_o}\right) \ln\left(\frac{d_2}{d_1}\right) \tag{3.23}$$

To predict the sparkover voltage of a gap d_3, it follows from (3.23) that:

$$U_{50}(d_3) - U_{50}(d_2) = \Delta U_{23} = \left(\frac{q_{cr}}{2\pi\varepsilon_o}\right) \ln\left(\frac{d_3}{d_2}\right) \tag{3.24}$$

From (23), (24) it follows that:

$$\Delta U_{23} = \Delta U_{12} \frac{\ln\left(\frac{d_3}{d_2}\right)}{\ln\left(\frac{d_2}{d_1}\right)} \tag{3.25}$$

The procedure is repeated to extrapolate the sparkover characteristics to longer gaps.

Jones Model [3.17]

This model deals with the rod-plane gap and attempts to account for the U-shape of the dependence of positive switching impulse strength on the time-to-crest.

Considering a gap of length d, partly penetrated by the leader, then at any position of the leader tip, the condition for continued leader propagation is:

$$V(t) > V_{pc}(l_s) + l_s E_{ml} \tag{3.26}$$

where

- V(t) is the instantaneous applied voltage
- V_{pc} is the critical leader tip potential corresponding to any length l_s
- E_{ml} is the mean leader gradient

At leader inception a simplified theoretical analysis

as well as regression of measured values yield the approximate relationship:

$$U_{lc} = V_{pc}(l_s=0) = 270\sqrt{d} \quad (kV,m) \qquad (3.27)$$

For any leader length l_s, the critical tip potential V_{pc} will then be given by:

$$V_{pc} = 270\sqrt{(d - l_s)} \quad (kV,m) \qquad (3.28)$$

Differentiating (3.26) with respect to t provides an expression for the rate of growth of the leader:

$$\frac{dl_s}{dt} = \frac{\left(\frac{dV}{dt} - l_s\frac{dE_{al}}{dt}\right)}{\left[E_{al} + \frac{d}{dl_s}(V_{pc}(l_s))\right]} \qquad (3.29)$$

According to this model, leader growth stops when the numerator of (3.29) vanishes. On the other hand as the denominator tends to zero breakdown is produced in a final jump.

The current during leader propagation is given by:

$$i = \frac{d}{dt}(l_s q_o) = q_o\frac{dl_s}{dt} + l_s\frac{dq_o}{dV}\frac{dV}{dt} \qquad (3.30)$$

where q_o is the charge per unit leader length.

The leader gradient for an element with life time t was found, in analogy with the electric arc to be:

$$E_l = E_\infty + (E_i - E_\infty)\,e^{-\frac{t}{\vartheta}} \qquad (3.31)$$

where

- E_i is the initial leader gradient at t=0, taken as 500 kV/m
- E_∞ is the ultimate gradient; $E_\infty = 100/i^{0.4}$ (kV/m, A)
- ϑ is an effective time constant taken as 50 μs.

Considering a critical impulse, with the leader progressing with constant speed along the gap axis and taking only the first term of (3.30), the breakdown time $t_b = q_o d/i$ and the corresponding average breakdown gradient becomes:

$$E_b = E_\infty(i) + [E_i - E_\infty(i)]\left(\frac{i\vartheta}{q_o d}\right)\left(1 - e^{-\frac{q_o d}{i\vartheta}}\right) \qquad (3.32)$$

Note that in this expression, the breakdown gradient is taken as that of a leader spanning the whole gap, without taking the final jump into consideration. While expression (3.27) yields reasonable values of the continuous leader inception voltage, evaluation of (3.32) with known values of i and q results in values of E_b which are generally on the low side.

Carrara-Thione Model [3.18]

The model starts from observations on rod-plane and conductor-plane configurations under positive impulses having critical front time. The 50% sparkover voltage is considered as the sum of three components:

1. U_{lc} is the continuous leader inception voltage
2. ΔU_l is the voltage increase during leader propagation
3. ΔU_s is the difference between U_{50} and U_s, where $U_s = U_{lc} + \Delta U_l$ is the minimum sparkover voltage.

A fundamental experimental observation is that for each gap length, there is a critical size of the positive electrode above which corona and continuous leader inception voltages practically coincide. For electrode sizes below critical, the continuous leader inception voltage remains practically constant at a level corresponding to the corona inception voltage of the critical electrode.

The critical radius can then be determined from experimental sparkover voltages of gaps with fixed distance but with positive electrodes of different radii, as shown in Figure 3.23 for a rod-plane configuration. Figure 3.24 shows the variation of the critical radius R_c with gap distance for rod-plane and conductor-plane configurations.

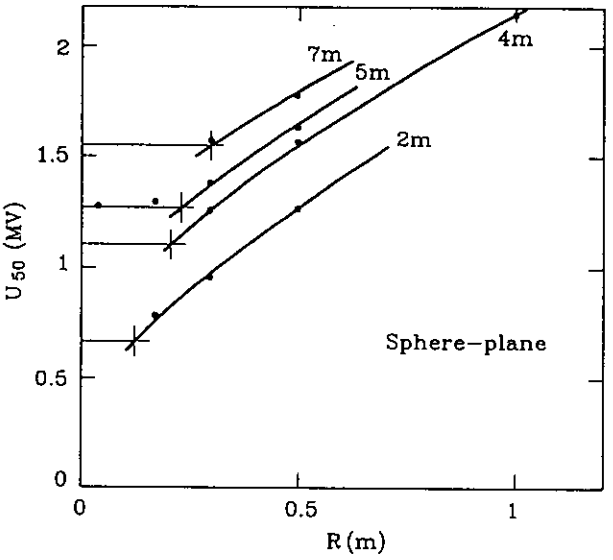

Figure 3.23 50% breakdown voltage versus electrode radius for different gap spacings.

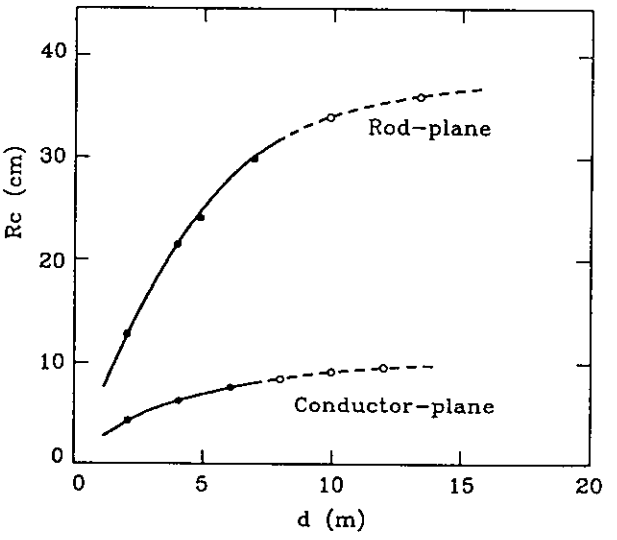

Figure 3.24 Critical radius as function of the gap spacing d.

In extending the application of the model to more complex configurations distinction is made between rod-type gaps for which the equipotential surfaces close to the electrode in the direction of maximum gradient are considered spheres and conductor-type gaps for which such equipotential are considered cylinders. The corresponding basic configurations are the rod-plane and conductor-plane gaps.

Two rather arbitrary criteria are proposed to establish the equivalence between a configuration of one type and its basic configuration.

The criterion of equivalence to determine R_c reads:

"With reference to corona to leader stem transition, a configuration is equivalent to the basic configuration of its group with spacing H_e, if the ratio between the electric field strength E_1 and E_2, evaluated at the distances R_2 and $R_1 < R_2$ from the center of positively charged conductor, in the direction where this ratio is maximum, is the same in both configurations".

For rod-type gaps the following values were adopted R_1 = 20 cm, R_2 = 40 cm while the corresponding values for conductor-type gaps are R_1 = 5 cm and R_2 = 15 cm.

In order to apply this criterion in practice, a field strength factor ϵ was defined as:

$$\epsilon = \left(\frac{E_2}{E_1}\right)\left(\frac{R_2}{R_1}\right)^n - 1 \qquad (3.33)$$

where n=1 for conductor-type gaps and n=2 for rod-type gaps.

Computed values of ϵ are shown in Figure 3.25 for rod- and conductor-gaps. From the calculation of ϵ for a configuration under study, Figure 3.25 yields the equivalent distance H_e from which the critical radius R_c can be determined.

The second criterion of equivalence relates to the determination of ΔU_1 and reads:

"With reference to continuous leader progression starting from leader inception, a stress situation on a configuration is equivalent to the critical positive impulse applied to the basic configuration of spacing H_e, if the charge increase on the electrode considered during leader propagation is the same in both configurations''.

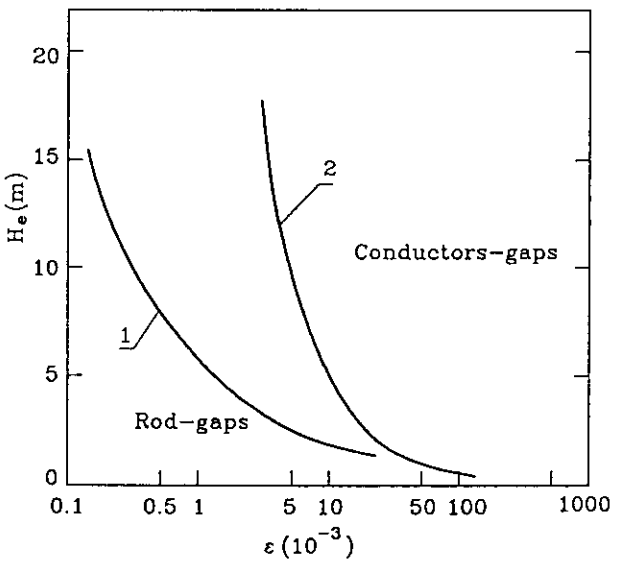

Figure 3.25 Equivalent gap spacing H_e as a function of the field strength factor ϵ.

For practical application of this criterion, the voltage increase ΔU_1 for the required configuration is obtained as:

$$\Delta U_1 = \beta(\Delta U_1)_e \qquad (3.34)$$

where β is the ratio between the coefficient relating the charge to voltage in the basic configuration and the coefficient relating the charge on the electrode considered to the voltage which is used as reference to define the stress in the configuration under consideration.

The model have been extensively applied to phase to ground and phase-to-phase configurations, finding generally a good agreement between the computed and the experimental results.

Hutzler Model [3.19], [3.20]

This model builds on Jones' model to simulate the temporal development of the leader in a rod-plane gap. It could account for the effect of impulse shape and for the statistical dispersion associated with leader propagation.

An equivalent leader radius r is defined, for which an arbitrary value of 30 cm was assumed. A critical field E_c of 31 kV/cm at the equivalent radius was assumed to be the necessary condition for leader propagation.

The leader current, associated with leader corona, follows Townsend's expression in terms of the electric field:

$$i = h\,E\,(E - E_c) \qquad (3.35)$$

where h = 10^{-11} Am^2/V^2.

The leader current is also related to the linear charge q_o and leader speed v by:

$$i = v\,q_o \qquad (3.36)$$

Similar to Jones, the leader gradient during propagation is governed by the differential equation:

$$\frac{dE}{dt} = \frac{[E_\infty(i) - E]}{\theta} \qquad (3.37)$$

with $E_\infty(i) = \frac{50}{i^{0.4}}$ $\left(\frac{kV}{m}, A\right)$

and $\theta = 30\mu s$

For $E \le E_c$, the leader current vanishes, propagation stops and the gradient recovers according to the differential equation:

$$\frac{dE}{dt} = \frac{E}{\theta_r} \qquad (3.38)$$

where θ_r is a recovery time constant taken as 500 μs.

The condition at the final jump was taken as:

$$470\,(d - l_d) \le V(t) \quad (m, kV) \qquad (3.39)$$

where V(t) is the instantaneous applied voltage.

Finally it was assumed that the leader progresses in straight segments, making a random angle Φ with the gap axis. The probability density function of Φ is assumed as:

$$f(\Phi) = \left(\frac{\sin\Phi}{a}\right) e^{-\frac{(1-\cos\Phi)}{a}} \qquad (3.40)$$

where a is a parameter which depends on dV/dt and the radius of the geometric equipotential surface at the point considered.

Figure 3.26 shows interesting simulation results of leader current and position during sparkover and withstand tests. Figure 3.27 shows a comparison between calculated values of U_{50} and $U_o(=U_0)$ and the well known EdF formula.

While the agreement is fairly good with respect to the complexity of the problem, it is clear that for gaps below 5 m the model results are too high while for very long gaps they are too low. This discrepancy could be the result of the simplified criterion of leader propagation, in the sense that for shorter gaps the adopted leader inception voltage may be too high while the opposite may be true for longer gaps.

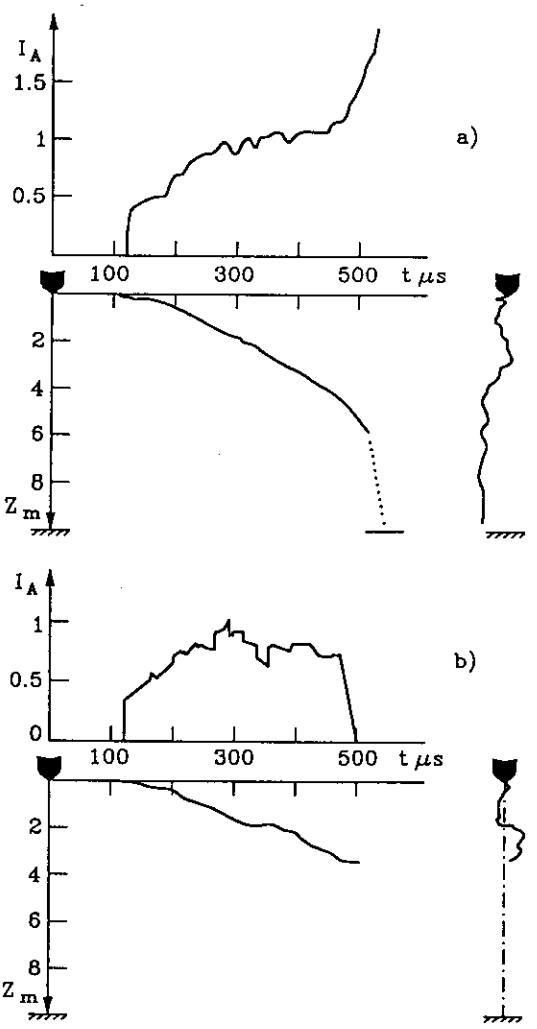

Figure 3.26 Simulation of current oscillogram, image converter recording and static picture, d=10 m, R=30 cm. Impulse 500/10000 μs, $U_{crest}=U_{50}=1859$ kV.
a) breakdown b) withstand

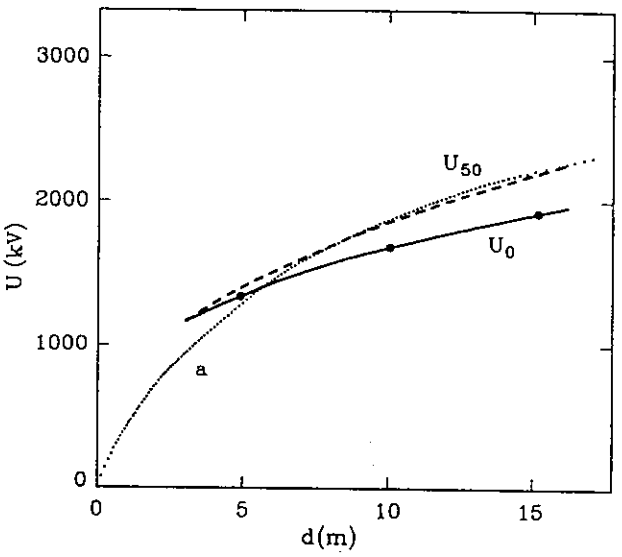

Figure 3.27 U_{50} and U_o levels as a function of gap spacing d. Impulse shape: 500/10000 μs, R=30 cm
(a) $U_{50}=3400/(1+8/d)$

Bazelyan Model [3.21]

Bazelyan takes the electrostatic energy stored in the equivalent capacitance of a spark channel as an upper limit to the energy released in the channel.
For a leader discharge the charge jacket contributes the major part of the equivalent leader capacitance (estimated roughly as 25 pF/m). An estimate of the minimum voltage at which transition from streamer to leader is possible is 200-300 kV.

Considering the leader corona zone, starting from a leader tip of radius r_p and potential V_p, the charge per unit length q_o and length s of streamer zone were obtained as:

$$q_o = \frac{4\pi\varepsilon_o V_p}{\ln\left(\frac{s}{r_p}\right)} \qquad (3.41)$$

$$s = \frac{V_p}{E_o}\left[1-\frac{1}{\ln\left(\frac{s}{r_p}\right)}\right] \qquad (3.42)$$

with the streamer gradient E_o taken as 4.65 kV/cm and the radius at the leader tip assumed as 1 cm. As an example, evaluation of (3.41) and (3.42) yields q_o of 21 μC/m and s of 1.7 m at V_p = 1000 kV.

An empirical formula for the leader gradient in terms of the leader current i and life time t takes the form:

$$E_l = \frac{800}{i^{0.5}\, t^{0.55}} \quad \left(\frac{kV}{m},\ A,\ \mu s\right) \qquad (3.43)$$

This formula means, for example, that for a leader current of 1A, the gradient of a leader segment will drop to 50 kV/m in 155 μs and will eventually reach 10 kV/m in 2.9 ms.

Another empirical expression relates the leader speed v to the tip potential V_p:

$$v = 12\, V_p^{0.5} \qquad (3.44)$$

This rather strong dependence of v on V_p is somewhat

different from results of Les Renardieres Group, as reported by Waters [3.22], which indicates that the leader velocity is less sensitive to the application of overvoltage, anode geometry and gap length which may all contribute to change the tip potential.

Bazelyan used the model to evaluate the strength of gaps up to 100 m long, but stressed that the calculations are in the nature of estimates claiming to establish only qualitative regularities.

Rizk Model [3.23], [3.24]

This model introduces criteria for leader inception and breakdown of different electrode configurations under positive switching impulses with critical time-to-crest. It accounts for conditions in the vicinity of the high voltage positive electrode at leader inception as well as for conditions at the threshold of the final jump.

Figure 3.28a presents a simplified schematic diagram of a rod-plane gap at leader inception, subjected to a positive switching impulse having a critical front time. Positive streamers converge into an ionized stem zone leading to the high voltage electrode. The streamer and stem zone are characterized by the critical charge Q_o and the distances s and s_o. The elements of the model at continuous leader inception [3.24] can be explained with reference to Figure 3.28b:

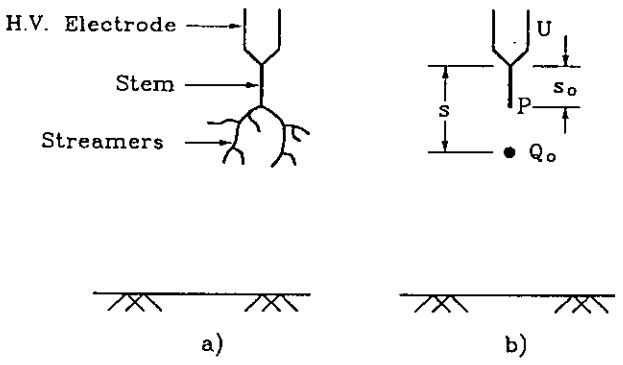

Figure 3.28 Schematic representation of a rod-plane gap at continuous leader inception
a) simplified physical picture
b) simplified equivalent scheme

- the distances s and s_o are much shorter than, and practically independent of, the gap length d.
- the stem, at continuous leader inception and for the purpose of calculating the field at its tip, is considered as an extension of the high voltage electrode.
- the applied electric field E_{1c} at the stem tip P is given by U_{1c}/r_{eq}, where U_{1c} is the applied voltage and r_{eq} is an equivalent radius characterizing the thin stem and is very little influenced by the dimensions of the high voltage electrode or the gap length.
- r_{eq} is much smaller than both s and s_o.
- the first prerequisite for continuous leader inception is that the streamer reaches a critical size, characterized in the model by the ratio Q_o/U_{1c}.
- Q_o and its image charges produce an opposing field E_{1n} at the stem tip P.
- As the flow of the critical charge Q_o ensures adequate electrical conductivity of the stem, continuous leader propagation starts when the resultant electric field at P exceeds a critical level E_c.
- E_{1n} and E_c are respectively correlated to the space charge induced potential U_{1n} and a critical potential U_c through the equivalent stem radius r_{eq}.
- the continuous leader penetrates the gap, surrounded by a positive space charge sheath of constant charge q_o per unit axial length.
- the continuous leader penetrates the gap with practically constant speed and the leader tip potential is practically maintained constant at the inception level U_{1c}.

The situation at the threshold of the final jump is described in the model as follows:

- the tip potential U_{1c} must be equal to the positive streamer gradient E_s multiplied by the length h_f of the final jump.
- the electric field E_g at the ground plane must exceed a critical value E_{cr} in order to permit the penetration of the gap by the streamers ahead of the leader discharge (leader corona).
- for rod-type positive high voltage electrode, the field E_g results almost totally from the effect of the leader space charge sheath.
- for conductor-type positive high voltage electrode, the geometry of that electrode will play a role, although the leader space charge is still the determining factor of E_g.

The model results in expressions of continuous leader inception voltage U_{1c} for different gap configurations. For example, the expression for a rod-plane gap reads:

$$U_{1c} = \frac{1556}{1+\frac{3.89}{d}} \quad (kV,\ m) \tag{3.45}$$

The corresponding expression for conductor-plane gap:

$$U_{1c} = \frac{2247}{1+\frac{5.15-5.49\ \ln a}{d\ \ln\frac{2d}{a}}} \quad (kV,\ m) \tag{3.46}$$

where a is the conductor radius.

For a rod-rod gaps of 4 m or more, with a grounded rod of height h so that h≤2d, the expression for the continuous leader inception voltage reads:

$$U_{1c} = \frac{1556}{1+\frac{3.89}{h+d}} \quad (kV,\ m) \tag{3.47}$$

and the corresponding expression for a conductor- grounded rod gap:

$$U_{1c} = \frac{2247}{1+\frac{5.15-5.49\ \ln a}{(d+h)\ \ln\left(\frac{2(d+h)}{a}\right)}} \quad (kV,\ m) \tag{3.48}$$

The leader gradient is calculated slightly differently from Jones and Hutzler, in that the leader conductance per unit length G rather than the leader voltage gradient E_l is governed by the Hochrainer's equation:

$$\frac{dG}{dt} = \frac{(G_\infty - G)}{\theta} \tag{3.49}$$

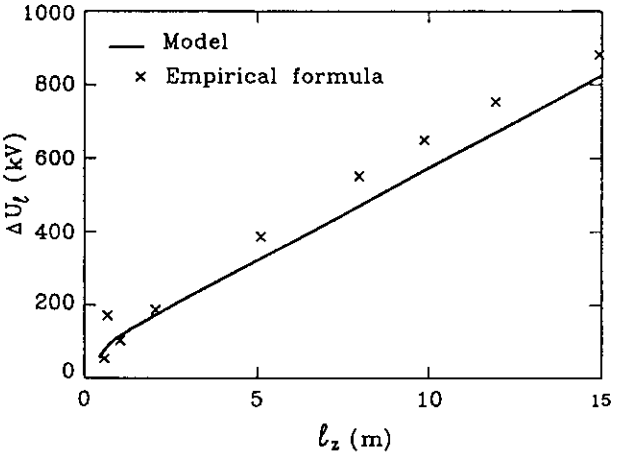

Figure 3.29 Leader voltage drop as a function of axial leader length.

with a time constant Θ taken as 50 μs.

The conductance per unit length G is obviously related to the gradient E_l through:

$$G = \frac{i}{E_l} \tag{3.50}$$

For a constant leader current, G_∞ is constant and (3.49) yields:

$$G(t) = G_\infty + (G_l - G_\infty)\, e^{-\frac{t}{\Theta}} \tag{3.51}$$

with $G_\infty = i/E_\infty$ and $G_l = i/E_l$, E_∞ and E_l being taken as 50 kV/m and 400 kV/m respectively.

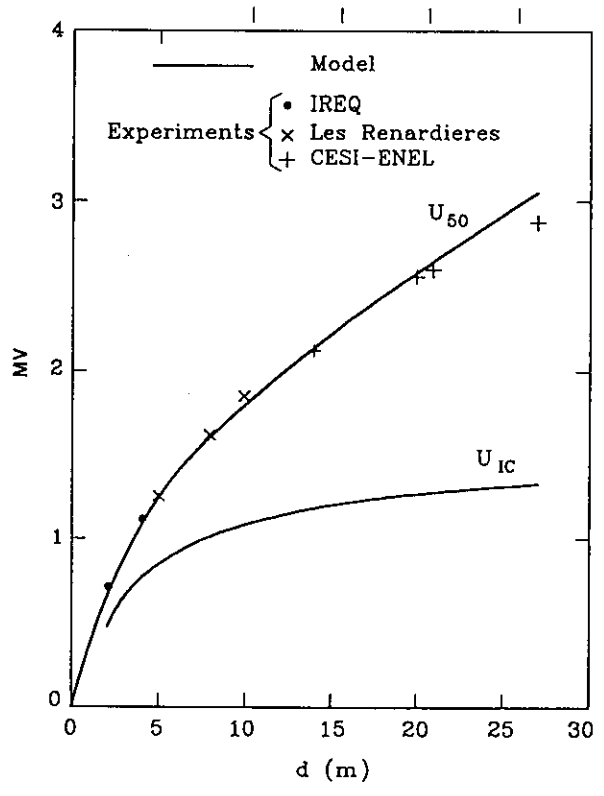

Figure 3.30 Continuous leader inception voltage and 50% breakdown voltage of rod-plane gaps under critical positive switching impulse.

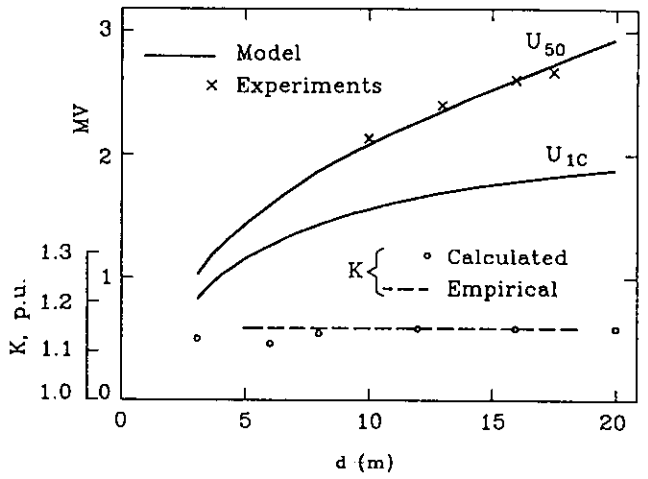

Figure 3.31 Critical positive switching impulse sparkover characteristics of conductor-plane gaps.

Figure 3.29 shows a comparison of the calculated leader voltage drop ΔU_l as a function of leader axial length l_z, to an empirical formula given in [3.25].

Figure 3.30 shows the variation of continuous leader inception voltage U_{lc} and U_{50} with gap spacing for a rod-plane gap. Experimental values from [3.26] and [3.27] are also indicated.

The agreement between theory and experiment for U_{50} is within ±2.5% except for the 27 m gap where the theory predicts a value 6% higher than that reported in [3.27].

Figure 3.31 shows similar model results and comparison with experiments for a conductor-plane gap [3.27].

Figure 3.32 shows the results of calculation of the

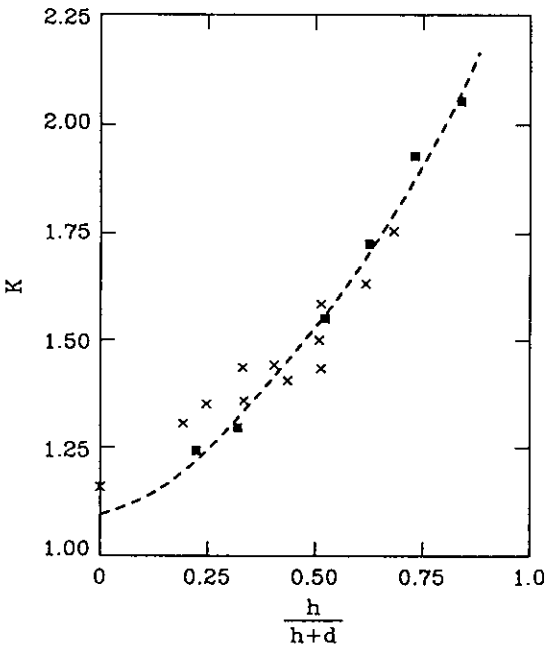

Figure 3.32 Comparison of model (x), and measured values, of gap factor of conductor-rod configuration.

gap factor of a conductor-rod gap together with experimental values from [3.28].

As shown the agreement between the model and experiment is excellent. More detailed results are given in [3.23] and [3.24]. Application of this model to air density effects is reported in [3.29] and to exposure of transmission lines to direct lightning strokes in [3.30].

3.6 CONCLUSIONS

The knowledge of breakdown mechanism in long air gaps, when stressed by transient voltages, has been highly improved during the last thirty years by performing a large amount of experimental work. By applying advanced diagnostic techniques, as high speed photography, spectroscopy and strioscopy, together with traditional measurements, a detailed description of the various phases of the discharge process has been obtained.

In the same period, many basic processes has been better clarified so that good physical models of the various phases have been proposed.

At the same time, due to the continuous increase of the voltage in transmission systems, it was necessary develop engineering models which allow either for the calculation of the strength of air insulations or for the correct extrapolation of the existing data at lower voltage. Several models have been put forward and their complexity, generality, degree of sophistication and precision increased as the knowledge of the discharge phenomena improved.

For lightning impulses, models exist which describe the discharge development in terms of streamer phase and, mainly, of leader elongation. These models allow for the determination of breakdown voltages and time to breakdown with sufficient accuracy.

For switching positive impulses, several models have been put forward to account for leader inception and its propagation. These models, which contribute to establish general trends and to rationalize experimental works, calculate the critical strength of simple configurations of practical interest, with accuracy as good as that of widely used empirical formulas.

Models have been generally proposed for simple configurations in standard conditions. Modelling of more complex configurations and conditions taking into account the influence of insulators, of environmental conditions (e.g. humidity, rain, ice, fire) requires additional work.

3.7 REFERENCES

[3.1] Les Renardieres Group, "Positive discharge in long air gaps at Les Renardieres: 1975 results and conclusions", Electra, 53, 1977.

[3.2] L.B. Loeb, J.M Meek, "The mechanism of the electric spark", Stanford University Press, 1941.

[3.3] R.F. Griffiths, C.T. Phelps, "The effect of air pressure and water vapour content on the propagation of positive corona streamers", Quart. J. R. Met. Soc., 102, 1976.

[3.4] S. Badaloni, I. Gallimberti, "The inception mechanism of the first corona in non uniform field", Padova University, Report UPee 72/03,1972.

[3.5] I.S. Stekolnikov, "The nature of the long spark", Izd. Ak. Nauk SSSR, 1960

[3.6] G.N. Alexandrov, "Mechanism of corona-to-spark transition in long air gap", Zh. Tekhn. Fiz., 35, 1965.

[3.7] I. Gallimberti, "The mechanism of the long spark formation", Journal de Physique, C7, 40, 1979.

[3.8] I. Gallimberti, "The characteristics of the leader channel in long gaps", World Electotech. Conf., Moscow, 1977.

[3.9] Les Renardieres Group, "Negative discharges in long air gaps at Les Renardieres: 1978 results", Electra, 74, 1981.

[3.10] G. Baldo, G. Pesavento, "Floating potential bodies and their interaction with discharge development", 6th ISH, New Orleans, 1989.

[3.11] A. Pigini et al., "Performance of large air gaps under lightning overvoltages: experimental study and analysis of accuracy of predetermination methods", IEEE Trans., Power Delivery, 4, 1989.

[3.12] Les Renardieres Group, " Long Air Gap Discharges at Les Renardieres: 1973 Results", Electra, No. 23, July 1972, pp. 105-120.

[3.13] E. Lemke, " Beitrag zur Abschatzung der Durchschlagspannung langer Luftfunkenstrecken", Z. elecktr. Inform. u. Energietechnik, Leipzig, Vol. 3, 1973, No. 4, pp.186-192.

[3.14] W. Mosch, E. Lemke, " Ein Modell zum Durchschlagprozess langer Luftfunkenstrecke", ETZ-A, Vol. 95, 1974, No. 5, pp. 256-260.

[3.15] G.N. Aleksandrov, " Special Features of Spark Discharge Development in Long Air Clearances of Insulating Structures", Elektrichestvo, No. 8, 1975, pp. 15-18.

[3.16] G.N. Aleksandrov, G.V. Podporkyn, " Analysis of Experimental Data on the Electric Strength of Long Air Gaps", IEEE Trans., Vol. PAS-98, No. 2, March/April 1979, pp. 597-605.

[3.17] B. Jones, "Switching Surges and Air Insulation", Phil. Trans. R. Soc. Lond. A., Vol. 275, 1973, pp. 165-180.

[3.18] G.Carrara, L.Thione, "Switching Surge Strength of Large Air Gaps: A Physical Approach", IEEE Trans., Vol. PAS-95, No. 2, March/April 1976, pp. 512-524.

[3.19] B. Hutzler, D. Hutzler-Barre, " Leader Propagation for Determination of Switching Surge Flashover Voltage of Large Air Gaps", IEEE Trans., Vol. Pas-97, No. 4, July/Aug. 1978, pp. 1087-1096.

[3.20] B. Hutzler, D. Hutzler-Barre, " A Model of the Breakdown in Large Air Gaps", EdF, Bulletin Etudes et Recherche, Serie B, No. 4, 1982, pp.11-39.

[3.21] E. M. Bazelyan, " The Leader of a Long Positive Spark", Electric Technology USSR, 1987, No. 2, pp.47-60.

[3.22] R.T. Waters, " Breakdown in Nonuniform Field", Proc IEE, Vol. 128, PEA, No. 4, May 1981, pp. 319-325.

[3.23] F.A.M. Rizk, " A Model for Switching Impulse Leader Inception and Breakdown of Long Air--Gaps", IEEE Trans. on Power Delivery, Vol. 4, No. 1, Jan. 1989, pp. 596-606.

[3.24] F.A.M. Rizk, " Switching Impulse Strength of Air Insulation: Leader Inception Criterion", IEEE Trans. on Power Delivery, Vol. 4, No. 4, Oct. 1989, pp. 2187-2195.

[3.25] L. Thione, " The Electric Strength of Air Insulation", in Surges in High Voltage Networks, Edited by K. Ragaller, 1979, pp. 165.

[3.26] Les Renardieres Group, " Research on Long Air Gap Discharges at Les Renardieres - 1973 Results", Electra No. 35, 1974, pp. 49-156.

[3.27] A. Pigini, G. Rizzi, R. Brambilla, E. Garbagnati, " Switching Impulse Strength of Very Large Air Gaps", ISH, Milano 1979, paper no. 52.15.

[3.28] G. Gallet, M. Bettler, G. Leroy, " Switching Impulse Results Obtained on the Outdoor Test Area at Les Renardieres", IEEE Trans., Vol. PAS-95, No. 2, 1976, pp. 580-585.

[3.29] F.A.M. Rizk, "Critical Switching Impulse Strength of Long Air Gaps: Modelling of Air Effects", IEEE Trans. paper, Summer Power Meeting, San Diego, Calif., July/Aug. 1991.

[3.30] F.A.M. Rizk, " Modelling of Transmission Line Exposure to Direct Lightning Strokes", IEEE Trans. on Power Delivery, Vol. 5, No. 4, Nov. 1990, pp. 1983-1997.

4 STRENGTH UNDER SWITCHING OVERVOLTAGES IN REFERENCE AMBIENT CONDITIONS

by B. HUTZLER, E. GARBAGNATI, E. LEMKE, A. PIGINI

4.1 INTRODUCTION

As shown in detail in chapter 3, the dielectric strength of an air gap depends on ionization phenomena. The various mechanisms have been identified. However they mutually interact in a complex way so that a generalized and easy to handle modelisation can not be envisaged in the short term.

Nevertheless, in some specific cases, simplifications can be made so that models are thus available.

These difficulties come from the fact that flashover is the result of a series of events which develop according to the entire history of the gap (the phenomenon is not instantaneous), and each individual event obeys statistical laws.

Furthermore, a large number of parameters have to be taken into account. As a matter of fact, ionization phenomena result from the interaction of an electric field with a gas, and any parameter which modifies either the characteristics of the electric field or gas has to be considered.

The electric field can be characterized by two sets of parameters: (1) Those which define the static (or geometric) distribution of the field such the gap length, the shape of the electrodes, the distance from the ground or from surrounding electrodes (energized or not) and (2) Those which define the temporal variation of the field such the shape of the voltage stress (or stresses when more than one electrode is energized).

The air can be characterized by its physical parameters (pressure, temperature) and by its chemical composition (humidity).

During the discharge process, it must be recognized that both the electric field distribution and the gas characteristics are continuously modified through the ionization phenomena which create space charges.

Unless explicitly specified, the conditions defined in this chapter are those which are known to prevail before the test. In other words, the test conditions are defined by external parameters.
This qualitative presentation of the influencing parameters illustrates the complexity of the problem. It is thus easy to understand that a quantitative description cannot cover all the possible cases.

As far as statistics are concerned, the test results will be characterized by the crest value of the voltage which produces a discharge in 50% of the cases when it is applied (U_{50}) and by the conventional deviation z. Once U_{50} and z are known the voltages having different discharge probabilities can, in principle, be easily calculated.

The influence of the geometrical parameters will be analyzed for the case of idealized geometries, as the detail of all actual structure geometries cannot be taken into account.

Concerning the effect of the electrical parameters, it has to be noted that the laboratory tests are, in most cases, conducted either with Marx generators or transformers, so that the results generally refer to bi-exponential impulses or, in a limited number of cases, to sinusoidal waves.

As the influence of air density and air humidity are treated in another chapter, most of the content of this chapter refers to standard conditions as defined by IEC 60 [4.1] i.e:

Temperature	:	20 °C
Pressure	:	101.3 kPa (1013 mbar)
Humidity	:	11 g/m³.

The strength under standard rain will be also considered.

4.2 ANALYSIS OF GENERAL TRENDS AND MAIN INFLUENCING PARAMETERS

4.2.1 Electrical parameters

In the simplest case, when only one electrode is energized, the electrical parameters define the impulse shape and the polarity. In phase to phase tests a second impulse is applied to the other electrode. In order to represent more closely actual configurations a DC or AC stress can be applied prior to the impulse. The influence of these different parameters will be successively examined.

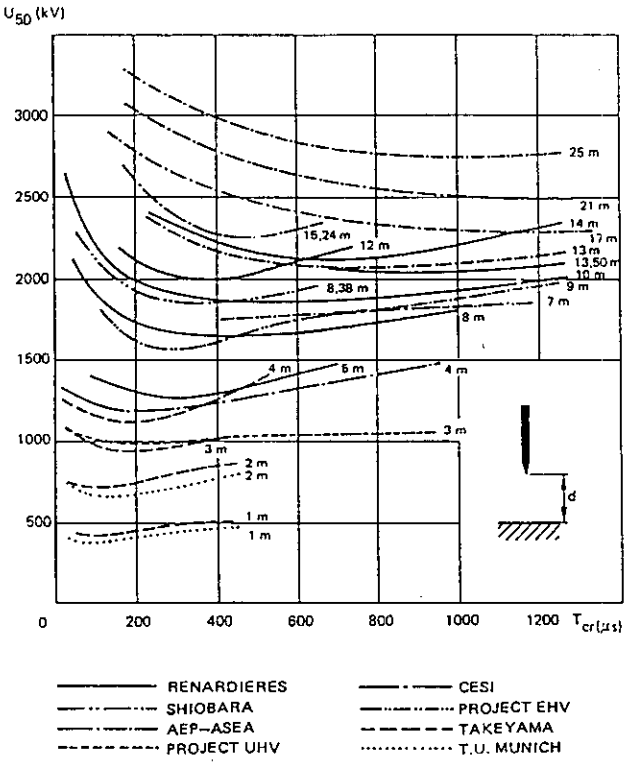

Figure 4.1 U-Curves for rod-plane gaps of various lengths under positive polarity impulses [4.12].

a) Positive polarity impulses

In the laboratory, the impulses most frequently obtained are of bi-exponential shape. However, damped sine waves, or composite front waves, are also sometimes used.

A bi-exponential impulse is characterized by two parameters, which may be time-to-crest, T_{cr}, and time to half value, T_2. When these parameters are modified, the dielectric strength of an air gap may be considerably changed. It has been noted in particular that when T_{cr} varies, the voltage U_{50} passes through a minimum having as coordinates $T_{cr\,crit}$, $U_{50\,crit}$. This curve is known as the U-curve (Figure 4.1).

The existence of this minimum is of paramount interest as it will simplify the characterization of air gaps. It can be seen in Figures 4.1 and 4.2 that this behaviour is qualitatively general and remains valid for all electrode shapes, gap lengths, types of stress and polarity. As the minimum of the U-curve is rather flat, $T_{cr\,crit}$ is not very precisely defined and a quantitative evaluation remains questionable. Nevertheless, a number of important variations are recognizable.

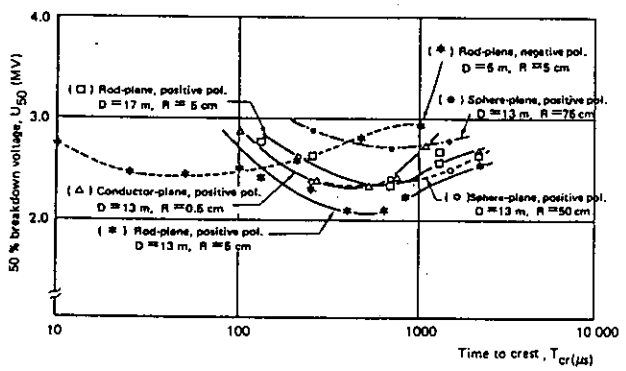

Figure 4.2 50% breakdown voltage (U_{50}) versus time to crest (T_{cr}) of the applied impulse of rod-plane, sphere-plane and conductor-plane configurations (d=gap spacing, R=radius of the electrode) [4.15].

From a physical point of view, it is known that the critical time to crest is directly linked to the duration of the leader propagation before the beginning of the final jump. Consequently:

- The critical time to crest is smaller under negative than under positive polarity, as, on the average a negative leader propagates quicker than a positive leader.

- The critical time to crest increases nearly linearly with the gap length, as the leader length increases nearly linearly with the gap length.

- The critical time to crest is changed when the cathode shape is modified. As an example, for a constant gap length, changing the cathode from a plane to a rod leads to a decrease in the leader length, the final jump starts earlier, and thus there is an associated decrease of the critical time to crest.

- The influence of the anode shape is less marked. Example: the critical time to crest is slightly lower for a conductor plane gap than for a rod plane gap (See Figure 4.2).

If, instead of using bi-exponential impulses, tests are performed with sine waves, the amplitude at the minimum of the U-curve is maintained. On the other hand, values of $T_{cr\,crit}$ are higher for sinusoidal waves than for bi-exponential impulses ; the ratio is about 2 [4.2], [4.3].

To better understand the influence of waveform, tests were also conducted with composite front waves. By varying both impulse test parameters (waveform, amplitude, polarity) and the timing of the impulse superimposed on the baseline impulse, it is thus possible to cover a greater diversity of impulse forms. Tests performed to date have never lead to a reduction of dielectric strength below $U_{50\,crit}$ [4.4].

Another example of this U-curve, for an air gap of 10 m, complemented by the variations of z and the mean flashover time T_B for bi-exponential impulses, is given in Figure 4.3. It can be seen that z is of the order of 5% for T_{cr} values which are in the range of $T_{cr\,crit}$. This result is generally assumed as representative of all geometries in the case of positive polarity.

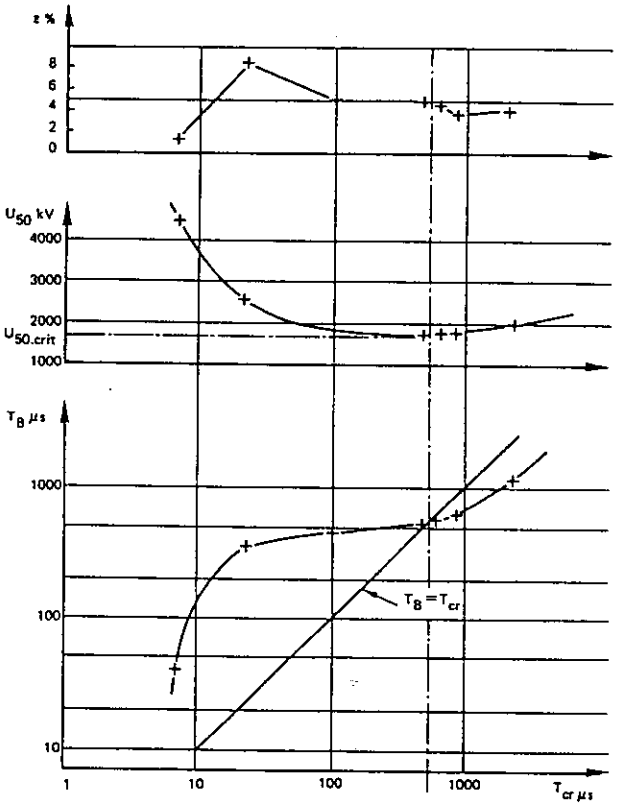

Figure 4.3 z, U_{50} and T_B as a function of T_{cr}. Positive rod-plane gap (d=10 m) [4.24].

To the right of the minimum of the U-curve, the time after which flashover occurs is less than T_{cr}. Flashover occurs on the front of the wave, and time to half value T_2 obviously has no influence on the withstand of the air gap.

To the left of the minimum, T_B is greater than T_{cr} and we therefore can anticipate a distinct influence of T_2 on the flashover characteristics of the air gap considered. By way of example, for a rod-plane air gap 8 m in length, Table 4.1 shows that there is relatively little difference in U_{50} when the time-to-crest increases from 7 to 22 μs, provided that time T_2 remains constant.

The influence of time to half value is illustrated using another presentation format in Figure 4.4. It can be seen that for constant T_{cr}, variations of T_2 are accompanied by substantial variations of U_{50}. When an impulse shape is modified, T_2 and T_{cr} are thus

Table 4.1 Influence of time to crest and time to half value on the dielectric strength of a positive rod-plane gap (d=8 m)

T_{cr} [μs]	T_2 [μs]	U_{50} [kV]	z [kV]	T_B [μs]
7	1400	2304	370	250
7	80	3805	33	34
22	1500	2277	217	274

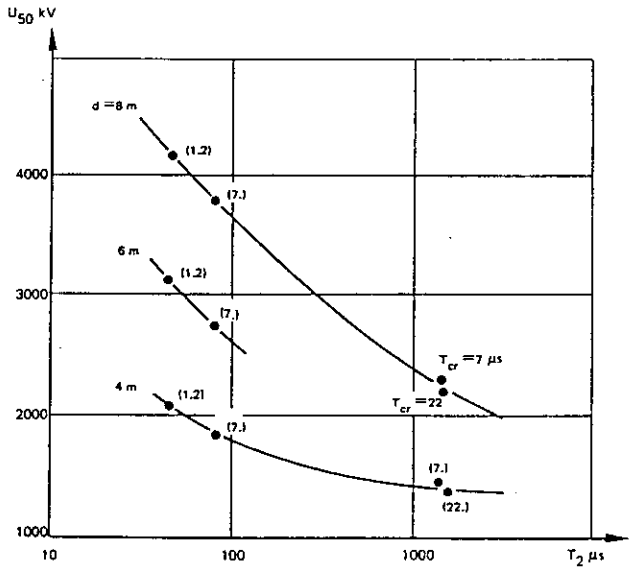

Figure 4.4 U_{50} as a function of time to half value T_1. Positive rod-plane gap (d=4, 6 and 8 m) [4.24].

simultaneously modified for practical reasons. Thus presentations such as Figure 4.1 can be criticized because T_{cr} is not the only variable shown. Moreover, Figure 4.4 shows that most of the variation of U_{50} for small T_{cr} is in fact due to T_1. However, even for a constant T_1, $U_{50} = f(T_{cr})$ is still a U-curve since leader corona liberates charge carriers which have two opposing effects.

From the physical analysis, corona generates electrons which heat the leader channel and acts as the motor of the discharge. However, when electrons are created, positive ions are released and generate a space charge field which opposes to the applied voltage field. On the left of the U-curve, the motor of the discharge (the electrons) is very active, but the brakes (the positive ions) are nearly blocked. On the right of the critical time to crest, the brakes have no action, but the motor is so weak that the discharge propagates with difficulty. At the critical time to crest the best compromise is reached in terms of discharge propagation between the motor and the brakes.

In summary, even if transient overvoltages cannot be characterized by a single impulse shape, the withstand voltage of any air gap has a lower limit, $U_{50\,crit}$. Thus the dimensioning of air gaps can be based on the value $U_{50\,crit}$.

b) Negative polarity impulses

The discussion of 4.2.1.a concerned positive polarity.

Currently available data on the dielectric strength of air gaps in negative polarity are much less

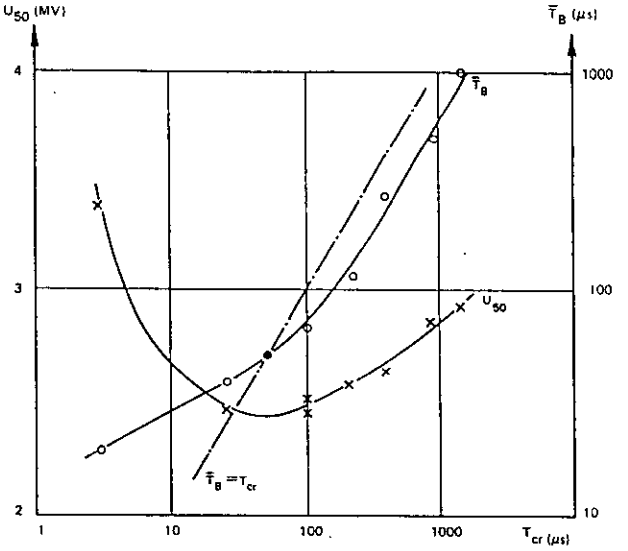

Figure 4.5 Variation of U_{50} and T_B versus T_{cr} (d=5 m). Negative rod-plane gap [4.24].

numerous than for positive polarity. This is due to the fact that positive stresses are more severe than negative stresses in the vast majority of practical cases and therefore less studied.

It is essential to note that the characteristics described in the case of positive polarity also apply to negative polarity. In particular, the flashover voltage follows a U-curve (Figure 4.5). However, as already mentioned, the critical time-to-crest is less than that obtained with positive polarity. If the time-to-crest is less than critical, flashover occurs after the crest; if not, it occurs on the impulse front (Figure 4.5)

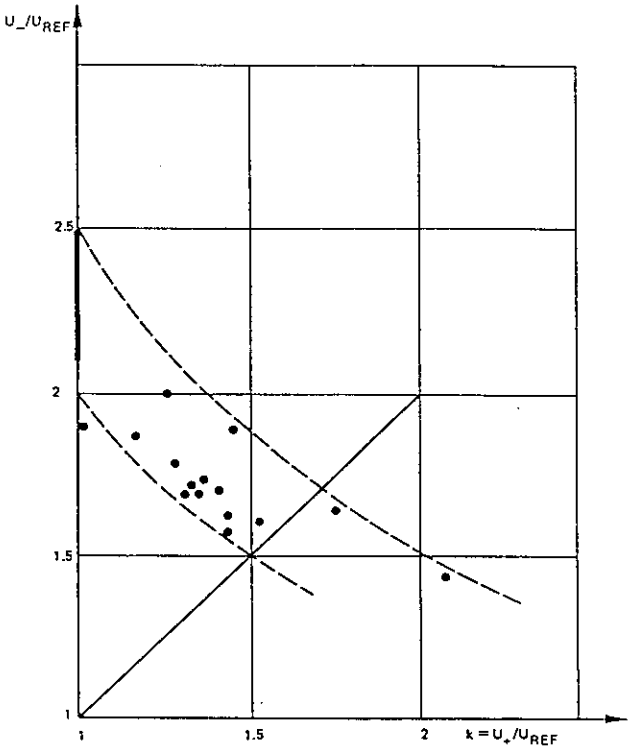

Figure 4.6 Correlation between strength under negative polarity and strength under positive polarity for a variety of configurations.
U_{REF}= 3400/(1+8/d) [4.24].

The conventional deviation z appears to be greater than with positive polarity - the scatter of the experimental results is very large. An average value of 8% can be taken as representative.

The strength under negative polarity U_- is compared to the strength under positive polarity U_+, in Figure 4.6. Both strengths are normalised to U_{REF}, which is the strength of the positive rod-plane gap of the same spacing. All the experimental results lie between the dotted lines. For a given air spacing, and despite a significant scatter, the gap which has the higher strength under positive polarity tends to have the lower strength under negative polarity. In other words, the order of merit is reversed when the polarity of the stress is changed. Most of the data points lie above the bisectrix, which means that most of the air gaps have a higher strength under negative polarity than under positive polarity. However, if under positive polarity, the strength of a gap is larger than 1.5 - 1.7 times the reference strength, the strength under negative polarity may be lower than under positive polarity.

c) Phase-to-phase conditions

The experimental study of the problems posed by the dimensioning of air gaps in cases where both electrodes may be stressed simultaneously was undertaken more recently [4.5, 4.6]. These studies require more test equipment and the number of parameters to be evaluated is greater than in the case of phase-to-earth stressing. The definition of these parameters is given on Figure 4.7. The result is that the level of our knowledge to date is far more superficial.

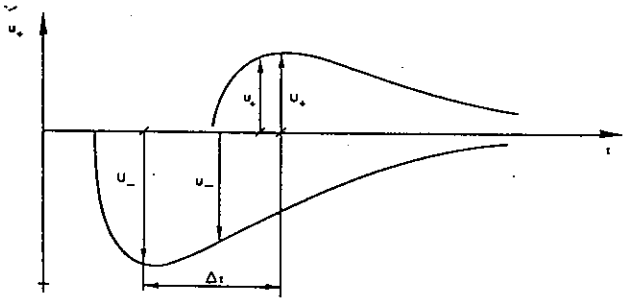

Figure 4.7 Definition of the various parameters useful for phase-to-phase testing.

Testing is generally conducted with two impulses of amplitudes U_- and U_+. Their relative amplitude is characterised by the parameter α[1] defined as:

$$\alpha = \frac{U_-}{U_+ + U_-} \qquad (4.1)$$

The reference condition is considered to be that where the peaks of the two impulses are synchronous, the negative polarity impulse having a time-to-crest equal to or greater than that of the positive polarity impulse. While this reference case does not correspond to minimal dielectric strength, it provides a good order of magnitude and, as it has been the subject of much study, enables the main characteristics of the dielectric strength of phase-to-phase air gaps to be presented.

[1] The use of the parameter α and of total voltage $(U_+ + U_-)$ enables a synthetic presentation of test results. The current trend however is to use the representation $U_+ = f(U_-)$ which is better suited to the study of phase-to-phase and phase-to-earth insulation coordination. Reference [4.7] contains an exhaustive study of this subject.

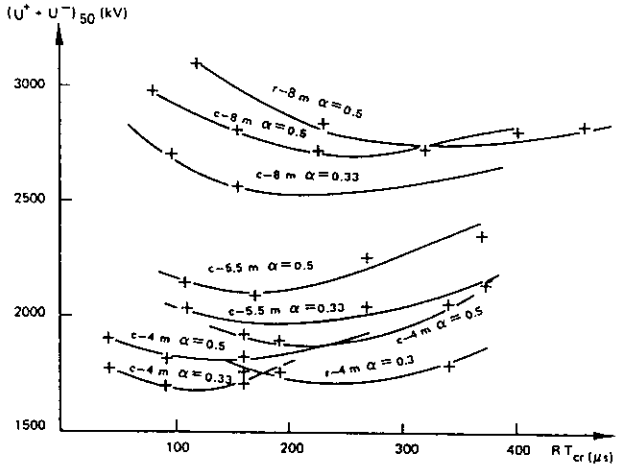

Figure 4.8 Phase to phase tests: Influence of the positive time-to-crest on U_{50} [4.5]
r=rod-rod configuration
c=conductor-conductor configuration

As in the case of phase-to-earth stresses, the U_{50} voltage passes through a minimum value when the time-to-crest of the positive polarity impulse varies (Figure 4.8). For a given spacing, this critical time-to-crest is between the critical times-to-crest observed under positive voltage alone and under only negative voltage. The exact position of the curve is dependent on parameter α.

When the relative importance of the positive and negative components varies (variations of α), the total voltage $(U_+ + U_-)$ varies more or less linearly between the voltage measured under positive voltage alone and that measured under only negative voltage (Figure 4.9). For the requirements of insulation coordination, particular interest is taken in values of α = 0.33 and 0.5.

This behaviour of the strength is, in fact, due to the presence of the ground. As an example, let us consider

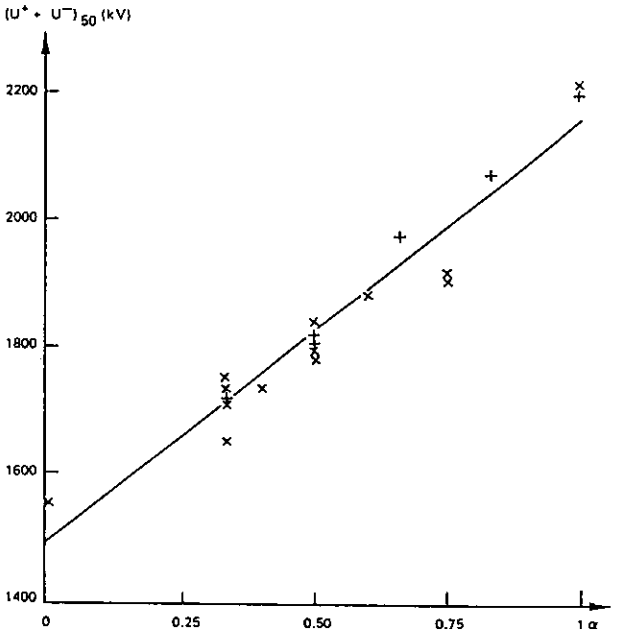

Figure 4.9 Phase to phase tests: Influence of the parameter α for 2 parallel conductors 4 m apart, 9 m above ground [4.24].

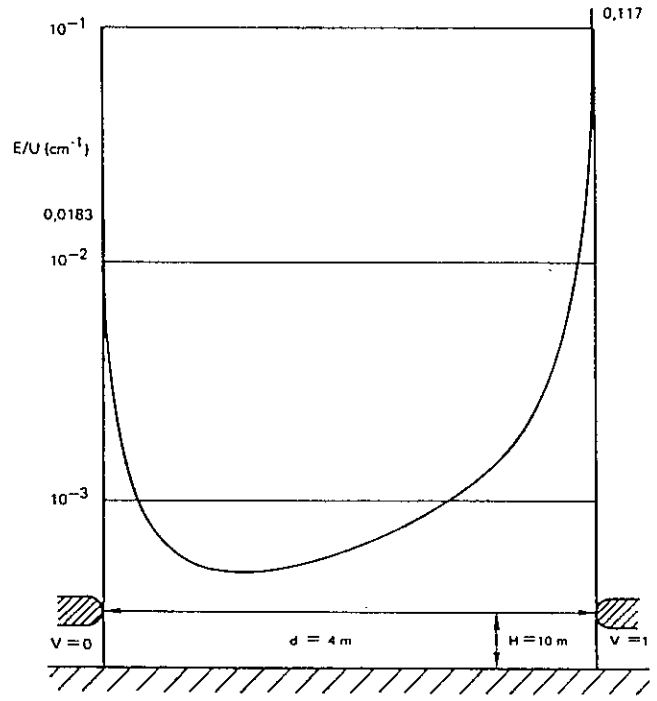

Figure 4.10 Distribution of electrical field in a geometrically symmetrical rod-rod gap. Gap spacing 4 m. Gap axis H=10 m above ground. Rod radii 5 cm.

a 4 m rod-rod air gap with a horizontal axis 10 m above the ground. Each rod is composed of a 10 cm diameter tube ending in a hemisphere of the same diameter. Geometrically, the air gap is symmetrical. We then apply a unit voltage (1 V) to the right-hand electrode, the left electrode being earthed. Under these conditions, the electric field calculated along the axis of the air gap is given by Figure 4.10. The asymmetry is evident. At the surface of the energized electrode the field is 11.7 V/m, whereas it attains a mere 1.83 V/m (more than six times less) at the earthed electrode. Thus the energized electrode is electrically more "pointed" than the earthed electrode. This asymmetry is caused by the presence of ground. As a matter of fact, if the gap axis is installed at a larger height above ground, the asymmetry will be attenuated. In the idealised case where the ground is completely removed, the field distribution becomes symmetrical whatever the value of α. On the other hand, if α = 0.5, the field distribution remains symmetrical whatever the height of the gap axis. This duality between α and the height above ground H appears on Figure 4.11 where it can be seen that the flashover voltage does not depend on H for α = 0.5 on one hand, and increases with H for α = 0,33, tending asymptotically toward the value for α = 0.5 on the other hand.

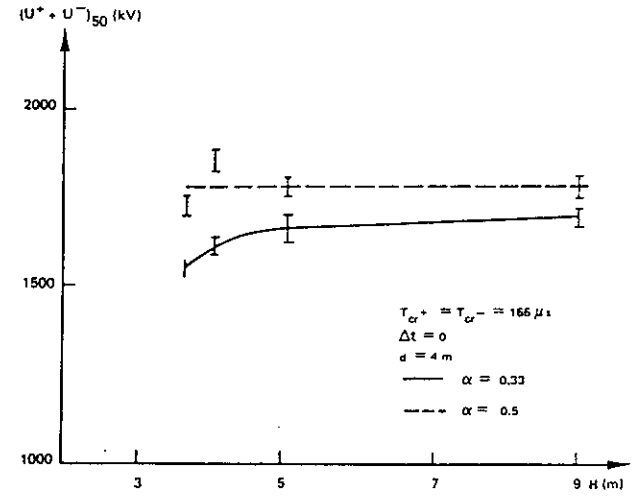

Figure 4.11 Disruptive phase-to-phase voltage dependent on height above ground. Conductor-conductor gap [4.5].

Figure 4.12 gives test results in a more complex case: a phase-to-phase configuration which, as in the previous case, is influenced by the ground, but where in addition, the role played by a fourth electrode (the third phase) is studied as a whole. The role played by the third phase is slight, and only just statistically significant. It should be noted, however, that the configuration studied is horizontal. Furthermore, in the case of Figure 4.12 the voltage applied to the 3rd phase is a sine-wave and equal to the phase-to-earth voltage of the 400 kV system. In practice, in the case of a voltage transient on both phases, the voltage of the third phase is also affected. Tests [4.6] have shown that the influence of the third phase could reach 10% in certain unfavourable cases. For a triangular configuration the influence would probably be more marked. However, the "realism" of these unfavourable laboratory conditions needs to be looked into more closely before drawing any final conclusions.

When the first tests of phase-to-phase dielectric strength were conducted [4.9], a certain number of parameters were defined on a theoretical basis. In particular, flashover voltage between phases was defined as the sum ($U_+ + U_-$) of the peak values of two components, positive and negative. When the peaks are simultaneous, ($U_+ + U_-$) do actually represent the voltage applied to the air gap at the time of flashover.
Contrariwise, when the time differential, Δt, between peaks differs from zero, this value ($U_+ + U_-$) is only

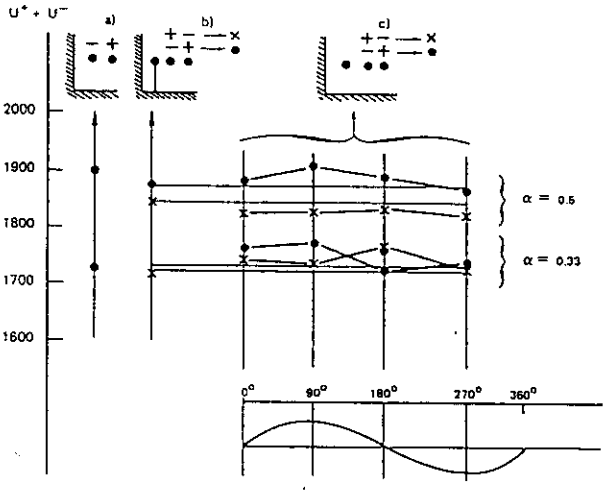

Figure 4.12 Influence of the third phase. Conductor-conductor gap (d=4 m, h=9 m) [4.5]. From left to right:
a) reference case with 2 conductors only
b) 3 conductors with the third earthed
c) 3 conductors with the third energized by a 50 Hz power frequency voltage (the two phase + and - impulses are synchronised at different times compared to the third phase sine curve).

of conventional significance. Initially, it was observed that ($U_+ + U_-$) passed through a minimum value for $\Delta t = 0$, and this value served as a reference for the determination of the general characteristics of phase-to-phase air gaps. Since then, by examining the matter in greater detail, it has been noted [4.8] that the minimum of ($u_+ + u_-$) was not obtained at $\Delta t = 0$ (u_+ and u_- are instantaneous voltages applied to the air gap at the time of flashover, see Figure 4.7). Experimentation now shows that u_+ and U_+ could be considered to be identical, since flashover always occurs in the neighbourhood of the peak of the positive component. The same does not apply to u_- and U_-, which can differ considerably when $\Delta t \neq 0$.

By way of example, Figure 4.13 gives the flashover parameters (u_- and U_+) for various characteristics of the negative component (shape and amplitude) and for various values of Δt. Compared to the reference case, the reduction in withstand voltage may be as great as 20%. Fortunately, such extreme reductions are obtained for amplitudes of negative components far greater than those encountered in service. However, reductions of 12% to 15% are not impossible, as can be derived from Figure 4.13.

d) Influence of a prestress

In actual configurations, when a switching surge occurs, the air clearance is already stressed by the AC or DC operating voltage.

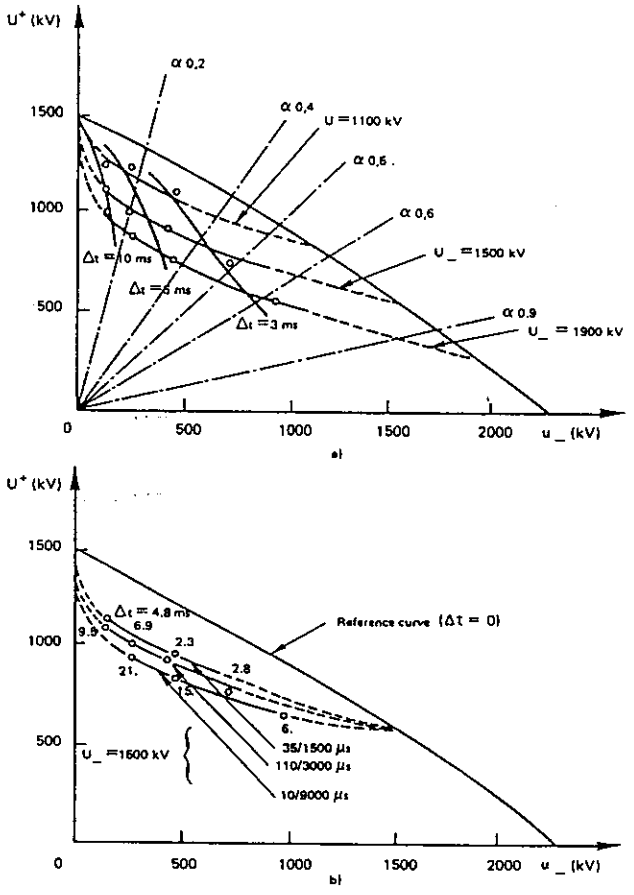

Figure 4.13 Rod-rod gap (d=4 m). Effects of phase-shifting Δt between negative and positive impulse on flashover (see Figure 4.7 for definition of parameters) [4.8].
a) for a given negative impulse shape: 110/3000 µs
b) for a given value of U_: 1500 kV

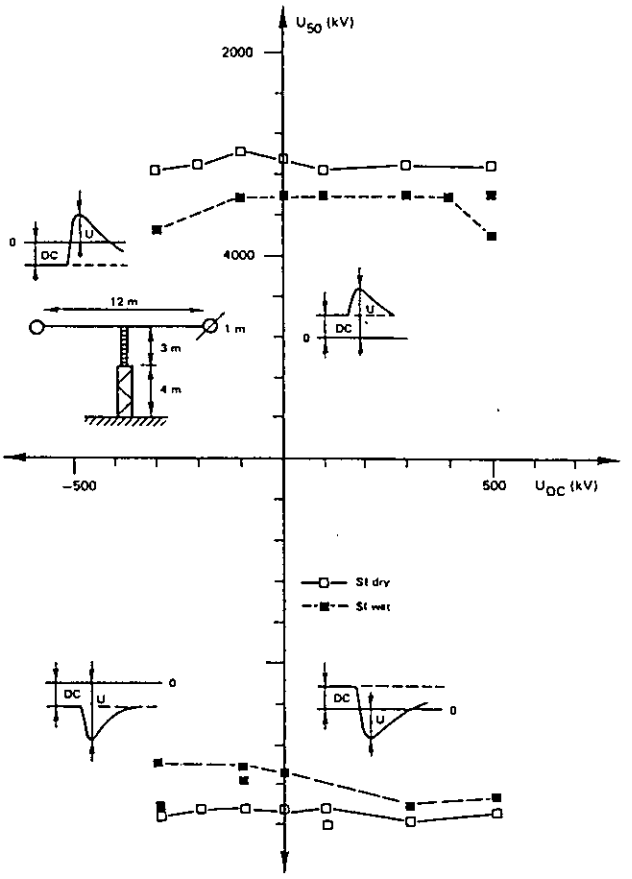

Figure 4.14 Performance of clean insulators under composite voltage stresses, DC + impulse, in both dry and wet conditions [4.10]. Test object: conductor-structure (supported bus bars). Analysis of the influence of the DC prestress for different polarity combinations.

As an example Figure 4.14 shows how the flashover voltage varies as a function of a DC prestress in case of a substation structure. It can be seen that the strength is lower under positive impulse than under negative impulse. Furthermore, the flashover voltage is practically unaffected by the D.C. prestress in dry condition [4.10].

4.2.2 Influence of geometry

a) Rod-plane gap

All the air gaps can be characterized by the minimum strength observed for the critical time to crest (minimum of the U-curve). This value will be given, in the following, as a function of the geometrical characteristics of the air gaps which are mainly the gap spacing d and the electrode shape. Among the different gaps of spacing d, the positive rod-plane gap has the lowest strength and is used as a reference.

Its characteristics will be first detailed. The influence of the radius of curvature of the positive rod (anode) can be shown in simplified form in Figure 4.15. When the anode radius is less than a certain critical value R_{cr} (which is dependent on air gap spacing) [4.11], voltage U_{50} remains constant as a first approximation.

This is the direct consequence of the streamer to leader transition. As a matter of fact, the condition

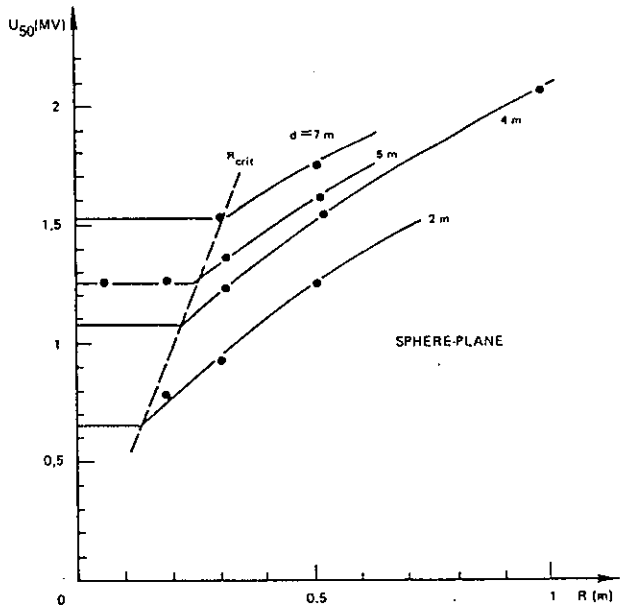

Figure 4.15 Influence of the radius R of spherical electrodes on U_{50} under positive polarity [4.11].

for this transition is a corona strong enough which requires a given voltage across the gap, independently of the anode radii, provided it is lower than the critical radius. For R > R_{crit}, we note that U_{50} increases with R. This increase is needed for the first corona to occur. It has to be noted that in this case the U curve is modified. An example is given by Figure 4.16 for a 10 m long air gap. Most of the lower part of the U curve disappears and its minimum becomes very flat.

It is important to point out that for the majority of practical problems, the anode radius is less than the critical radius. In this case, the strength depends only on the gap length and is usually expressed by the formula [4.12]:

$$U_{50\ crit} = \frac{3400}{1+\frac{8}{d}} \qquad (4.2)$$

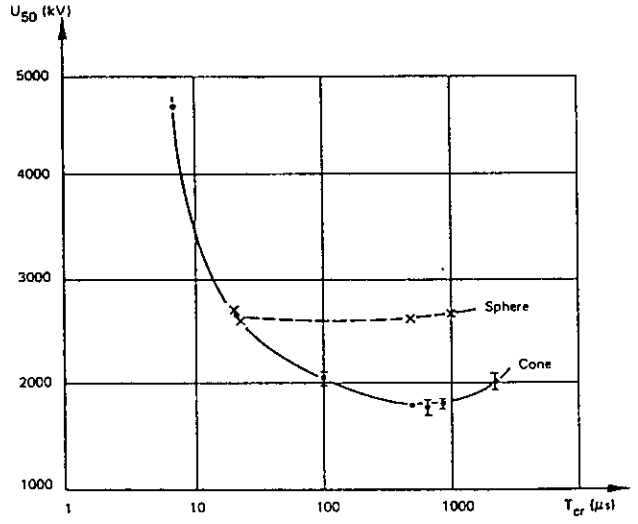

Figure 4.16 U_{50} versus T_{cr} for a 10 m air gap and two electrode geometries [4.24]:
- a cone (•) R < R_{crit}
- a sphere (x) R = 0.75 m > R_{crit}

with 2 m < d < 15 m

As the scatter (conventional deviation z) does not vary significantly an approximation is provided by:

$$z = 5\% \qquad (4.3)$$

The essential characteristic of the curve developed from equation (4.2) is its distinct saturation with increasing distance. This is one of the fundamental laws limiting the increase of the operating voltage of overhead lines. For example, to go from 1000 kV to 2000 kV, insulation distance must be tripled (from 3.5 m to 11 m). However, it has been shown [4.13] that for distances greater than 15 m, saturation is less distinct than indicated by formula (4.2). Up to d = 30 m, experimental results are relatively well represented by formula [4.15]:

$$U_{50\ crit} = 1400+55\ d \quad (kV, m) \qquad (4.4)$$

with 15 m < d < 30 m.

The UHV study committee of CRIEPI has also proposed [4.14] a formula which is not as simple as formulae 4.2 and 4.4, but has the advantage of being unique for larger range of gap spacings (up to 25 m). It also better represents the experimental results in the lower range of gap spacing. This formula is:

$$U_{50} = 1080\ \ln\ (0.46\ d + 1) \qquad (4.5)$$

and is shown on Figure 4.17.

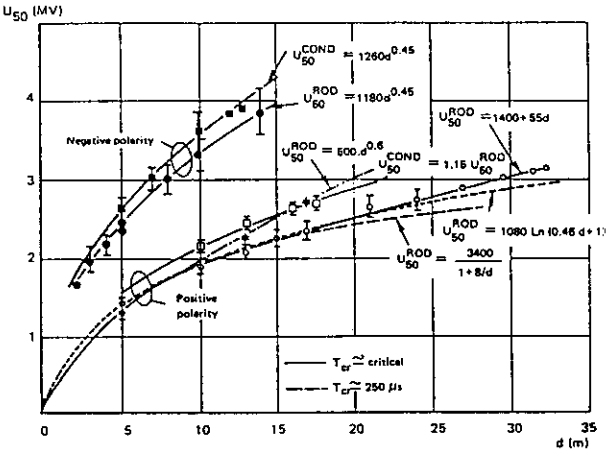

Figure 4.17 U_{50} versus d for rod-plane and conductor-plane gaps, with critical impulse shape and standard impulse shape (250/2500 μs) [4.15].

The impulse which is standardized as switching impulse by IEC Publication 60 has a 250/2500 μs shape. It is recognized, that for this specific wave shape, the Paris formula [4.16] gives a better evaluation of the dielectric strength of rod-plane air gaps:

$$U_{50} = 500\ d^{0.6} \qquad (4.6)$$

Up to 10 m, formula 4.6 does not differ very much from the equations listed in Figure 4.17, because U-curves are flat near the minimum of U_{50}.

A summary of the influence of the anode radius and of the gap length is given in Figure 4.18 for positive rod-plane gaps. Three regions can be distinguished.

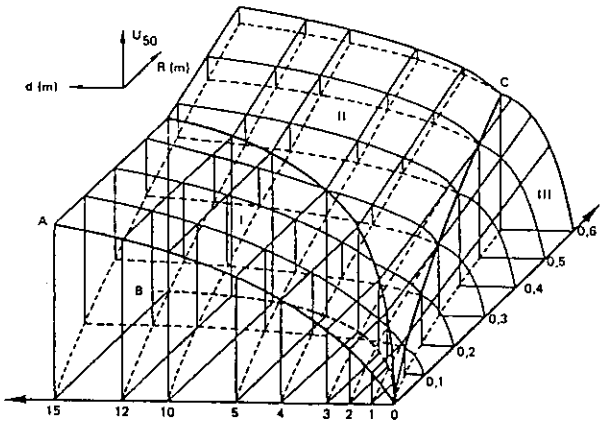

Figure 4.18 Influence of the geometrical characteristics of a positive rod-plane gap on the U_{50} breakdown voltage.
R : radius
d : gap length
U_{50} : breakdown voltage
--- corona threshold
—— breakdown voltage

Region I corresponds to conditions where the flashover voltage has the lowest value for a given gap spacing. It is delineated from region II by a curve whose projection on the d.U. plane (curve A) is equation 4.2 (or 4.5). On the d.R plane the projection of this limiting curve is curve B which gives the critical radius as a function of the gap spacing. In this region I, breakdown is the consequence of two or more successive corona and a leader development. In region II, the leader development is triggered by the first corona, while in region III the final jump is triggered by first corona. The limit between regions II and III is defined by U/d = 4.5 kV/cm.

Under negative impulses, rod plane air gaps have qualitatively the same characteristics as under positive impulses. Figure 4.17 shows that depending on air gap length a relatively more marked saturation than under positive voltage is observed. It gives a few experimental results, which can be fairly well represented between 2 m and 14 m by the formula:

$$U_{50\ crit} = 1180\ d^{0.45} \quad (kV, m) \qquad (4.7)$$

Thus, the ratio U_{50}/U_{50+} decays from 2.4 (for d = 2 m) to 1.94 (for d = 4 m) and thereafter remains constant at 1.8 for d ranging from 6 to 14 m. As already mentioned, the conventional deviation is higher than in positive polarity and reaches values of 8%.

b) Conductor-plane gap

Conductor-plane air gaps exhibit the same tendency as rod plane gaps. The general trend as a function of the gap length is the same, with breakdown voltages which are 7% to 15% higher than for the rod-plane gaps (figure 4.17).

The standard deviation and the U_{50} values are related to the length of the conductor. This is due to the fact that a conductor can be considered as a number of gaps in parallel. For a given voltage, the breakdown probabilities P_1 and P_2 of conductor-plane gaps with conductor lengths t_1 and t_2 are related by the formula $(1-P_1)^{t_2} = (1-P_2)^{t_1}$, and U_{50} and z values can be derived accordingly [4.17]. As a result, the z value is lower for conductor-plane gaps than for rod plane gaps, but the decrease of z is in fact limited down to values of about 2% due to the sag of the conductor, which cannot be avoided.

c) Actual air gaps

The rod-plane air gap, the main characteristics of which are presented in clause 4.2.2a, is a very important configuration for design because it has the lowest strength. Furthermore this is an ideal configuration for research purposes as the number of its characteristic parameters is relatively small. However, even in this case, the variety of electrical and climatic conditions to which it can be submitted is so large that the description of its properties is still incomplete. It is not surprising, therefore, that available data concerning actual air gaps is even more incomplete. They are sufficiently numerous, however, to enable us to derive a few general guidelines. For this reason, rather than presenting partial findings for specific air gaps, we shall set out these guidelines in the following.

In the case of a positive rod-plane air gap, the electrical field vector is oriented from the rod towards the plane. In the vicinity of the rod, the field is divergent. Should the rod be negative, the field is convergent close to the rod. In either case, the field is practically uniform close to the plane. Examination of the results of Figure 4.17 shows clearly that flashover occurs more readily in a divergent field than in a convergent field. Furthermore, available physical data show that in a rod-rod air gap (or in any other air gap where the field is convergent at the cathode and divergent at the anode) the development of the discharge is essentially determined by the electric field distribution in the divergent region of that gap near the anode.

Let us assume, therefore, that the distribution of the voltage inducing flashover in a positive rod-plane air gap is represented by Figure 4.19a. The voltage applied to this air gap is obtained by (for instance) the formula (4.6):

$$U_{50} = 500\ d^{0.6}$$

Let us imagine that, at this air gap, we attach a negative rod-plane air gap to which the same voltage is applied. For reasons of both electrical and geometrical symmetry, the plane will represent the equipotential V = 0 and it is possible to eliminate this hypothetical plane without changing the voltage distribution between the positive and the negative rod. We have thus defined a symmetrical positive rod-negative rod air gap of length 2 d to which the following voltage is applied (Fig. 4.19b):

$$U_{r.r.}(2\ d) = 2 \times 500\ d^{0.6} \qquad (4.8)$$

When passing from the positive rod-plane air gap of spacing d to the symmetrical rod-rod air gap of spacing 2 d, the voltage distribution in the area where the field is divergent has not been modified. Consequently, the conditions governing the development of the discharge are the same. Formula (4.8) gives the flashover voltage for the rod-plane air gap of spacing d. Likewise formula (4.9) gives the flashover voltage for a rod-rod air gap of spacing 2 d. The flashover voltage of a rod-plane air gap of length 2 d is given by:

$$U_{r.p.}(2\ d) = 500\ 2^{0.6}\ d^{0.6} \qquad (4.9)$$

Comparison of formulas (4.8) and (4.9) shows that the flashover voltage of a symmetrical rod-rod air gap is $2^{0.4} = 1.32$ times greater than that for a rod-plane air gap of the same spacing.

Naturally, the foregoing explanation is idealised. It does not take into account space charges or ionisation

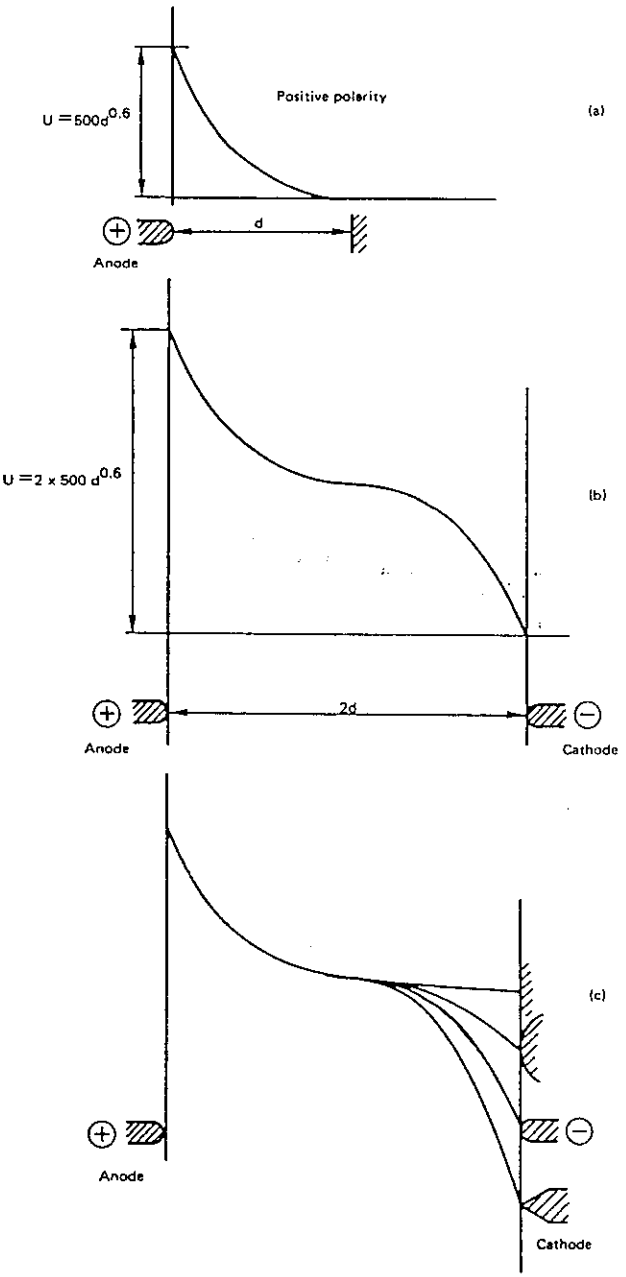

Figure 4.19 Voltage distribution
a) rod-plane gap of spacing d
b) rod-rod gap of spacing 2d without earth plane effect
c) changes in U_{50} depending upon electrode shape for the cathode only.

phenomena close to the negative rod and was developed for a very specific geometric case. Nevertheless, it does bring out clearly an entirely general rule which, incidentally, contradicts a certain number of preconceived notions (Figure 4.19c). This rule could be expressed as follows:

The more "pointed" the <u>cathode</u>, the <u>greater</u> the flashover voltage of a large air gap.

In fact, this result is quite easily understandable. In order to achieve the appropriate field distribution in the anodic region to ensure discharge propagation, a voltage drop has to be spent in the cathodic region. This voltage drop is higher for more pointed cathode (see Figure 4.19c) and plays the decisive role in the variation of U_{50} as a function of the cathode shape.

For the anodic region, where the field is divergent, the results found in the case of the positive rod-plane air gap -and illustrated by Figures 4.15 or 4.18 for the anode remain valid, i.e.

The more "pointed" the <u>anode</u>, the <u>lower</u> the flashover voltage of a large air gap.

The term "pointed" used in the above guidelines represents more abstract concepts concerning the convergence or divergence of the electric field. Its meaning is thus rather different from its usual geometrical meaning.

To quantify this fact, the concept of "equivalent radius" is frequently used. It is known that the electric field E at the surface of an isolated sphere and at an applied voltage U is written: E = U/R, R being the sphere radius. By analogy, the equivalent radius of a given electrode placed in a specified electrical and geometric environment is defined as the ratio between the potential of this electrode and its surface electric field. In the case of an isolated sphere this calculated equivalent radius is equal to the geometric radius. In the example of Figure 4.10 the equivalent radius of the energized electrode is 8.5 cm. For the earthed electrode, the equivalent radius cannot be directly defined as the applied voltage is zero. However, it can be defined by comparison with the equivalent radius of the H.V. electrode. In the preceding example we would have obtained an equivalent radius of 54.6 cm.

The concept of equivalent radius described here and illustrated in Figure 4.10 forms the basis of the gap factor approach which will be presented in clause 4.3.

d) Phase to phase configuration

When the height above ground (e.g. zero voltage surface) of the two phase electrodes is large compared to the phase to phase gap length (Figure 4.8), even if the ground influences the field distribution, the insulation still behaves as a phase to phase configur-

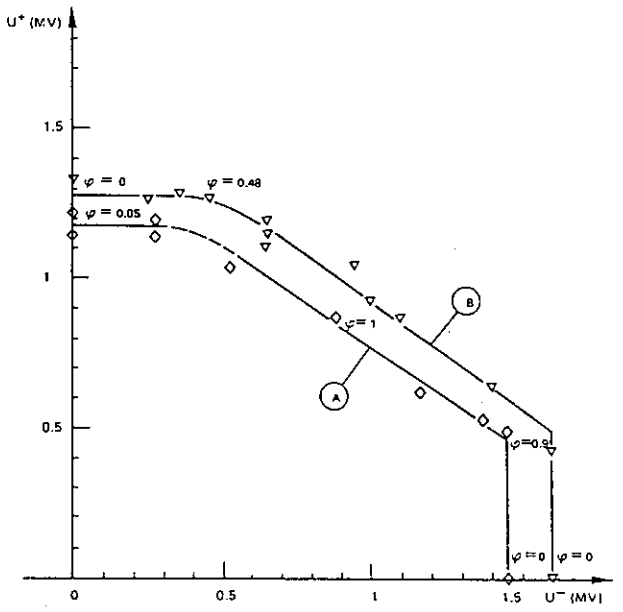

Figure 4.20 Characteristics $U^+_{50} = f(U^-)$ for actual phase-phase earth configurations [4.9].
A: ring-ring pedestals d=3 m, H=6 m, HG=2.5 m
B: disconnectors d=4 m, H=6.5 m, HG=3 m

ation for the complete range of α. In other words, any phase-to-ground insulation(s) still has such large strength that it is "protected" by the phase-to-phase insulation. The ratio of the probability P_ϕ of discharge between phases to the overall probability of discharge P_T is $\phi = P_\phi/P_T$. In the idealised case ϕ is always equal to 1.

In configurations which are closer to actual system conditions such as disconnectors or bus bars, the phase to ground strength is not as large, and the $U_- = f(U_+)$ curve is truncated at both extremities. When U_- or U_+ is small, the phase to phase stress is relatively low compared to the phase to ground stress and all discharges occur in the phase to ground gaps ($\phi = 0$). Examples are given by Figure 4.20.

e) Influence of insulators

In many cases, air gaps are modified by the presence of insulators, either insulators strings or post insulators.

By way of example, Table 4.2 compares two conductor cross-arm air gaps which are strictly identical except for the presence of a string of 19 cap-and-pin insulators in the second case.

Table 4.2 Influence of the presence of insulators on the dielectric strength of a conductor-cross arm gap (dry insulators)

Polarity	Air gap without insulators		Air gap with string of 19 insulators	
	U_{50} [kV]	z [%]	U_{50} [kV]	z [%]
positive	1160	3.1	1132	4.2
negative	1478	1.3	1449	1

The influence of cap and pin insulators in the gap is secondary: data in [4.18] indicate an influence lower than 3%. Given experimental error and the statistical uncertainty of these results plus the imprecise nature of the evaluation of the geometrical characteristics of the insulator-less air gap, the presence of dry insulators in an air gap does not modify its behaviour significantly [4.16, 4.19, 4.20]. Nevertheless a correction factor has been proposed [4.21].

In the case of insulator strings, the field distribution is evenly perturbed by the metallic caps and pins. In the case of post insulators, or of long rod suspension insulators, the field is locally perturbed by any metallic flanges present and this may impair more drastically the dielectric strength of the insulation.
It has been shown (Figure 4.21) [4.22] that the maximum strength reduction is observed when the flange is located between one quarter and one third of the gap length measured from the energized electrode. The reduction can reach 15% to 18%. In cases of a second flange the strength reduction may be larger. More extensive data are given in reference [4.22].

4.2.3 - Influence of rain

As environmental conditions modifies the characteristics of the insulating medium it is important to evaluate their impact on the dielectric strength of external insulation. Other chapters are devoted to the influence of pressure, temperature (or air density), ice and snow, humidity, and fires. In this paragraph we describe the influence of rain.

The tests which have been carried out show that the

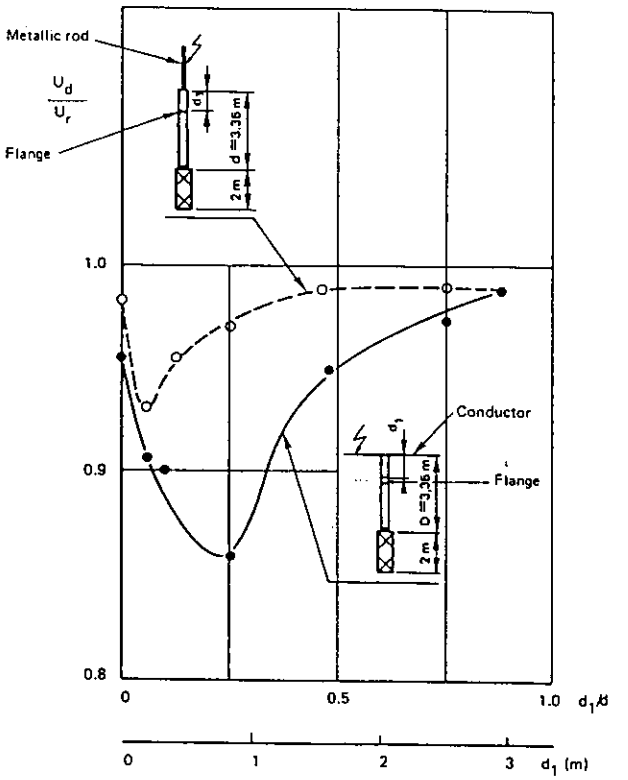

Figure 4.21 Rod-lower structure and conductor-lower structure configuration equipped with insulator model, dry conditions. Effect of the distance of the top metal flange from energized electrode on the positive SI strength U_r [4.22].

rain, as a perturbation of the insulation medium, has no significant effect on the dielectric strength of air gaps neither under positive polarity nor under negative polarity. The physics of the discharge is not modified. However, in some cases, due to streaming of water, the rain can modify the shape of the electrodes and can accordingly decrease the dielectric strength of an air gap.

In other words, if rain is observed to modify the dielectric strength of an air gap, this is due to the modification of the electrode shape rather than to a change in the insulating medium.

When insulators are present within the gap (cap and pin, long rod, string, post insulators) the existence of a physical support may make the rain cascade on the sheds. The physical mechanism of the discharge is modified. Instead of a discharge propagating through the air, the discharge closely follows the sheds and jumps from shed to shed. This type of discharge is characterized by a flashover voltage which is not very much polarity dependant and which, under positive polarity, is not very different from the air gap flashover voltage.

As a result, rain does not materially reduce the dielectric strength of some configurations (e.g. insulator strings with cap and pin insulators having a large distance between sheds). However the data are much more scattered for post insulators (Figure 4.22) and in some extreme cases, the reduction may reach 30% [4.22] particularly if the gap factor of the gap where the insulator is inserted is large. Generally speaking, the reduction is higher for larger sheds and for small shed spacings.

The dielectric strength under negative polarity is

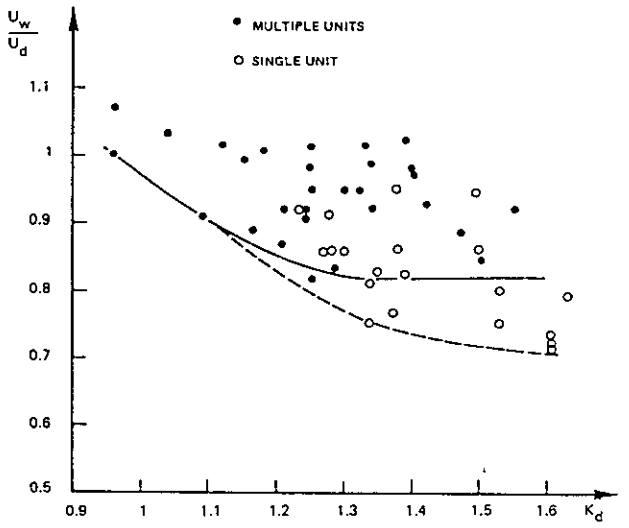

Figure 4.22 Configuration with actual insulators (single and multiple units). Ratio U_w/U_d with positive SI versus gap factor.

nearly reduced down to the strength under positive polarity.

In both cases, the standard deviation is increased, so that the question of the reproducibility of rain tests still remains.

4.3 METHODS AND CRITERIA FOR THE ASSESSMENT OF THE STRENGTH

4.3.1 Evaluation of the phase to ground switching impulse strength

The different parameters examined in clause 4.2 influence the strength of external insulation in different ways:

- some have a decisive influence, like the air clearance, the shape of the cathode, the balance between positive and negative components for phase to phase configurations,
- some have a significant influence. This is the case of the impulse shape. When the shape of the impulse varies, the strength passes through a minimum value so that reference is often made to this critical value having the time to crest $T_r=T_{rm}$. Alternatively, reference can also be made to a standard value (standard impulse having $T_r=250$ μs),
- some, have a lower influence, like pre-stressing by the operating voltage and can be forgotten in a first approximation.

The various studies undertaken in this field have led to some simplifications. The concept of "a gap factor" proposed by L. Paris in 1966 is one of the more interesting [4.23].

The gap factor, k, of any air gap is the ratio between the flashover voltage of the air gap to the positive rod-plane air gap flashover voltage, with air gaps of identical spacings and submitted to the same switching impulse. The main interest of this concept is that the gap factor is practically independent of the length of the air gap considered.

In summary, this means that under a positive switching impulse, the flashover voltage U of any air gap is obtained by:

$$U = k \frac{3400}{1 + \frac{\theta}{d}} \quad for\ T_{cr} = T_{crit}$$

$$U = k\ 500\ d^{0.6} \quad for\ T_{cr} = 250\ \mu s \qquad 4.10$$

$$z = 0.05\ U$$

k is the gap factor determined by the overall distribution of the electric field.

As an example, as shown in paragraph 4.2.2 the gap factor of an electrically symmetrical air gap is 1.32.

Values of the gap factor for some basic configurations are given in Table 4.3.

Table 4.3 Gap factor of a number of basic configurations. If k > 1.6, withstand in negative polarity is less than in positive.

Configuration		k
Rod-plane	d	1
Conductor-plane	d	1.1 to 1.15
Rod-rod	H, d, H'	$1 + 0.6 \frac{H'}{H}$
Conductor-rod	H, d, H'	$(1.1 \text{ to } 1.15) \exp\left(0.7 \frac{H'}{H}\right)$
Protrusions	H, d, H'	$k_0 \exp\left(\pm 0.7 \frac{H'}{H}\right)^*$ $k \geq 1$

*Sign + for protrusions from the negative electrode
Sign – for protrusions from at the positive electrode
k_0 : gap factor without protrusions.

For overhead lines or air-insulated substations, it is not always possible to simplify the configuration without making large errors. Table 4.4 gives the gap factor for some configurations which are more realistic. Two evaluations are given. The first one (right column) is a rough value which can be taken as an order of magnitude. The second one (central column) is a formula [4.21] which takes into account some secondary geometrical characteristics of the actual configuration, and which can be used to assess the influence of these secondary characteristics.

Furthermore, the following indications may be given about the influence of other secondary geometrical parameters.

Influence of the type of conductor The gap factor, referred to the clearance d measured from the axis of the bundle, slightly increases with the number of sub-conductors, N, according to the expression :

$$k_{bundle} = k_{single} + 0.01\ (N-2) \qquad (4.11)$$

This equation is applicable for N = 2÷8 and spacing between sub-conductors of about 40÷50 cm.

Influence of high voltage fittings The presence of high voltage fittings, as conductor yoke, shielding rings and similar, has two effects: to modify the field distribution of the HV conductor and to reduce the clearance from the HV parts to the structure. With reference to Figure 4.23, on condition that $l/d < 0.2$, the gap factors of Table 4 are still applicable, provided they are referred to the actual minimum clearance $d' < d$. If large fittings are present, the correction for the bundle should not be applied.

Influence of earth fittings The influence of a suspension rod hanging from the structure (see Figure 4.23) is negligible in V-string configurations, provided the length of the string exceeds the gap minimum clearance d. In I-string configurations, the gap factor, referred to the distance from the conductor to the structure d is slightly reduced with the increase of the length of the rod l' according to the expression:

$$k = k_{l=0} - 0.4\ \frac{l'}{d} \qquad (4.12)$$

valid as far as $l'/d < 0.2$.

Influence of the impulse shape All the above mentioned gap factors hold, as a first approximation,

Table 4.4 Gap factor for some actual configurations.

Configuration	Formula	Typical value
«conductor-cross-arm» 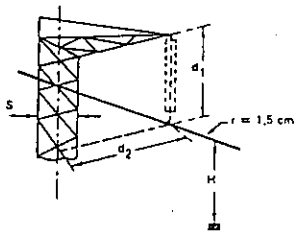	$k = 1.45 + 0.015\left(\frac{H}{d_1} - 6\right) + 0.35\,(e^{-8\,S/d_1} - 0.2) + 0.135\left(\frac{d_2}{d_1} - 1.5\right)$ Applicable in the range : $d_1 = 2 \div 10$ m $\quad d_2/d_1 = 1 \div 2$ $S/d_1 = 0.1 \div 1 \quad H/d_1 = 2 \div 10$	$k = 1.45$
«conductor-window» 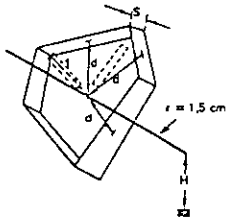	$k = 1.25 + 0.005\left(\frac{H}{d} - 6\right) + 0.25\,(e^{-8\,S/d} - 0.2)$ Applicable in the range : $d = 2 \div 10$ m $\quad S/d = 0.1 \div 1 \quad H/d = 2 \div 10$	$k = 1.25$
«conductor-lower structure» 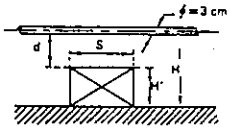	$k = 1.15 + 0.81\left(\frac{H'}{H}\right)^{1.167} + 0.02\ \frac{H'}{d} - A\left[1.209\left(\frac{H'}{H}\right)^{1.167} + 0.03\left(\frac{H'}{H}\right)\right](0.67 - e^{-2\,S/d})$ where A = 0 if $S/d < 0.2$ and A = 1 if $S/d \geq 0.2$. Applicable in the range : $d = 2 \div 10$ m $\quad S/d = 0 \div \infty \quad H'/H = 0 \div 1$	$k = 1.15$ for cond-plane to 1.5 or more
«conductor-lateral structure» 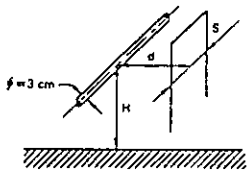	$k = 1.45 + 0.024\left(\frac{H'}{H}\right) - 6 + 0.35\,(e^{-8\,S/d} - 0.2)$ Applicable in the range : $d = 2 \div 10$ m $\quad S/d = 0.1 \div 1 \quad H/d = 2 \div 10$	$k = 1.45$
«rod-rod structure» (open switchgear) 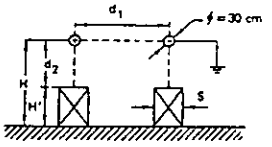	Horizontal rod-rod-structure $k_1 = 1.35 - 0.1\ \frac{H'}{H} - \left(\frac{d_1}{H} - 0.5\right)$ Rod-lower structure $k_2 = 1 + 0.6\ \frac{H'}{H} - A\ 1.093\ \frac{H'}{H}\,(0.549 - e^{-3\,S/d_2})$ where A = 0 if $S/d_2 < 0.2$ and A = 1 if $S/d_2 \geq 0.2$. Applicable in the range : $(k_1)\ d_1 = 2 \div 10$ m $\quad d_1/H = 0.1 \div 0.8 \quad d_1 < d_2$ $(k_2)\ d_2 = 2 \div 10$ m $\quad S/d_2 = 0 \div \infty \quad d_2 < d_1$	$k_1 = 1.3$ $k_2 = 1 + 0.6\ \frac{H'}{H}$

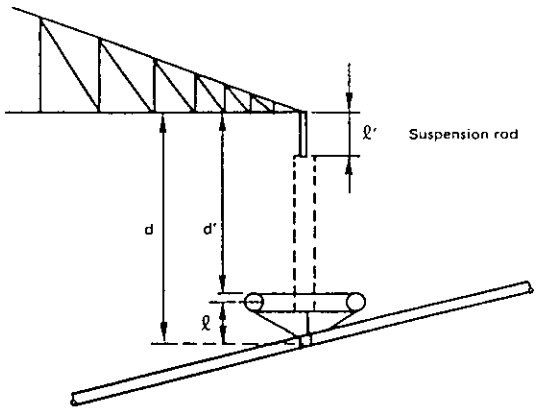

Figure 4.23 Sketch of high voltage and earth fittings.

both for critical impulse shape and for the standard one (depending on the rod plane characteristic of reference).
The dependence of the strength on the impulse shape is then strongly related to the configuration considered.
For switching impulse of positive polarity, the dependence of the critical time to crest, T_{crit}, on the above mentioned parameters is roughly given by the expression:

$$T_{crit} = [50 - 35(k-1)]\ d \qquad (4.13)$$

- T_{crit}: critical time to crest in μsec;
- d : gap spacing (m);
- k : gap factor of the configuration ($1 < k < 1.8$).

As far as the dependence of the breakdown voltage on the time to breakdown (U-curves), it is not easy to indicate equations of general application; direct reference can be made to the experimental data.

Influence of insulators in dry conditions Starting from gap factors k relevant to configurations in air (see Table 4.4), the influence of cap and pin insulators may be roughly expressed by the formula [4.21]:

$$k_i = [0.85 + 0.15\ e^{-(k-1)}]\ k \qquad (4.14)$$

where k_i = gap factor with insulators.

The influence of post insulators may be expressed with the formula [4.22]:

$$k_i = k\left[1-0.4(k-1)^{0.5}\left(1-\frac{0.1\ d_i}{h_f}\right)(n-1)^{0.5}\right] \qquad (4.15)$$

with:

d_i= length of each unit (in the range 0.8-1.7 m)
n= number of units (1 to 4)
h_f= sum of the lengths of the flanges line side and earth side (assumed equal to intermediate ones) (0.15 to 0.35 m).

The above expressions interpolate the results with an accuracy of ± 5%. The presence of the live and earth flanges was taken into account, as a first approximation, evaluating k and $U_{rod\text{-}plane}$ with reference to the distances d and d' = d - h_f respectively.

Influence of insulators in wet conditions For configurations with cap and pin insulators the influence of rain may be assessed on the base of the following equation [4.21]:

$$k_{wet} = \left[1-0.54\ e^{-\frac{1}{k_i-1}}\right] k_i \qquad (4.16)$$

For configurations with post insulators, the influence of rain is given by the following formula optimized on the basis of experimental results relevant to conductor-lower structure and rod-lower structure configurations [4.22]:

$$k_{wet} = k_i\left[1.05-0.6(k_i-1)\ \frac{\left(1-0.5\ \frac{p}{\phi}-n^{0.5}\frac{p}{\phi}\right)}{n^{0.4}}\right] \qquad (4.17)$$

with:

p= distance between sheds (0.035 to 0.13 m)
ϕ= external diameter of the insulator; average value in case of different diameters in the stack (0.15 to 0.4 m)
n= number of units (1 to 4).

The above expressions interpolate the results with an accuracy of about ± 8%.

4.3.2 Evaluation of the phase to phase Switching Impulse strength

As for phase to earth configurations, the gap factor approach can be used to evaluate the phase to phase Switching Impulse strength with critical impulse shape of ideal phase-phase configurations. According to [4.5] the following formula can be adopted for positive impulses of critical impulses shape:

$$(U^+ + u^-)_{50} = k\ \frac{3400}{1+\frac{8}{d}} \qquad (4.18)$$

k values are given in Table 4.5 for α = 0.33 and 0.5.

Table 4.5 Gap factor k for usual phase-to-phase configurations.

Flashover voltager is calculated by:
$(U^+ + u^-)_{50} = k\ 3400/(1+8/d)$.

Configuration	α=0.5	α=0.33
Ring-Ring or large smooth electrodes	1.80	1.70
Crossed conductors	1.65	1.53
Rod-Rod or conductor-conductor (along the span)	1.62	1.52
Supported busbars (fittings)	1.50	1.40
Asymetrical geometries	1.45	1.36

More detailed equations have been proposed for the phase conductor-phase conductor configuration (long span). The data may be approximated by the following equation:

$$U^+_{50} = U^+_{0\text{-}50} - \beta\ u^- \qquad (4.19)$$

where $U^+_{0\text{-}50}$ is the breakdown voltage between the conductors at $u^- = 0$ and is given by the expression:

$$U^+_{0\text{-}50} = 640\ d^{0.6}\left(1-\frac{0.25\ d}{H}\right) \quad (kV, m) \qquad (4.20)$$

and β represents the slope of the $U^+ = f(u^-)$ characteristics, and is given by the formula:

$$\beta = 0.86 - 0.54\ \frac{d}{H} \qquad (4.21)$$

The above equations are applicable in the range d =

5÷18 m, d/H = 0.2÷1 and u^-/u^+ = 0÷1.

These equations fit the experimental curves with an accuracy generally better than 3%.
The phase to phase strength may be also expressed in the form of the 50% breakdown voltage between phases, as a function of the stress parameter $\alpha = u^-/(u^-+U^+)$, as per the following equation:

$$(U^+ + u^-) = \frac{640\ d^{0.4}\left(1-0.25\ \frac{d}{H}\right)}{1-\alpha\left(0.14+0.54\ \frac{d}{H}\right)} \quad (kV,\ m) \qquad (4.22)$$

which has the same range of applicability as (4.19) through (4.21). The withstand voltage, $U_w = U_{50} - 3\ z$, z = 3%, may be obtained applying a reduction factor of about 10%.

If both phase to phase and phase to ground break downs have to be taken into consideration (as in Figure 4.20) the procedure for the determination of $U^+_{50} = f(u-)$ becomes more complex and less accurate; an example is given in [4.7].

4.4 REFERENCES

[4.1] IEC Publication 60-1. Second Edition 11-89. High voltage test techniques Part 1 : general definitions and test requirements.

[4.2] T. Harada, Y. Aihara, Y. Aoshima, "Influence of switching impulse wave shape on flashover voltages of air gaps", IEEE Transactions on Power Apparatus and Systems, Vol. PAS, n° 92, May 1973, p. 1085-1093.

[4.3] O. V. Volkova, A. R. Koriavin, "For the evaluation of the critical parameters of the impulse voltage for the insulating construction test", Int. Colloquium on high voltage testing technique. Leningrad 1988 - Report III.24C.

[4.4] J. Lalot, B. Hutzler, "Influence of non standard switching impulses on the flashover mechanisms of an air gap", IEEE Trans. on P.A.S. vol 97 n° 3 May-June 1978, pp. 848-856.

[4.5] G. Gallet, B. Hutzler, J. P. Riu, "Analysis of the switching impulse strength of phase-to-phase air gaps", IEEE Trans. on PAS, Vol. PAS 97, n° 2, march 1978, p. 485-494.

[4.6] K. H. Weck, H. Studinger, L. Thione, A. Pigini, G. N. Alexandrov, "Phase-to-phase and longitudinal insulation test technique", CIGRE Report 33-09, 1976 session.

[4.7] CIGRE Study Committee n° 33, "Phase-to-phase insulation coordination", Electra, n° 64, may 1979, p. 137-236.

[4.8] G. Baldo, A. Fisher, B. Hutzler, G. Pesavento, J. P. Riu, Z. Zacke, "Phase to phase insulation: Effect of time shift between the two components of the applied voltage", 3rd I.S.H. Milan, august 1979 : articles 51-12 et 52-18.

[4.9] CIGRE TF 33.03.03, "Switching impulse test procedure for phase to-phase air insulation", Electra. n° 30. October 1973, p. 55-69.

[4.10] R. Cortina, G. Marrone, A. Pigini, L. Thione, W. Petrusch, M. P. Verma, "Study of the dielectric strength of external insulation of HVDC systems and application to design and testing", CIGRE - 1984 Session - paper 33-12.

[4.11] G. Carrara, L. Thione, "Switching surge strength of large air gaps: a physical approach", IEEE Transactions on Power Apparatus and Systems, Vol. 95, n° 2, March/April 1976.

[4.12] G. Gallet, G. Leroy, R. Lacey, I. Kromer, "General expression for positive switching impulse strength valid up to extra long air gaps", IEEE Transactions on Power Apparatus and Systems, Vol. PAS 94, n° 6, 1975, pp. 1989-1993.

[4.13] A. Pigini, G. Rizzi, R. Brambilla, E. Garbagnati, "Switching impulse strength of very large air gaps", 3rd I.S.H. Milan 1979, article 526-15.

[4.14] I. Kishizima, K. Matsumoto, Y. Watanabe ,"New facilities for phase to phase switching impulse tests and some tests results", IEEE PAS 103 n° 6, June 1984, pp. 1211-1216.

[4.15] R. Cortina, E. Garbagnati, A. Pigini, G. Sartorio, L. Thione, "Switching impulse strength of phase to earth UHV external insulation", Research at the 1000 kV project, IEEE Trans. on P.A.S. - Vol PAS 104, n° 11 november 1985 p. 3161-3168.

[4.16] L. Paris, R. Cortina, "Switching and lightning impulse discharge characteristics of large air gaps and long insulator strings", IEEE. Trans. on PAS, Vol. 87, n° 4, April 1968, p. 947-957.

[4.17] G. N. Aleksandrov, Y. A. Gerasimov, "Generalised characteristics for the electric strength of phase to phase insulation in EHV overhead transmission lines and substations", IEE Proc. Vol 133. Pt A. N° 8. Nov. 1986, pp. 543-546.

[4.18] B. Hutzler, J. P. Riu, "Behaviour of long insulator strings in dry conditions", IEEE Transactions on Power Apparatus and Systems, Vol. PAS 98, n° 3, may-june 1979, p. 982-991.

[4.19] V. YE. Kizevetter, "Discharge characteristics of insulator strings", Elektrichestvo, n° 4, 1974, p. 38-42.

[4.20] O. V. Volkova, B. P. Koburin, L. S. Slutskii, "Electric characteristics of extra-high-voltage support insulation", Electrichestvo, n° 8, 1974, p. 26-29.

[4.21] CIGRE Task Force 33.03.03 "Evaluation of the switching impulse strength of external insulation", ELECTRA, n° 94, may 1984, pp.77-95.

[4.22] CIGRE Task Force 33.03.03, "Switching impulse performance of post insulators", ELECTRA, n° 109, December 1986, pp. 115-132.

[4.23] L. Paris, "Influence of air gaps characteristics of line to ground switching surges", IEEE trans on PAS, Vol. PAS 86, n° 8, august 1967, p. 936-947.

[4.24] G. Le Roy et al., "Les propriétés diélectriques de l'air et les très hautes tensions", Ed. EYROLLES PARIS, 1984.

[4.25] R. Cortina, P. Nicolini, A. Pigini, L. Thione, "Space occupation of EHV and UHV transmission lines as affected by the switching impulse strength of phse-to-phse insulation", CIGRE Symposium on Compact Lines, Stockholm, 23-25 June 1981.

5 DIELECTRIC STRENGTH UNDER FAST FRONT OVERVOLTAGES IN REFERENCE AMBIENT CONDITIONS

by G.BALDO, B.HUTZLER, A.PIGINI, E.GARBAGNATI

5.1 GENERAL

Fast front overvoltages are usually simulated in laboratory for type and routine testing with a standard impulse, of double exponential type, with a time to crest T_1=1.2 μs and a time to half value T_2=50 μs (Figure 5.1). Lightning strokes to lines may lead to travelling waves the shape of which might be similar to standard impulse. However, lightning overvoltages (see example in Figure 5.2) with shapes substantially deviating from the standard double exponential one, may be generated in many practical conditions. Namely back flashovers at the tower generate travelling waves with fast linearly rising fronts; sparkover of protective gaps introduce either full or partial chopping of the impulse; oscillations may occur due to reflections in substations, etc.

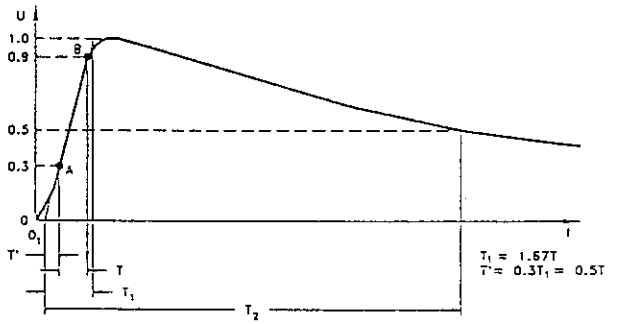

Figure 5.1 Standard Lightning impulse

For application purpose, the following information is needed for any given impulse, gap and geometry:

- the crest value of the voltage producing a discharge in 50% of the applications (U_{50}) and the conventional deviation z. Once U_{50} and z are known the voltages having different discharge probabilities may be easily evaluated.
- the volt-time characteristics which relate the maximum voltage reached before breakdown, U_s, to the time to breakdown T_s (see Figure 5.3). They

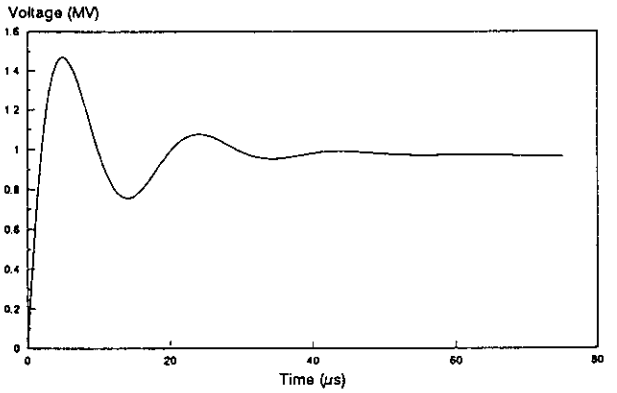

Figure 5.2 Examples of non standard lightning impulses

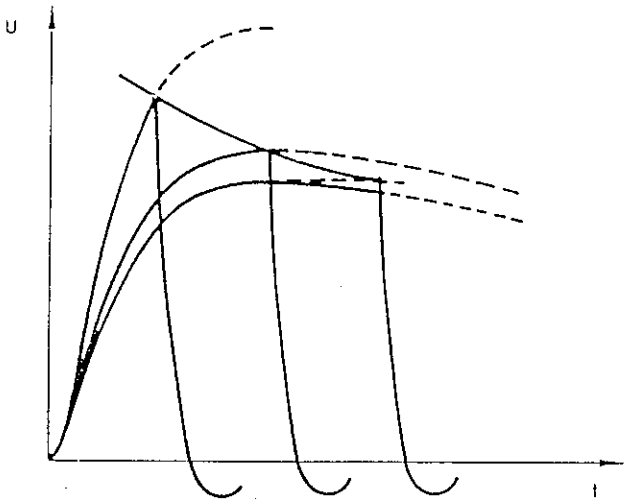

Figure 5.3 Volt-time curve for impulses of constant prospective shape

are obtained by applying voltages of various levels, with values ranging from the minimum discharge voltage to much higher values.

A large amount of work was carried out to obtain the above characteristics (see references [5.1] to [5.29]).

In the following standard lightning impulses will be mainly examined. However, indications will given on the possibility of evaluating the strength with non standard lightning impulses.

5.2 SURVEY OF EXPERIMENTAL DATA

5.2.1 Standard lightning impulses

5.2.1.1 U_{50}

Air gaps (without insulators)

Many sets of data are available in the literature ([5.1] to [5.29]). Examples of the obtained results are given in Figures 5.4 and 5.5, which report the U_{50} for rod-plane and conductor-cross arm configuration, respectively. The data refer to dry condition even if other data indicate that the influence of rain is negligible for configurations without insulator in the gap.

For rod-plane configuration the U_{50} with negative polarity is much higher than that with positive polarity. Furthermore, the U_{50} when plotted against the gap clearance is nonlinear with negative polarity while it is linear with the positive one.

For the conductor-cross arm configuration the U_{50} with positive polarity is very close to that with negative polarity. The U_{50} is higher than that with rod-plane under positive polarity.

A generalization of the influence of the gap geometry

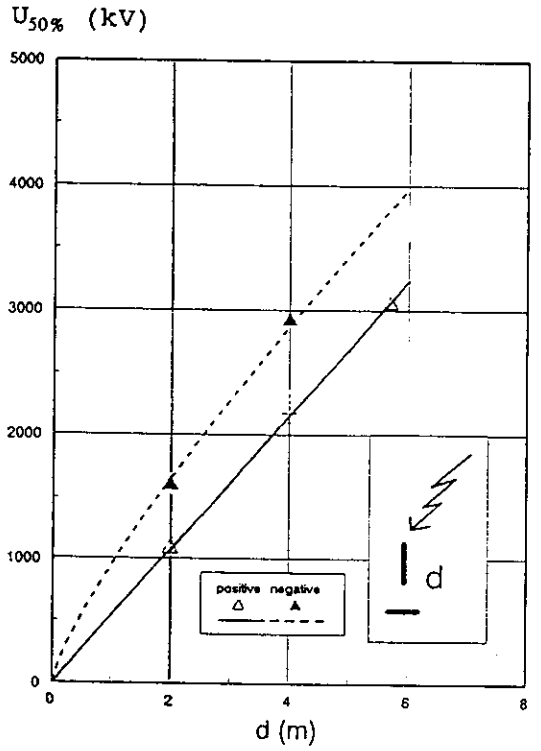

Figure 5.4 Results of LI (1.2/50 μs) tests on rod-plane configuration without insulators [5.4].

(clearance and configurations) on the U_{50} is given in Figs. 5.6 and 5.7 [5.1].

Figure 5.6, which refers to the rod-plane configuration, gives the average gradient in the gap ($E_{50}=U_{50}/d$) under positive and negative polarities, at 50% discharge probability, as a function of the gap

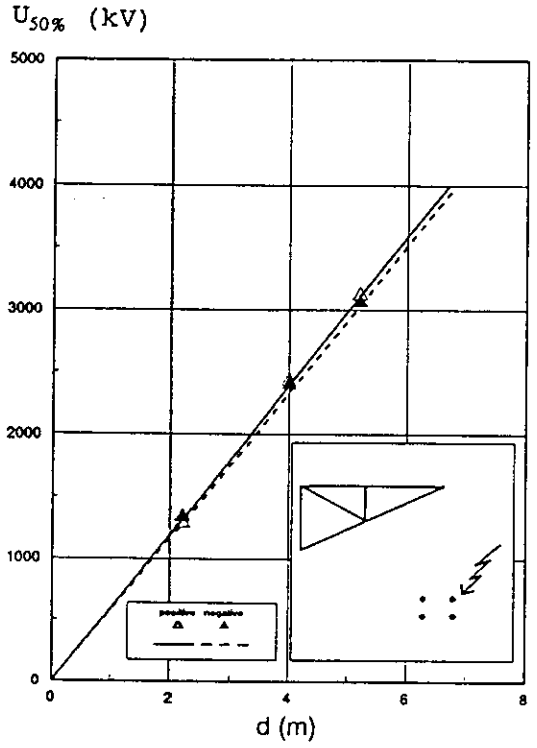

Figure 5.5 Results of LI (1.2/50 μs) tests on conductor-cross arm configuration without insulators [5.4].

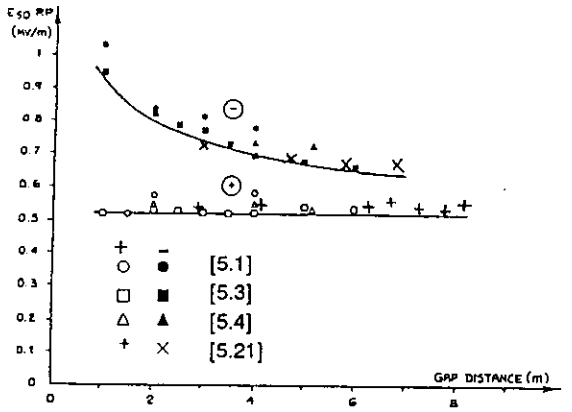

Figure 5.6 Rod-plane configuration without insulators in the gap. Average gradient at U_{50} under LI as a function of the gap clearance [5.3], [5.4], [5.21].

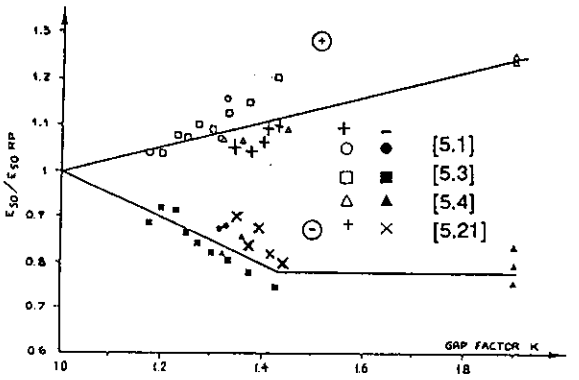

Figure 5.7 Other configurations without insulators in the gap. Average gradient in the gap at U_{50} under LI as a function of the gap factor of the configuration. Gradients given in p.u. of the values relevant to the rod-plane with the same gap length and under the same voltage polarity [5.3], [5.4], [5.21].

clearance (d). With positive polarity, E_{50} has a value of about 500 kV/m, independent of the clearance. With negative polarity, E_{50} is higher than that with positive polarity and decreases when the gap clearance increases.

Figure 5.7, which refers to various electrode configurations, gives the value of E_{50}, in p.u. of E_{50} of the rod-plane one, as a function of the "gap factor" K of the configuration with SI[5.1][1]. It is evident that E_{50} with positive polarity tends to increase as K increases, while with negative polarity an opposite trend is found. Combining the information in Figure 5.6 and 5.7, it can be found that the value of E_{50} is higher for negative than that for positive polarity voltage when K is close to 1, it becomes close for the two polarities when K values are about 1.3-1.4 (values typical for line and station configurations), finally the negative polarity becomes most critical when the highest gap factors are considered.

[1] As more deeply analyzed in the chapter dealing with switching impulses, the gap factor is defined, with reference to positive polarity impulses, as the ratio between the U_{50} of the examined configuration and that of the rod-plane having the same gap clearance under switching impulse. For a given gap distance the gap factor gives an order of merit to the configuration. It is found useful to adopt the same order of merit also with lightning impulse. The gap factor of the configurations of interest can be obtained from chapter 4.

Another way to rationalize the data was proposed in [5.28] on the basis of other sets of results. The lightning impulse strength was plotted as a function of the switching impulse strength of the same configuration with the same voltage polarity, as shown in Figure 5.8. The switching impulse strength is given in Figure 5.8 in p.u. of that with rod plane with the same clearance under positive switching impulse.

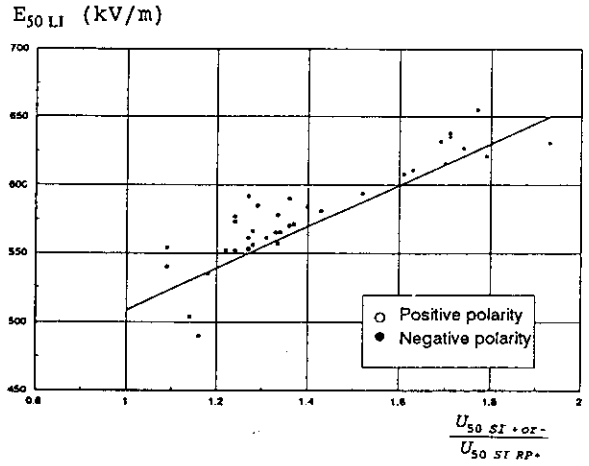

Figure 5.8 Lightning impulse strength (E_{50}) as a function of switching impulse strength (in p.u. of that with rod-plane, positive polarity) [5.29]

Air gaps with insulators

The presence of insulators between the electrodes can play an important role on the discharge process, thus also heavily affecting the U_{50}.

As an example Figure 5.9 reports the results obtained in case of rod plane configuration, inserting cap and pin insulators in the discharge gap. It can be seen that the presence of insulators strongly reduces

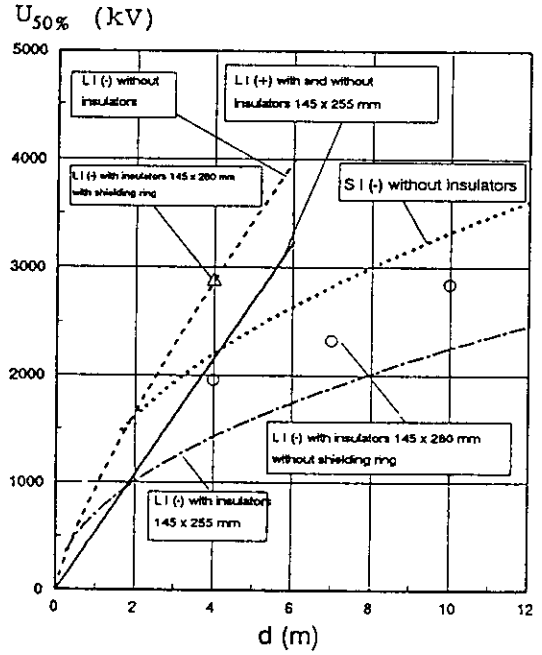

Figure 5.9 Results of LI (1.2/50 μs) tests on rod-plane configuration with cap and pin insulators in the gap [5.5]. Comparison with the strength of the pure air gap and with that in presence of insulators and a shielding ring.

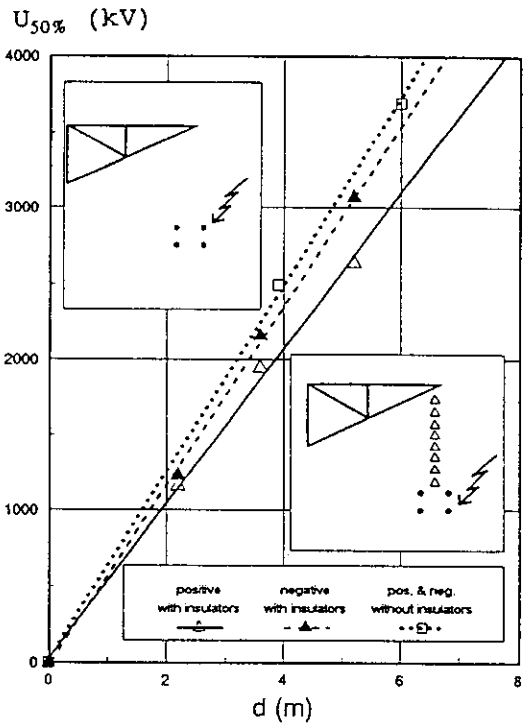

Figure 5.10 Results of LI (1.2/50 μs) tests on conductor-cross arm configuration with cap and pin insulators. Comparison with the strength of the pure air gap [5.4].

breakdown voltage in the case of negative polarity.

The influence of cap and pin insulators is reduced when the stress on the first insulator at both extremities of the string is reduced using shielding rings. It is also reduced for more practical configurations (see as an example Figure 5.10), with

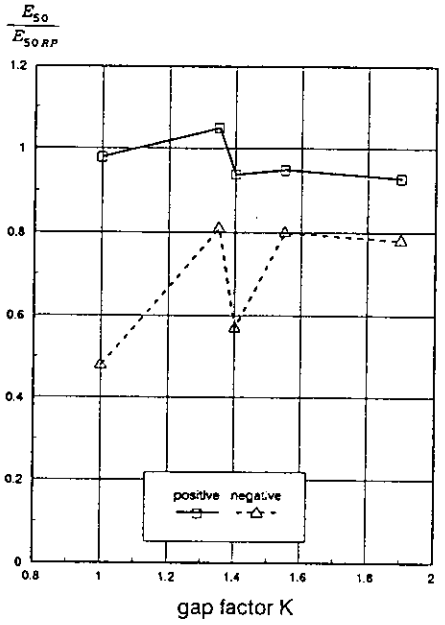

Figure 5.11 Configuration with cap and pin insulators in the gap (d = 4 m). Average gradient in the gap at U_{50} under LI as a function of the gap factor of the configuration. Gradients given in p.u. of the values relevant to the rod-plane (without insulators) with the same gap length and the same voltage polarity [5.4].

insulators at both extremities less stressed than in the case of rod-plane gap.

The E_{50} obtained with standard lightning impulse on typical configurations with and without cap and pin insulators are given in Table I [5.4], in order to get indications about the expected strength.

A generalization of the results similar to that made for configurations without insulators is not easy when cap and pin insulators are included in the gap, as shown, as an example, in Figure 5.11 where an attempt to present the data as in Figure 5.7 is made, always with reference to the basic case of the rod plane configuration without insulators.

For some configurations, as conductor upper structure, and even conductor cross-arm, the strength is to be considered close to that of air gaps, as given by Figures 5.6 and 5.7. For other more peculiar configurations, and especially when large clearances are involved, only a preliminary indication about the strength may be obtained by the results available and testing is advised to get accurate results.

It is to be mentioned that the dielectric performance depends on insulator type (capacitance between units, distance between metal parts along the insulator set). A lower influence is to be expected for insulators with few metal parts (e.g. post insulators, long rod, composite) [5.28] .

The influence of rain on the flashover voltage is, generally, secondary as in the case of air gaps.

5.2.1.2 The standard deviation

The standard deviation is of about 3% for air gaps under positive impulse. It is higher for negative impulses.

The standard deviation can also be largely affected by the presence of insulators, reaching a maximum of 5 to 9% in connection with the cases presenting the largest influence of the insulators on U_{50}. In the other cases a value close to that of air gaps is applicable.

TABLE I Comparison of the strength with and without insulators in the gap. Distance range 2÷5 m [5.4]

CONFIGURATION	GAP FACTOR	INSULATORS CAP & PIN	E_{50} POS. (kV)	NEG. (kV)
ROD-PLANE	1.00	NO	525	800-700[2]
		YES	520	520-250[3]
CONDUCTOR	1.35	NO	570	670-600[2]
STRUCTURE		YES	550	600
ROD-ROD	1.40	NO	580	650-600[2]
(lower 6m)		YES	530	550-250[3]
CONDUCTOR	1.55	NO	590	620-590[2]
CROSS-ARM		YES	530	600-570[3]
CONDUCTOR	1.90	NO	650	610-590[2]
UPPER ROD		YES	600-400[3]	580

([1]) Experimental gap factor [5.4].
([2]) Non linear trend: decreasing with the clearance, see Figure 5.4 and 5.6.
The range of the measured strength varying the gap clearance is given.
([3]) Non linear trend: remarkable reduction of the strength caused by insulators especially for large clearances. The range of the measured strength varying the gap distance is given.

5.2.1.3 Volt-time curves

Examples of volt-time curves, summarising the data in [5.2], are presented in Figures 5.12 to 5.15. The U_s (E_s) is given in p.u. of U_{50} (E_{50}). The spread of the results is partially due to the fact that they refer to gaps of different length. Furthermore the results were obtained in different laboratories using different circuits.

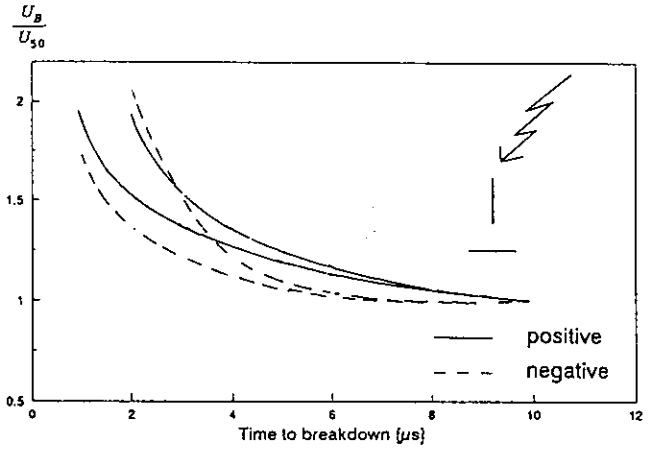

Figure 5.12 Volt-time curves for standard lightning impulses, rod-plane gap, 1 to 6 m.

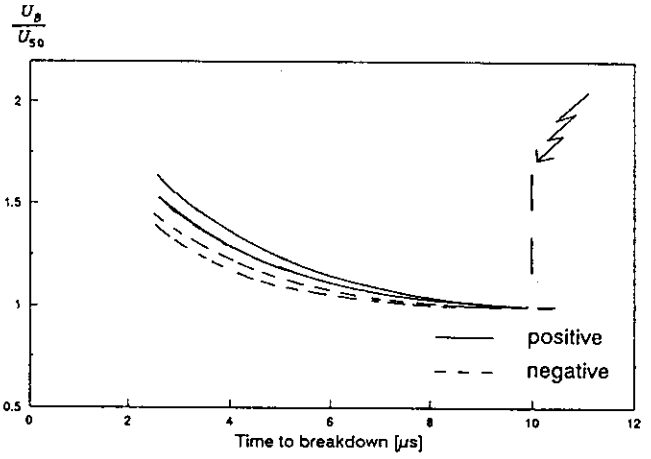

Figure 5.13 Volt-time curves for standard lightning impulses, rod-rod gap, 1 to 6 m.

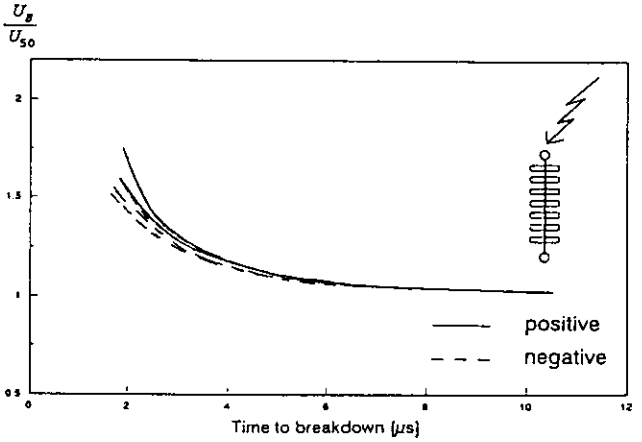

Figure 5.14 Volt-time curves for standard lightning impulses, long rod insulator string gap, 1 to 6 m.

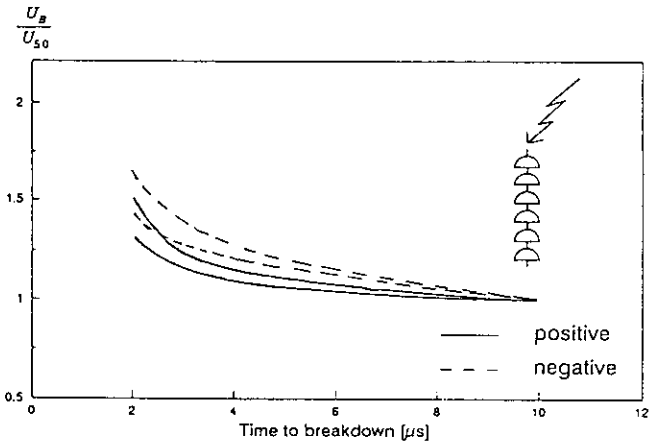

Figure 5.15 Volt-time curves for standard lightning impulses, cap and pin insulator string gap, 1 to 6 m.

It has to be mentioned that by increasing the applied voltage, the interaction between the phenomena and the generating circuit increases. Due to the large current associated with discharge development, large voltage drops can occur which changes the actual voltage applied to the gap. Attention has to be paid when comparing results at short time to breakdown.

5.2.2 Non standard impulses

The case of non standard impulses is much more complex. The variety of impulse shapes is very large

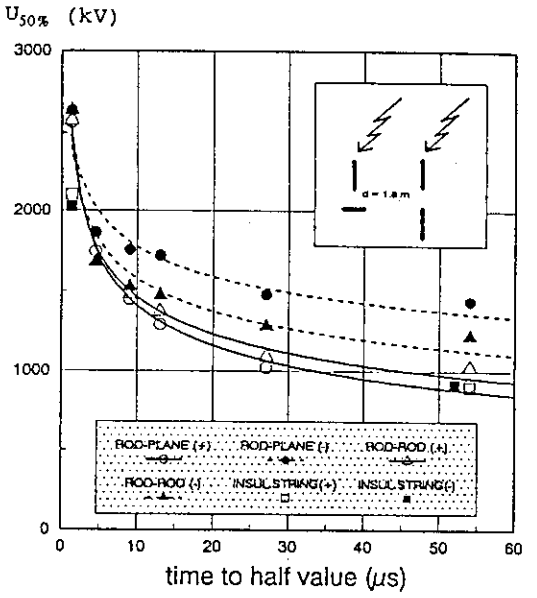

Figure 5.16 Influence of the impulse shape. 50 % breakdown voltage of various configurations as a function of the duration of the impulse tail [5.15].

and experimental results cannot cover all the possible cases. Figure 5.16 [5.15] and Figure 5.17 [5.1] give some examples of the influence of the impulse shape.

Figure 5.16 shows the influence of the tail duration of a double exponential impulse on 50% breakdown

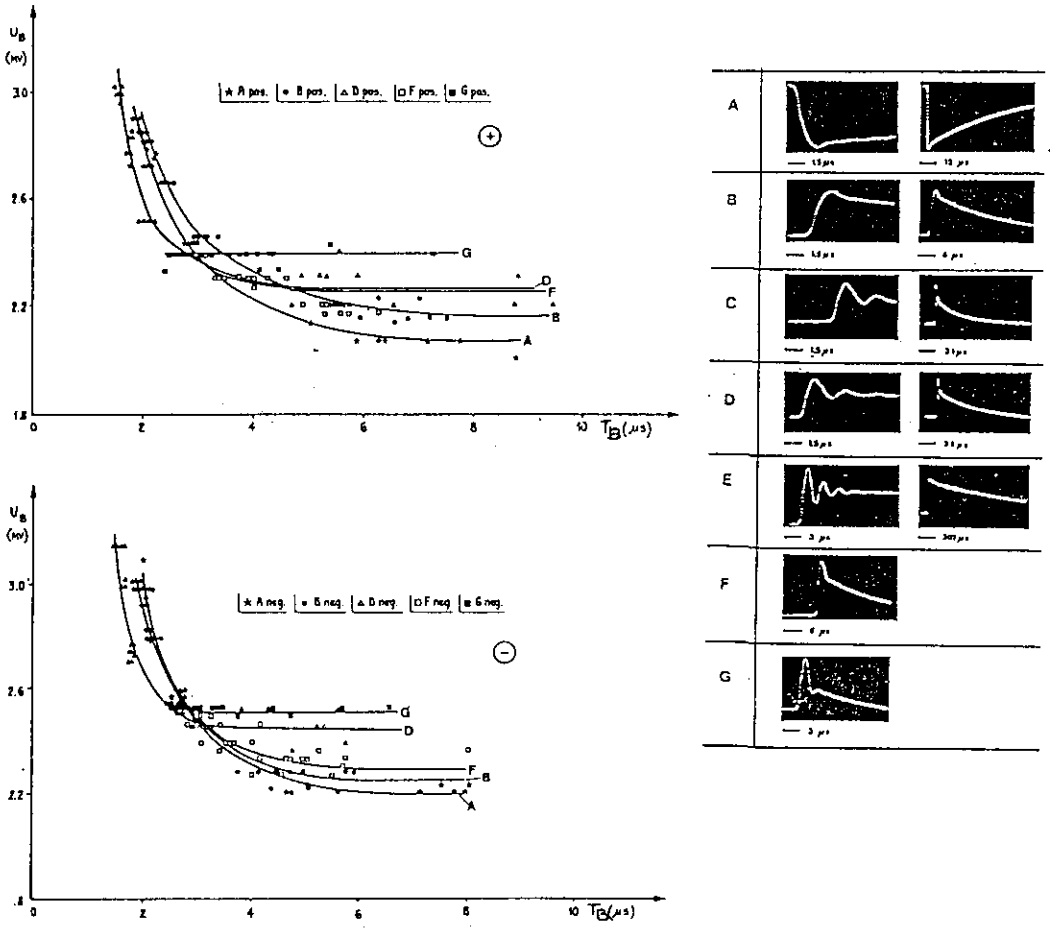

Figure 5.17 Volt-time curves for the various impulses shapes considered, conductor-cross arm configuration, d=3.6 m [5.1].

voltage of two simple configurations. The data clearly show the large influence of this parameter. The maximum influence pertains to the rod-plane gap with positive polarity, while this influence is less with negative polarity and high gap factor. Furthermore, results relevant to rod-plane with insulators in the gap are shown, confirming the insulator influence.

Figure 5.17 shows the volt-time curves of conductor-cross arm configuration for various non standard impulses. They provide, for long T_s, visual evidence of the different divergence between characteristics associated with the various impulse shapes, as well as further information on the contribution of the tail duration. Starting from impulse shape A which is close to standard, it can be seen that, by reducing the tail duration, U_s increases. The same trend is followed by oscillating impulses. The large difference between curves belonging to F and G impulses is clearly due to the different voltage remaining after chopping: in any case, when the voltage is increased so that all processes take place around the crest, differences in impulse shape tend to be less significant and all curves converge; minor differences in this case can be due to circuit interaction and to slight modifications associated with time parameters of the front.

Due to the variety of impulses and configurations, the available results cannot be generalized.

5.3 EVALUATION OF THE LI STRENGTH

In the case of standard impulses, experimental information is, in general, sufficient to estimate the dielectric strength of the configurations of practical interest.
In fact, once the configuration and gap distance are fixed,, the gap factor can be derived from chapter 4.
Entering with this data in Figure 5.6 and 5.7 the U_{50} can be derived.
Generally experimental results are also sufficient to obtain indications about the volt-time curve (see examples in Figures 5.12 to 5.15). An example of application is given in Appendix.

In the case of non standard impulses, on the contrary, experimental data cannot be generalized, as mentioned before. Therefore, suitable models have to be evolved to predict the behaviour of the insulation.

Various approaches have been proposed to evaluate the strength under the above mentioned overvoltages [5.2]. They may be obviously used to evaluate the volt-time curves under standard lightning impulse also.
The approaches may be grouped into three main categories, namely,

- **Physical approaches** [5.1], [5.6-5.15], which, in their general form, evaluate the time to breakdown, T_s, for a given applied voltage, as the sum of the times necessary for the development of the various phenomena involved in the discharge (time to corona inception T_i, time necessary for streamers propagation T_s, time necessary for leader propagation T_l, as schematically shown in Figure 5.18.
For a defined configuration (type, distance...) the calculation implies the following steps:

  * The instantaneous voltage u at the examined configuration is required for model application. In particular, in case of laboratory results, the voltage is evaluated by simulating the generating circuit through lump parameters with charging voltage as an input. The circuit simulation allows to take into account the interaction with the test object, once the current related to the discharge process is given. The model assumes that the current, i, is negligible

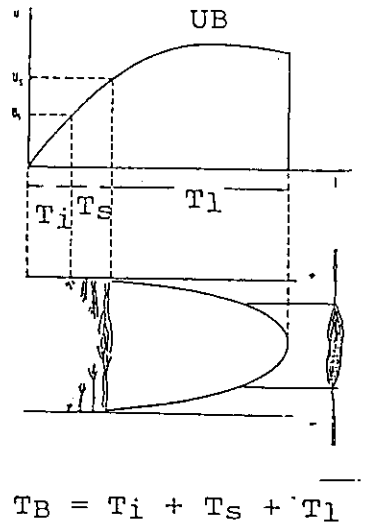

Figure 5.18 Scheme of the discharge development without insulators in the gap.

up to the leader inception while later it is linearly related to leader velocity, v, according to the equation

$$i = q\,v \qquad (5.1)$$

with q=400 μC/m, i in ampere and v in m/μs.

  * The streamer phase duration T_s is evaluated. Generally it is assumed that the streamer phase is completed when the average gradient in the gap u/d, reaches a fixed value, E_o, depending on the configuration and clearance considered. As a first approximation E_o can be assumed to be equal to E_{50} (data of Figure 5.6 and 5.7)

  * The leader phase duration T_l, is evaluated. It is assumed that leader phase starts when streamers have covered the whole gap (time T_i+T_s). The models consider an "equivalent" leader, which, for all the geometries, propagates from one electrode only, with a propagation time equal to that of the actual leaders. The duration of the leader phase is computed as the time necessary for a leader to cross a distance equal to the whole gap length. Many formulae have been proposed in the literature [5.1], in particular the following formula was recently proposed [5.1]:

$$v_l = 170\; d\; e^{\left(0.0015\,\frac{u}{d}\right)}\left(\frac{u}{x}-E_o\right) \qquad (5.2)$$

  where v_l= leader velocity (m/s);
  u = instantaneous voltage (kV)
  d = gap length (m);
  l = leader length (m);
  x = d-l (m)

- **Integration methods** (e.g. constant area criteria) [5.16],[5.17] which consider the time integral of the difference between the applied voltage and a fixed voltage (in some cases this difference is raised to a power n different from unity), as schematically shown in Figure 5.19. In particular, a coefficient n = 2.25 was proposed in [5.17]. Breakdown is assumed to take place when the integral reaches a fixed value, depending on configuration and voltage polarity.

- **Simple formulae** interpolating the various sets of data are available (e.g. those in [5.22]).

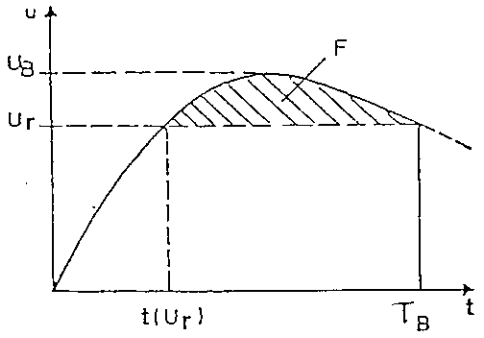

Figure 5.19 Integration method. Schematic representation of the method.

The accuracy of several approaches proposed in the literature have been checked against the experimental Volt-time curves obtained for pure air gaps. Those models based on physical approaches gave results of large generality and accuracy for pure air gaps. The models in [5.1] and [5.11] allowed to reach an accuracy generally much better than 10% for all the configurations without insulators considered, with a gap factor ranging from 1 to 1.4. Available integration methods did not give, in general, a good accuracy (errors extending up to 20-30%).

Examples of application of the approach in [5.1] to configurations without insulators are given in Figure 5.20.

The models generally showed low accuracy for cases with discharge heavily involving insulators (see the example in Figure 5.21) where the discharge assumes characteristics which are very different from those in air gaps, for which the models were set up. In this case the best evaluation accuracy was obtained by the integration methods, "calibrated" on a similar configuration.

5.4 Conclusions

Experimental data permit to evaluate the strength of the most common insulation configurations under standard lightning impulse.

The extrapolation of experimental data through modelling permits also to evaluate the strength under non standard LI with generally sufficient accuracy.

In the case of long insulators strings of cap and pin type peculiar behaviour may be encountered which still needs some understanding.

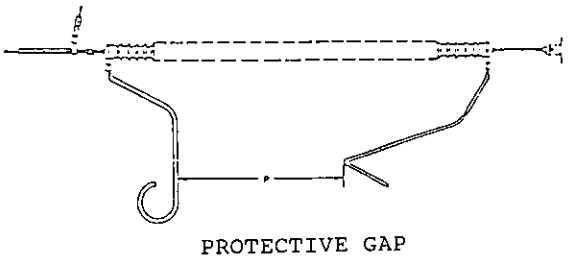

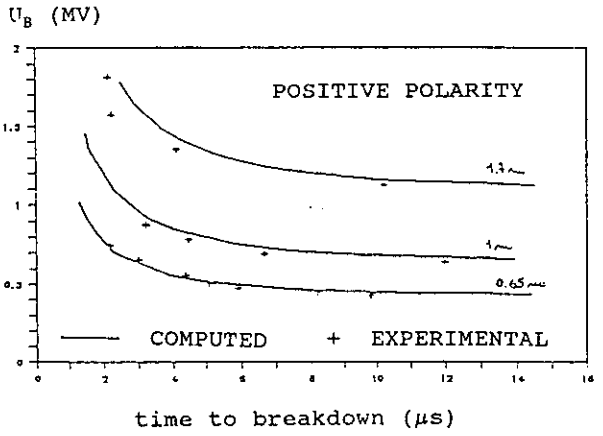

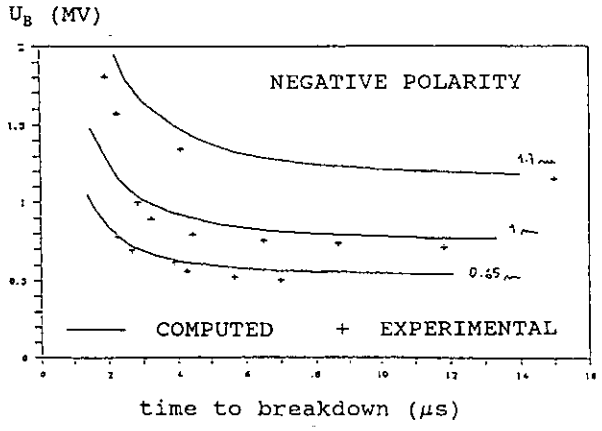

Figure 5.20 Example of application of the model in [5.1] to configurations without insulators in the gap .

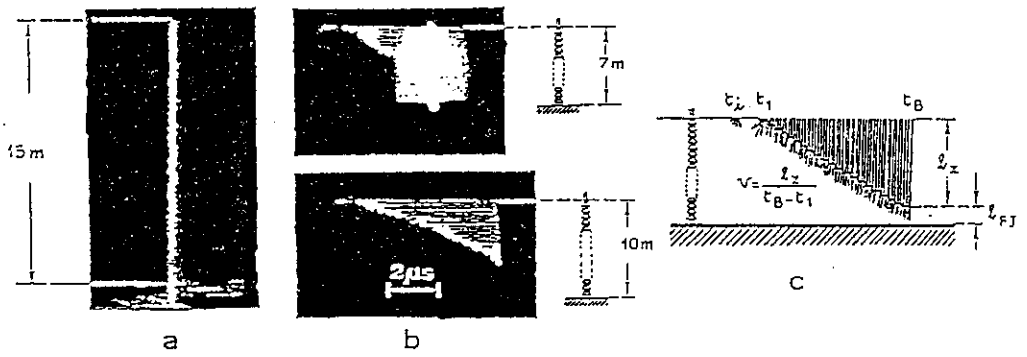

Figure 5.21 Rod-plane configuration with cap and pin insulators in the gap. LI of negative polarity.

a) Still picture of the discharge
b) Image converter picture
c) Scheme of the discharge process

5.5 REFERENCES

[5.1] A.Pigini, G.Rizzi, E.Garbagnati, A. Porrino, G.Baldo, G. Pesavento,"Performance of large air gaps under lightning overvoltages: experimental study and analysis of accuracy of predetermination methods", IEEE paper 88 SM 592-8.

[5.2] J. Eriksson, J. Huse, G. Baldo, A. Pigini and K.H. Weck,"Parameters influencing the lightning performance of electrical systems: Part IV: Non-standard lightning impulse strength", CIGRE SC 33 Colloquium-Rio de Janeiro 1981-Paper 03

[5.3] G. Carrara, "Impulse sparkover voltages of rod gaps", CIGRE General Session 1964. Annex II to the report N 328 of SC 8 by Prof.H.Baatz

[5.4] L.Paris and R. Cortina, "Switching and lightning impulse discharge characteristics of large air gaps and long insulator strings", IEEE Trans. PAS vol. 87, pp 947-957, April 1968

[5.5] R. Cortina, E. Garbagnati, F. Gallucci and A. Pigini, "Lightning impulse performance of long insulator strings" , ISH 83, Athens, paper N 44-10

[5.6] T. Suzuki and K. Miyake, "Experimental study of the breakdown voltage time characteristics of large air gaps with lightning impulses", IEEE Trans. PAS vol. 96, pp.227-233, 1977

[5.7] Les Renardieres Group, "Research on long air gap discharges at Les Renardieres", ELECTRA, N.23-1972, N.35-1975, N.53-1977, N.74-1981, N.111-1987

[5.8] G. Baldo, G. Pesavento, "Leader propagation under lightning overvoltages with different gap length", 3rd International Symposium on Gaseous Dielectrics, Knoxville, 1982

[5.9] A.A. Akopian, V.P. Larionov and A.S. Torosian "On impulse discharge voltages across high voltage insulation as related to the shape of the voltage wave ", CIGRE Paper 411, 1954

[5.10] C.F. Wagner, A.R. Hileman, "Mechanism of breakdown of laboratory gaps", AIEE Transactions on Power Apparatus and System, vol.80, pt. III, 1961

[5.11] K.H. Weck, "Dielectric strength of insulation under non standard lightning impulses", CIGRE SC 33 76 TF 33.01.02 IWD Private Communication

[5.12] G. Pesavento, "Leader development under non standard lightning impulses", ISH-Milan, 1979, Paper 51/13

[5.13] T. Harada, Y. Ayoshima and Y. Aihara, "V-t characteristics of air gaps for steep front impulses", ISH-Milan, 1979, Paper 52/06

[5.14] T. Shindo and T. Suzuki, "A new calculation method of breakdown voltage time characteristics of long air gaps", IEEE Trans. PAS vol.104, pp 1556-1563, June 1985

[5.15] B. Hutzler and J. Gibert, "Breakdown characteristics of air insulation exposed to short tailed lightning impulses", IEE Conf.Publ. N.236, pp. 158-162

[5.16] D. Kind, "Die Aufbaulache bei Stoss-spannungs-beanspruchung technischer Elektroden-anordnungen in Luft", ETZ-A, Bd-79, 1958, S.65

[5.17] K. Alstad, J. Huse, H.M. Paulsen, A. Schei, H. Wold, T. Henriksen and A. Rein, "Lightning impulse flashover criterion for overhead line insulation", ISH-Milan 1979 Paper 42.19

[5.18] Okada, Kimoto, Koga, "LI flashover characteristics of long disk insulator strings under polluted condition", IEEE Paper 71-CP 144-PWR, 1971

[5.19] Lushnikoff, Parnell, "The effects of pollution and surface discharges on the impulse strength of line insulation", IEEE PAS 90, N.4,1971

[5.20] Garbagnati, Marrone, Porrino, Perin, Pigini, "Switching impulse performance of post insulators in polluted conditions", 5th ISH, Braunschweigh 1987

[5.21] T. Udo, "Switching surge and impulse characteristics of large gap spacings and long insulator strings", IEEE Trans. on PAS April 1965

[5.22] Cortina, Garbagnati, Serravalli, Dellera, Pigini, Thione, "Some aspects of the evaluation of the lightning performance of electrical systems", CIGRE 33-13, 1980

[5.23] G. Baldo, G. Pesavento, "Floating potential bodies and their interaction with discharge development", ISH 1989, New Orleans

[5.24] B. Hutzler, J. P. Riu, "Behaviour of long insulator strings in dry conditions", IEEE Vol PAS 79 N3

[5.25] D. Rösler, "Stoßkennlinien von Freileitungen und Stützern", Hermsdorfer Techn. Mitt., 1976, H. 17.

[5.26] T. Udo, "Sparkover characteristics of large gap spaces and long insulators strings", IEEE Trans. PAS 83 (1964) 471.

[5.27] H. Biallas, P. Blasius, K. H. Weck, "Die elektrische Festigkeit von Freiluftisolationen bei Blitzüberspannungen", FGH Techn. Bericht 1-243, 1979.

[5.28] G. N. Alexandrov, YU. A. Gerasimov, P. V. Gorbunov," The electric strength of long insulators strings by lightning impulses",ISH Dresden, August 26-30, 1991.

[5.29] G. Le Roy, C. Gary, B. Hutzler, J. Lalot, C. Dubanton, "Les propriétés diélectriques de l'air et les très hautes tensions", Editions Eyrolles, 1984.

APPENDIX

EXAMPLE OF EVALUATION OF DIELECTRIC STRENGTH WITH STANDARD LIGHTNING IMPULSE

Configuration:	rod-rod without insulators, with a gap distance of 4 m and a height of the lower rod of 4 m.
Gap factor:	from chapter 4, K=1.3
U_{50}:	from Figure 5.6 $U_{50\,RP}$ positive=520 kV $U_{50\,RP}$ negative=700 kV from Figure 5.7 U_{50} positive=520 x 1.09=570 kV U_{50} negative=700 x 0.86=600 kV
Volt-time curves:	a first information can be derived from Figure 5.13. Additional information can be derived by the application of the proposed evaluation approach.

6 DIELECTRIC STRENGTH UNDER AC AND DC VOLTAGES

by A. PIGINI, L. THIONE, F. RIZK

6.1 INTRODUCTION

The analysis is made with reference to the strength of external insulation in clean conditions (dry and wet). The performance under continuous operating voltage and contaminated conditions, which is very important for the design of external insulation, is outside the scope of WG 33.07 and thus of this guide. The phenomena under contaminated conditions and transient overvoltages is examined in chapter 9.

6.2 DIELECTRIC STRENGTH UNDER AC VOLTAGE

Air gaps

Fundamental knowledge on dielectric strength of large air gaps is reported in chapters 2 and 3.
The breakdown behaviour of different types of air gaps (rod-plane, conductor-plane, conductor-structure, rod-rod, conductor-rod) under power frequency voltage, for different gap spacing, is shown in Figure 6.1.

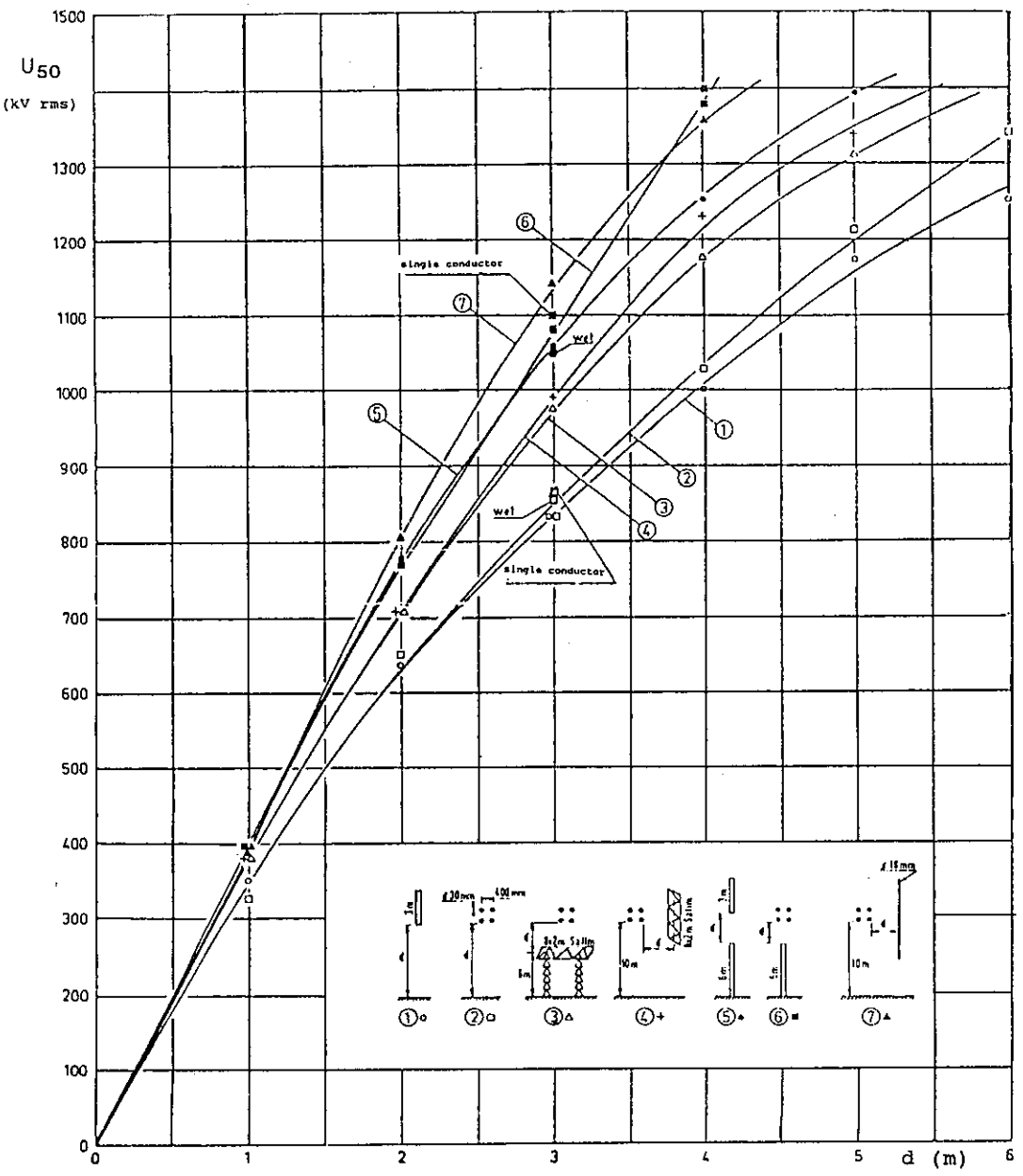

Figure 6.1 Power frequency tests. 50 % breakdown voltage for different types of air gaps.

The test results were obtained by increasing the voltage step by step and maintaining the voltage for 1 minute at each voltage step since the gap breakdown.

It can be observed that the tendencies of the curves relevant to the various air gaps considered, are quite similar.

Rod-plane has the lowest withstand voltage. Taking into account the data of Figure 6.1, its 50 % breakdown voltage can be approximated by the following equation:

$$U_{50RP} = 750 \ln (1 + 0.55\, d^{1.2}) \quad (kV\ rms,\ m) \qquad (6.1)$$

with d ≥ 2 m

The peak value of U_{50} under AC is about 20-30 % higher than the corresponding value under positive switching impulse (SI) of critical shape.

The influence of the configuration on the strength is generally lower under AC than under SI. It is quite small for gaps up to about 1 m clearance. For gaps larger than 2 m the strength can be evaluated according to the following equation (in dry conditions):

$$U_{50} = U_{50RP}(1.35\, K - 0.35\, k^2) \qquad (6.2)$$

where K is the gap factor, determined from SI tests (see chapter 4).
Values measured and calculated are presented in Annex I.

The influence of rain is negligible, specially for the configurations presenting the lowest strength.

It should be mentioned that the test results can be influenced by the test method. Information on this matter may be obtained from the tests carried out on a rod-plane air gap of 2.8 m with the following two procedures:

- AC voltage is increased in a linear way with different rise rates until the breakdown occurs (linearly rising voltage method);

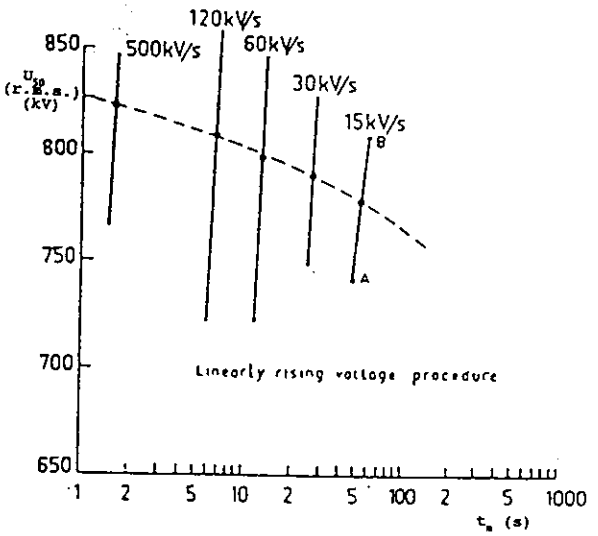

Figure 6.2 Linearly rising voltage method. Mean breakdown voltage Um, as a function of the mean time to breakdown t_a [6.2].

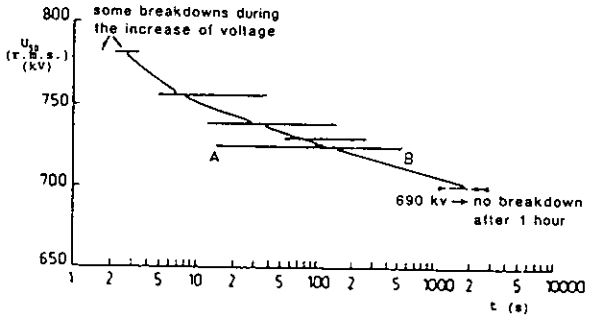

Figure 6.3 Voltage step method. Mean time to breakdown tm as a function of the step voltage [6.2].

- predetermined voltage levels are applied to the rod and maintained constant for a given time until the breakdown occurs (voltage step method).

Examples of the results obtained are given in Figure 6.2 and 6.3, indicating a decrease of the strength of about 5 % when the time to flashover is varied from 1 minute to 1 hour, with a tendency of saturation for longer times.

Influence of insulators

When insulators are present the flashover voltage can remarkably decrease with respect to the reference case (the same air gap without insulators) specially when post insulators are considered with large flanges close to the energised electrode. Reductions of the strength similar to that with SI may be expected (see chapter 4).

The influence of rain can be also important specially for post insulators with small distance between sheds.

Tests performed on single post insulator units and insulator columns (tested according to IEC 168) have given a ratio between the strength under rain and that in dry condition of 0.76 ± 0.06 and 0.87 ± 0.12 respectively. It is also interesting to compare the ratio of the strength under AC and SI, in wet condition, for the same insulators (referenced to peak values). The ratios obtained for units and columns are 0.90 ± 0.06 and 0.90 ± 0.09 respectively.

The spread in the above ratios depends partially on the insulator characteristics and partially on the poor repeatability of the rain test, specially under AC voltage.

The design of external insulation is usually not dictated by the performance under power frequency in clean condition. However test specifications still prescribe tests under AC and in rain condition at quite high voltages. These tests can be rather severe for some kind of insulators.

6.3 DIELECTRIC STRENGTH UNDER DC VOLTAGE

Air gaps

Fundamental knowledge on dielectric strength of large air gaps is reported in [6.3] to [6.6].
Examples of the results available are reported in Figure 6.4, 6.5 and 6.6.

For practical HVDC and EHVDC insulation configurations, with gap factors from 1.15 to 1.8 and clearances varying from 1 to 5 m (range investigated), the short time flashover voltage is almost proportional to the gap clearance.

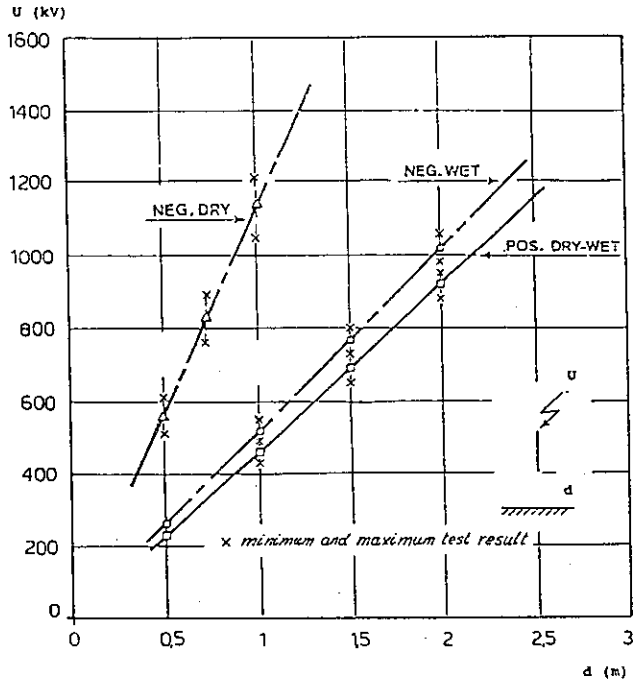

Figure 6.4 DC sparkover/ withstand voltage as a function of the gap clearance for a rod-plane configuration.

For both positive and negative polarities and in both dry and wet conditions, the mean flashover gradient, E_{50}, is close to a value of 500 kV/m, which is typical for the positive streamer discharge.
Much higher flashover gradients are observed only with negative polarity, in dry condition, on configurations of rod-plane type.

Taking into account the possible influence of the duration of the voltage application, values of about 400 kV/m may be retained as conservative figures for design of air clearances.

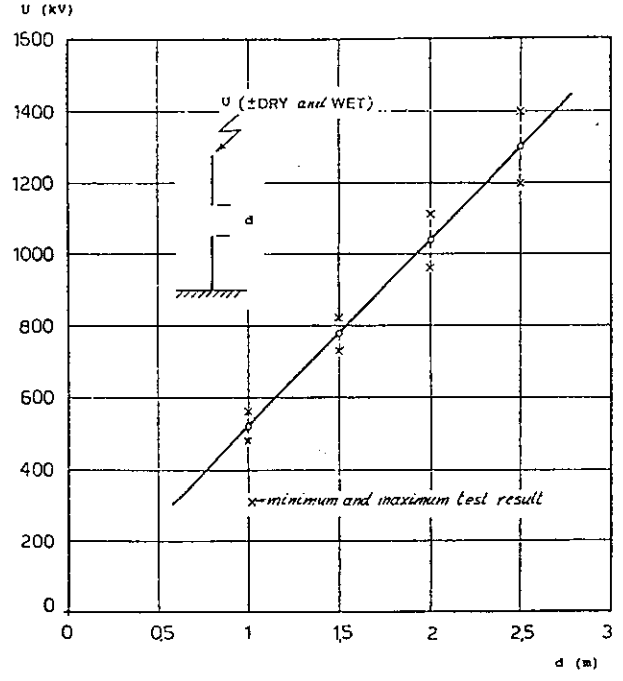

Figure 6.5 DC sparkover/ withstand voltage as a function of the gap clearance for a rod-rod configuration.

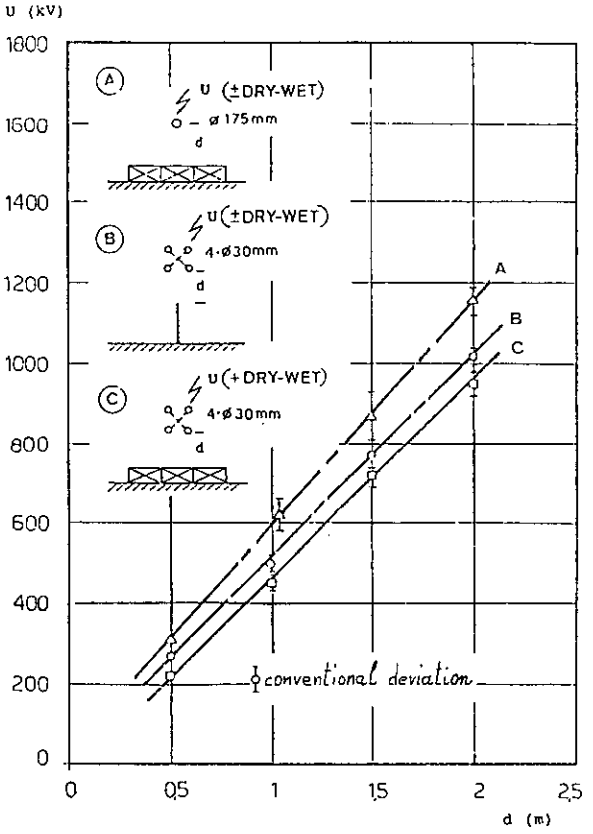

Figure 6.6 DC sparkover/ withstand voltage as a function of the gap clearance for a conductor-structure configuration.

Influence of insulators

The flashover voltage, in dry conditions, is only slightly lower than that of air gaps, for both positive and negative polarities; the minimum observed flashover gradient is about 400 kV/m [6.4].

On the contrary, the strength can be considerably reduced below that of the rod-plain air gap, under rain (wet) conditions.

Under rain the flashover voltage is generally lower with negative polarity than with positive, and is largely affected by a number of parameters, such as the insulator characteristics, the resistivity of the water, the uniformity of wetting, etc.

The short time flashover gradients, measured on wet insulators, for both line and station types, with lengths varying from 1 to 5 m, are ranging from 300 to 500 kV/m with positive polarity and 170 to 400 kV/m with negative polarity.

Recently, lower values of about 70-100 kV/m were obtained for large bushings for DC application under strongly non uniform wetting conditions, which is dealt in the following.

Behaviour of bushings

Background

The problem of the performance of bushings under non uniform wetting could dominate the design, ([6.7] to [6.13]).

Analysis of service records of major HVDC stations with voltages in the range ± 125 ÷ 500 kV revealed

that in 80 recorded flashovers, about 65 % related to wall bushings [6.7]. A study of the performance of HVDC wall bushings at Itaipu reported that the pollution severities in the range 3 ÷ 5 $\mu g/cm^2$ are too low to account for a conventional pollution flashover mechanism [6.10]. In a laboratory investigation of HVDC horizontally mounted insulators, nonuniform rain tests were carried out and the mean sparkover gradients obtained were as low as 60 ÷ 70 kV/m [6.13].

Bushing flashover mechanism under nonuniform wetting

Recently, the flashover mechanism on horizontally mounted wall bushing under nonuniform rain was investigated [6.11], [6.12].

Ref. [6.11] presents a simple model in which the bushing is characterized by a wet and a dry zone each having a constant surface resistance per unit length. The voltage distribution was determined by the relative length of the wet and dry parts. The model of ref. [6.11] gives a criterion for the sparkover of the dry zone, which constitutes a necessary but insufficient condition for the flashover of the complete bushing.
A more rigorous model of bushing flashover mechanism is given in ref. [6.12].
The basic elements and conclusions of the model are given below:

- Non-uniform voltage distribution along the bushing as well as within the dry zone itself constitute prerequisites for initiation of the flashover process.
- Stray capacitance to ground and between the wet surface and the high voltage conductor play a major role in streamer-to-arc transition across any bridged intershed gap.
- A fast collapse of the voltage across a bridged intershed gap is essential for exerting critical stress on the adjacent gap and allowing further propagation of the discharge leading eventually to complete flashover.
- The model confirms laboratory experience establishing that critical relative length of the dry zone results in minimum withstand stress.
- The model provides minimum withstand stresses of HVDC wall bushings under nonuniform rain which are in good agreement with experiment.
- The critical dry zone length is sensitive to the distribution of surface resistance within that zone and the model predictions are in the same range as experimental findings.
- The minimum withstand stress of an HVDC wall bushing on the positive pole is at least 10% higher than on the negative, confirming superior field performance of the positive pole.
- The minimum withstand stress of an empty shell can be as much as 50% higher than that of a complete bushing. Shells should therefore not be used as substitute during nonuniform rain tests.
- The minimum withstand stress of an HVDC wall bushing under nonuniform rain first drops gradually but then practically stabilizes with the increase of the wet layer conductance per unit leakage length.
- Increasing the specific leakage path keeping the same insulator length of the wall bushing does not constitute a viable alternative to improve performance under nonuniform rain.
- Under the same nonuniform wetting conditions, a lower voltage DC bushing performs better than a higher voltage bushing.

Preventive measures and ongoing research

Following are the preventive measures that are being applied and considered to alleviate the problems of the bushing performance:

* application of silicon grease;

* application of RTV coating;

* installation of booster sheds.

Research is being conducted to provide better understanding of the effects of such measures and hopefully to provide more elegant and more permanent solutions.

6.4 CONCLUSIONS

- For pure air gaps under AC the peak value of the breakdown voltage is higher than the corresponding breakdown voltage under positive SI of critical shape.
  The influence of the configuration on the AC strength is lower than in the case of SI.
  When insulator are presents then flashover voltage can remarkable decrease with respect to the case of a gap without insulators.

- For pure air gaps under DC the mean flashover gradient is about 400 kV/m.
  Insulators in dry condition have a little influence on the gap. Contrary, the strength can be noticely reduced when insulators are present in wet condition.
  Bushings may be particularly critical under DC voltage and in rain condition.

6.5 REFERENCES

[6.1] G. Baldo, R. Cortina, L. Thione "The dielectric strength of large air gaps in the light of the physics of discharge" Report 2.17, WELC, Moscow 1976

[6.2] Lalot, Gallet "Breakdown phenomena at power frequency" 3rd ISH, Milan 1979

[6.3] BPA "Transmission reference book HVDC to 600 ± EPRI 1976

[6.4] R. Cortina, G. Marrone, A. Pigini, L. Thione, W. Petrush, M. P. Verma "Study of the dielectric strength of external insulation of HVDC systems and application to design and testing" CIGRE paper 33-12, 1984

[6.5] W. Lampe and al. " Long term tests of HVDC insulators under natural pollution conditions at the big Eddy test center" IEEE paper 88 WM 081-2

[6.6] K. Naito, R. Matsuoka, S. Ito, S. Morikawa "An investigation of the horizontally mounted insulators for HVDC stations" IEEE Trans. on Power Delivery, vol. 4,no. 1, January 1989

[6.7] W. Lampe, K. A. Eriksson, C.A.O. Peixoto "Operating experience of HVDC stations with regard to natural pollution" CIGRE paper 33-01,1984

[6.8] S. S. Low "Operating and test experience with 500 kV DC wall bushings" CIGRE Inter-

national Colloquium on HVDC Power Transmission, 13-15 August 1989, Recife, Brazil, paper no. VII-02

[6.9] R. L. Crusius, A. I. Nigri "600 kV system external insulation performance - Four Years in Operation" CIGRE International Colloquium on HVDC Power Transmission, 13-15 August 1989, Recife, Brazil, paper no. VII-01

[6.10] W. Lampe "Pollution and rain on HVDC wall bushings" IEEE second international conference on properties and applications of dielectrics materials, September 1988

[6.11] H. M. Schneider, A. E. Lux "Mechanism of HVDC wall bushing flashover in non uniform rain" IEEE Trans. paper no. 90 WM 166-9 PWRD

[6.12] F. A. M. Rizk, S. I. Kamel "Modelling of HVDC wall bushing flashover in non uniform rain" IEEE 91 WM 124-8 PWRD

[6.13] P.J. Lambeth, "HVDC wall bushing performance in wet weather", IEEE Trans. paper No. 90 WM 167-7, Winter Meeting, Atlanta, Georgia, February 4-8, 1990

ANNEX I

Values of U_{50} (r.m.s.) measured and calculated for various configurations with the following formulae:

$$U_{50RP} = 750 \ln(1 + 0.55\, d^{1.2}) \quad (kV\ r.m.s.,\ m)$$

with d ≥ 2 m

$$U_{50} = U_{50RP}(1.35\, K - 0.35\, k^2)$$

d [m]	ROD-PLANE K = 1.00 mesured U50(rms) [kV]	ROD-PLANE K = 1.00 calculated U50(rms) [kV]	ROD-PLANE K = 1.00 difference %	CONDUCTOR-PLANE K = 1.05 mesured U50(rms) [kV]	CONDUCTOR-PLANE K = 1.05 calculated U50(rms) [kV]	CONDUCTOR-PLANE K = 1.05 difference %
1.00	350.00	328.69	-6.09	325.00	339.09	4.33
2.00	635.00	612.71	-3.51	650.00	632.08	-2.76
3.00	835.00	837.70	0.32	830.00	864.19	4.12
4.00	1000.00	1021.29	2.13	1030.00	1053.59	2.29
5.00	1170.00	1175.56	0.48	1210.00	1212.74	0.23
6.00	1250.00	1308.26	4.66	1345.00	1349.64	0.34
Mean value:			-0.33			1.43
Standard deviation:			3.54			2.47

d [m]	CONDUCTOR-STRUCT.(UNDER) K = 1.30 mesured U50(rms) [kV]	CONDUCTOR-STRUCT.(UNDER) K = 1.30 calculated U50(rms) [kV]	CONDUCTOR-STRUCT.(UNDER) K = 1.30 difference %	ROD-ROD K = 1.40 mesured U50(rms) [kV]	ROD-ROD K = 1.40 calculated U50(rms) [kV]	ROD-ROD K = 1.40 difference %
1.00	380.00	382.43	0.64	395.00	395.74	0.19
2.00	705.00	712.88	1.12	775.00	737.70	-4.81
3.00	975.00	974.66	-0.03	1060.00	1008.59	-4.85
4.00	1175.00	1188.27	1.13	1250.00	1229.64	-1.63
5.00	1310.00	1367.77	4.41	1395.00	1415.38	1.46
6.00						
Mean value:			1.45			-1.93
Standard deviation:			1.54			2.57

d [m]	CONDUCTOR-ROD K = 1.65 mesured U50(rms) [kV]	CONDUCTOR-ROD K = 1.65 calculated U50(rms) [kV]	CONDUCTOR-ROD K = 1.65 difference %	CONDUCTOR-ROPE K = 1.50 mesured U50(rms) [kV]	CONDUCTOR-ROPE K = 1.50 calculated U50(rms) [kV]	CONDUCTOR-ROPE K = 1.50 difference %
1.00	390.00	418.96	7.43	390.00	406.76	4.30
2.00	760.00	780.97	2.76	805.00	758.22	-5.81
3.00	1080.00	1067.75	-1.13	1140.00	1036.65	-9.07
4.00	1380.00	1301.77	-5.67	1360.00	1263.85	-7.07
5.00						
6.00						
Mean value:			0.85			-4.41
Standard deviation:			4.83			5.16

7 INFLUENCE OF AIR DENSITY ON THE DIELECTRIC STRENGTH OF EXTERNAL INSULATION

by M. MORENO, A. PIGINI, F. RIZK

7.1 INTRODUCTION

The experimental data on the dielectric strength considered in the previous chapters refer to standard conditions, i.e.:

- temperature t_o = 20 °C
- pressure b_o = 101.3 kPa
- absolute humidity h_o = 11 g/m³

The influence of air humidity is dealt with separately in chapter 8.

The influence of air temperature (t) and pressure (b) on the dielectric strength can be taken into account simultaneously, at least as a first approximation, considering their effect on the air density (δ) and the influence of this last on the breakdown voltage.

The dependence of relative air density (δ) on temperature and pressure is given by the following equation [7.1]:

$$\delta = \left(\frac{b}{b_o}\right)\left(\frac{273+t_o}{273+t}\right) \qquad (7.1)$$

with temperature t and t_o and atmospheric pressure b and b_o expressed in homogeneous units.

Air density and air humidity may vary significantly in the same location, as shown as an example in Figure 7.1.

Larger variation in air density are encountered when locations at different altitudes are considered.

The dependence of air density on altitude (A) can be approximated by equation 7.2 (based on data of [7.7]):

$$\delta = e^{-\alpha A}\left(\frac{273+t_o}{273+t}\right) \quad (m,\ ^\circ C) \qquad (7.2)$$

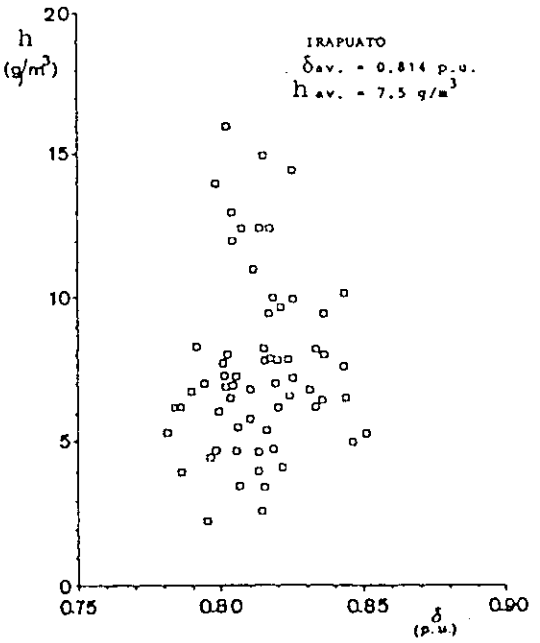

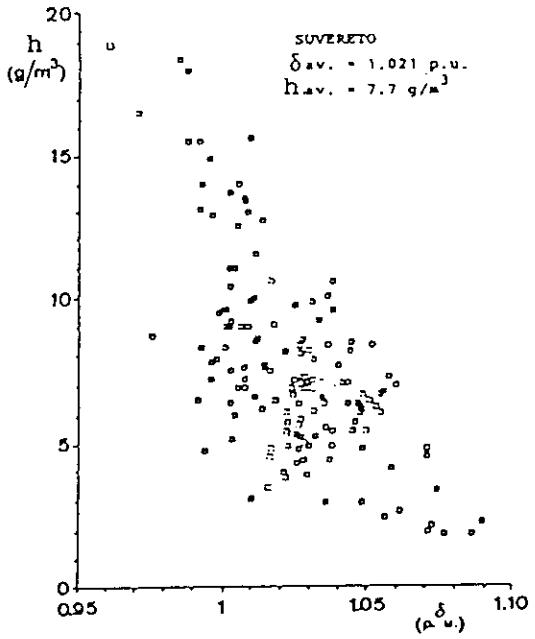

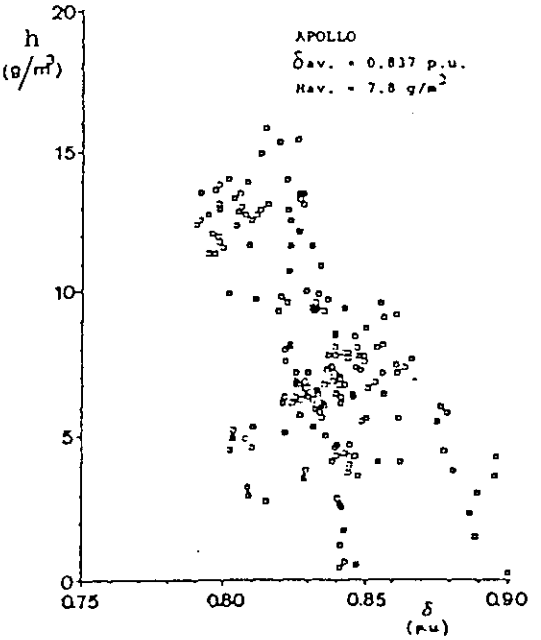

Figure 7.1: Atmospheric conditions during the tests in [7.2]. Absolute humidity versus relative air density.

with $\alpha = 121\ 10^{-4}$

In general the breakdown voltage is related to air density according to the following equation:

$$U = U_o\ \delta^m \qquad (7.3)$$

with m exponent which may vary with geometry and impulse characteristics.

In the following, after a brief analysis of the influence of air density on the breakdown process, correction procedures are described.

7.2 INFLUENCE OF AIR DENSITY ON THE BREAKDOWN PROCESS

As shown in chapter 3, the fundamental phases of the discharge in the breakdown process are: streamer formation and propagation, leader formation and growth and the final jump.

With reference to the final jump phase, the breakdown voltage U_o may be expressed by the equation:

$$U_o = E_l\ l_l + E_s\ l_s \qquad (7.4)$$

with:

E_l , E_s average gradient along the leader and streamer zone respectively.
l_l , l_s leader length and streamer length respectively.

Depending on the type of configuration, geometry and voltage characteristics, the part of the gap covered by leader and streamers may vary; furthermore positive and negative steamers may be present.

Experimental evidence indicates that for non uniform gaps [7.2], [7.3], [7.4]:

- the gradient necessary for positive streamer propagation is proportional to air density.
- the larger the part of the gap covered by positive streamers the larger is the influence of air density.
- density causes not only a variation of the gradient necessary for the propagation of streamers and leaders, but also a variation of their relative length (Figure 7.2).

A parameter g, which facilitates a rough estimate of the similarity of the analyzed discharge process with a pure positive streamer type discharge is that expressing the ratio of the average breakdown gradient to the average positive streamer gradient at the relevant atmospheric conditions:

$$g = \frac{U_{50}}{500\ \delta\ k_2\ d} \quad (kV,\ m) \qquad (7.5)$$

where:

U_{50} is the 50% breakdown voltage
d is the gap length
500 kV/m is the average streamer gradient at standard atmospheric conditions
k_2 is the humidity correction factor (see chapter 8). k_2=1 for standard humidity conditions.

For g close to 1 (e.g. positive lightning impulse applied to a rod plane)the discharge process is dominated by positive streamers and the dielectric strength is proportional to air density.

For g values lower than 1 (e.g. positive switching impulse applied to a rod plane) the discharge process is dominated by streamer and leaders and the dielectric strength is less influenced by air density.

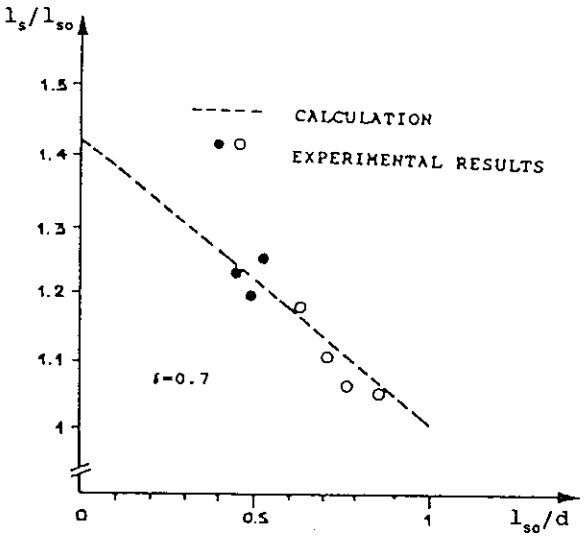

Figure 7.2: Rod plane configuration, positive switching impulse. Streamer length l_s at δ = 0.7, in p.u. of the value $l_{s\infty}$ at standard conditions, as a function of the ratio $l_{s\infty}/d$ [7.3] ($l_{s\infty}$: streamer length at standard atmosphere conditions, d: gap length).

For g values larger than 1 and lower than 2 (e.g. negative lightning impulse applied to a rod plane) the discharge process is dominated by positive and negative streamers and the situation is very complicated, generally indicating an air density influence lower than in the case of g=1.

For g values larger than 2 (e.g. uniform gaps) the discharge process is dominated by first corona and

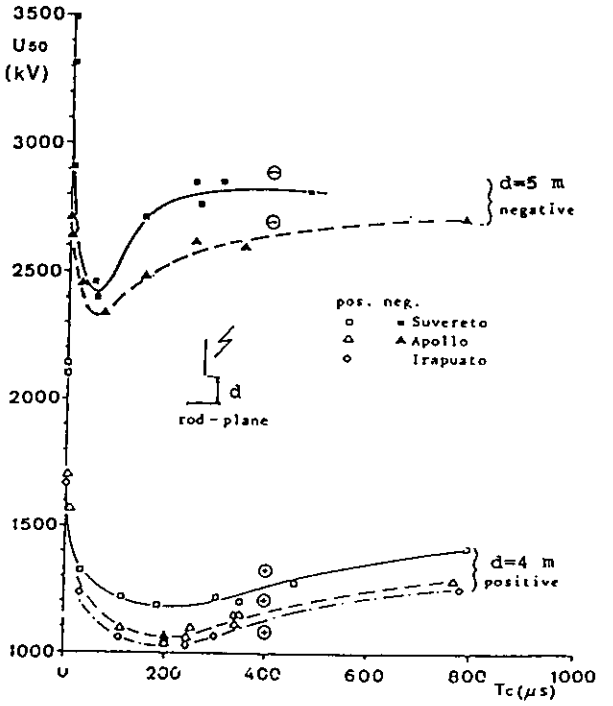

Figure 7.3: Examples of the dependence of the 50% breakdown voltage on relative air density for rod plane configuration, varying the impulse shape.

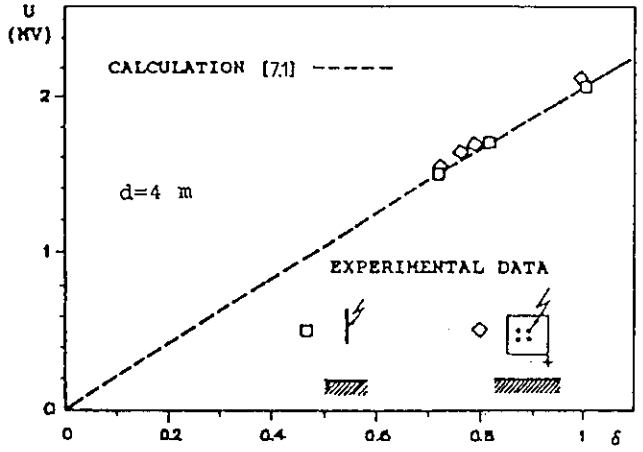

Figure 7.4: Standard positive LI. 50% breakdown voltage as a function of atmospheric conditions [7.3]. Comparison with calculations according to the standardized approach [7.1].

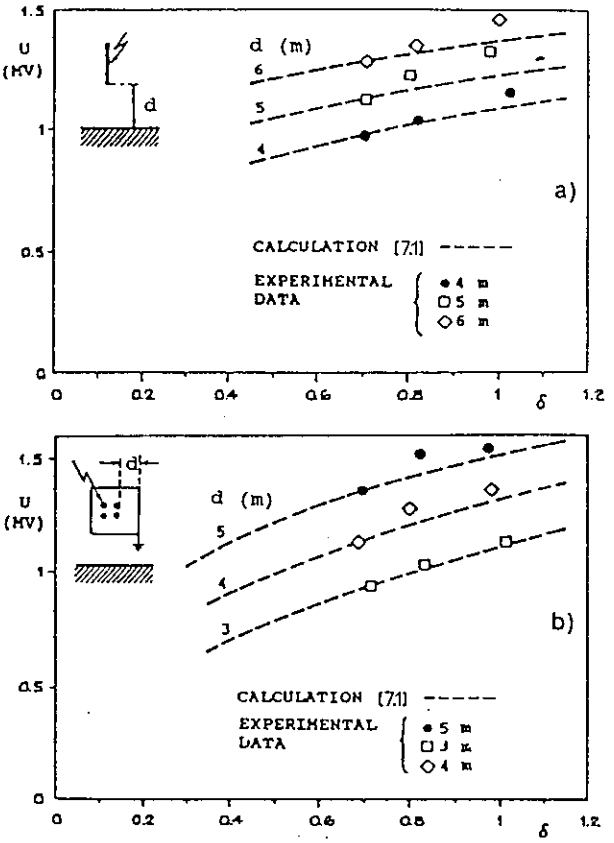

Figure 7.5: Positive SI of standard impulse shape. 50% breakdown voltage as a function of atmospheric conditions [7.3]. Comparison with calculations according to the standardized approach [7.1].

again the dielectric strength is proportional to the air density.

A general physical model describing the density influence is not yet available.

A model has been recently proposed limited to the important case of non uniform configuration under positive switching impulses [7.5]. The model permits to evaluate the influence of air density taking into account its influence on the voltage necessary for leader inception and for leader propagation. On the basis of the model an air density correction procedure has been derived, as reported in the relevant section.

7.3 GENERAL TRENDS

Examples of results obtained under positive and negative polarity impulses for rod plane configuration are given in Figure 7.3 [7.2].

Examples of the dependence of U_{50} on air density for positive polarity standard lightning (LI) and switching (SI) impulses are given in Figures 7.4 and 7.5 [7.3].

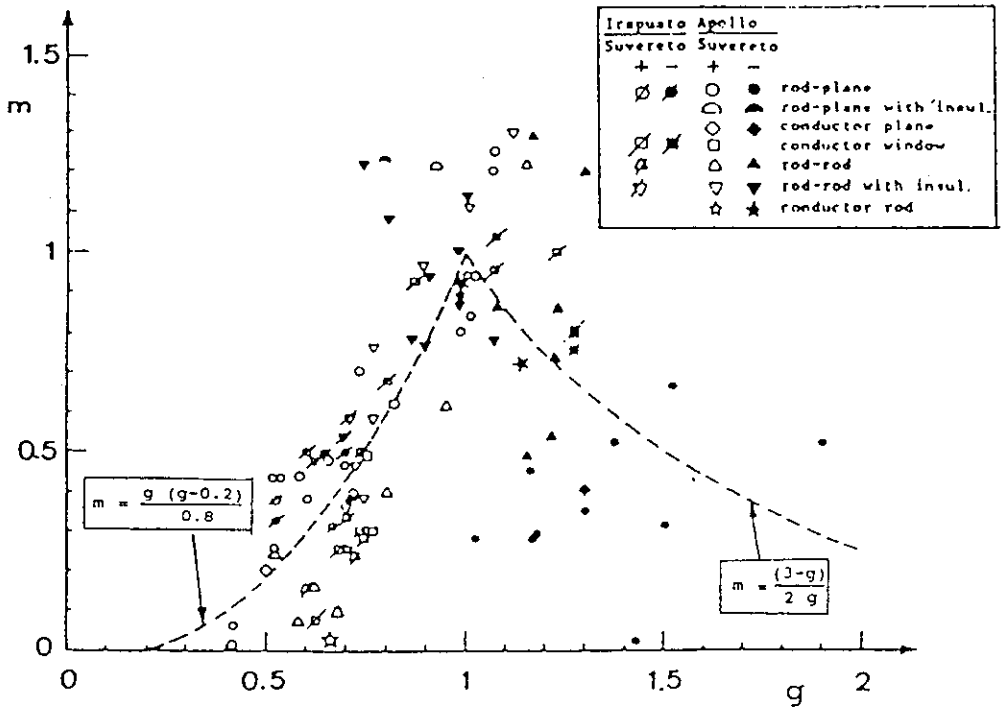

Figure 7.6: Experimental values of the exponent m versus parameter g [7.2].

The results indicates a linear dependence of U over δ for LI (m=1) and a less than linear dependence for SI (m<1).

An overview of the experimental results is given in Figure 7.6 [7.2] which gives experimental values of m as a function of experimental g values, obtained with different impulse shapes in different configurations.

The investigations regarding the influence of air density on the dielectric strength under alternating voltage (AC) and direct voltage (DC) are more limited [7.4]: the few results available agree with the picture given in Figure 7.6.

7.4 STANDARDIZED CORRECTION PROCEDURE

This procedure, developed on an empirical bases, is applicable for all voltage shapes and geometric configuration. It relates the m value to the g value, according to the curves given in Figure 7.7 [7.1], derived from Figure 7.6.

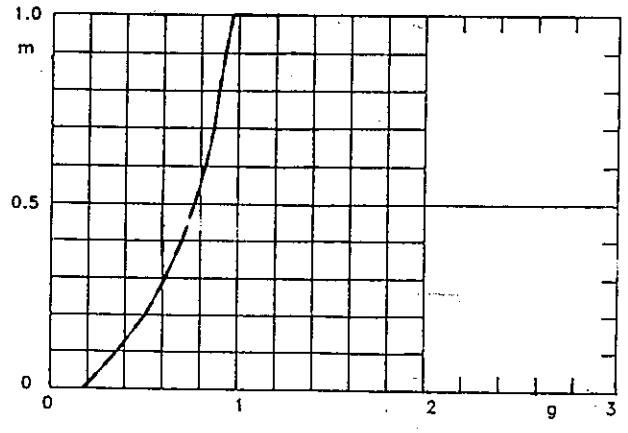

Figure 7.7: Exponent m versus parameter g, according to [7.1].

As a simplification, the method considers m=1 for all g values larger than 1. The simplification is adopted considering the large spread of the results for g>1 and the reduced importance of the conditions with 1.2<g<2 for design purposes (negative SI non relevant for non uniform gaps).

The method has been developed with special reference to phase to ground configurations. In the specific case of phase to phase configurations the method can be still applied, provided that reference to U_{50} between phases is made for the evaluation of the g value [7.6].

The method gives a good accuracy when applied in a limited air density range (with δ from 0.9 to 1.1)

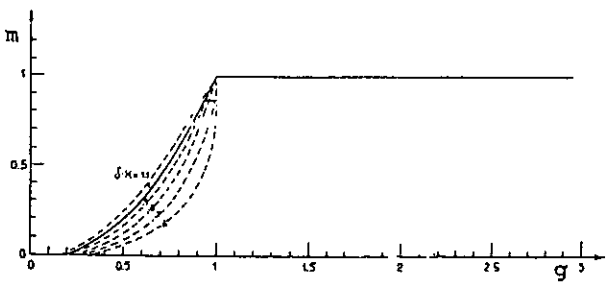

Figure 7.8: Exponent m versus parameter g, extending the approach in [7.1] to larger air density variations [7.4].

[7.2], [7.3]. However, is not recommended for larger air density variations, as those connected to large variations of altitudes, in all the cases g is different from 1 (in particular for positive switching impulses).

A technical reason for the limitation of the method is that various curves should be adopted when referring to different δ values, as shown in Figure 7.8 [7.4], when the g value is evaluated according to the prevailing atmospheric conditions. The reference to the various curves in Figure 7.8 permits to apply congruently the method: e.g. to correct from δ=1 to δ=0.7 and to correct back to δ=1, obtaining congruent results. Only by referring to close δ conditions (ranging from 0.9 to 1.1) one averaging curve can be assumed, as made in [7.1], as a first approximation.

A more important reason for the limitation is that the method is not sufficiently accurate when adopted to extrapolate air density influence for positive switching impulses in a large density range, as shown in Figure 7.5 [7.3].

7.5 HIGH ALTITUDE CORRECTION PROCEDURES FOR POSITIVE SWITCHING IMPULSES

New proposals were made with reference to the important case of positive switching impulses. Both proposals consider the dependence of m on air density.

Empirical proposal

On the basis of investigations up to 3000 m, the following expressions have been derived to fit experimental data obtained in various air gap configurations:

$$\frac{U}{U_o} = \frac{0.8\,[1+T(1-\delta)]\,(\delta-0.2g_o)}{(1-0.2g_o)} + 0.2 \qquad (7.6)$$

with:

U_o: breakdown voltage in standard conditions.

$$T = 1.4\,K^{1.6}\,\frac{1-0.8g_o}{1-0.2g_o}$$

$$g_o = \frac{U_o}{500\,d\left[1+\frac{(K-1)}{3}\right]}$$

K: gap factor (see chapter 4)

Physical proposal

On the basis of the physical approach illustrated in [7.5] the application curves of Figures 7.9, 7.10 and

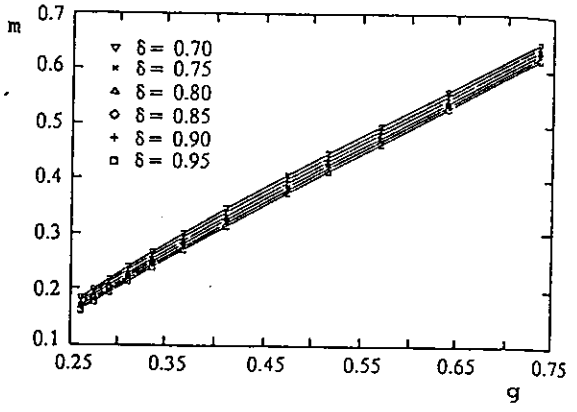

Figure 7.9: Physical approach [7.5]. Dependence of the exponent m of a rod plane gap on g for different values of δ.

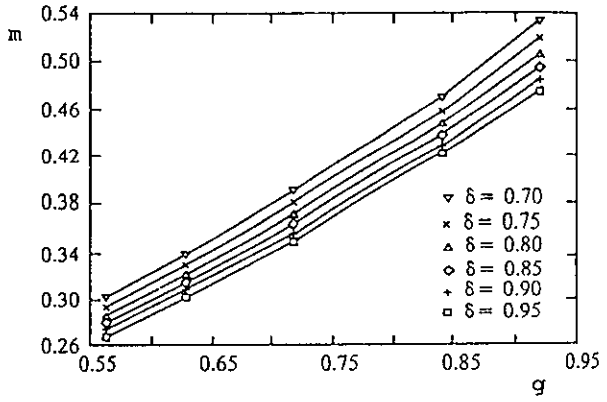

Figure 7.10: Physical approach [7.5]. Dependence of the exponent m of a rod-rod gap (with clearance equal to the height of lower rod) on g for different values of δ.

7.11 were derived.

It has been verified that the proposed approach permits to obtain a good accuracy when applied to positive SI in all the density range from 0.7 to 1.1 (discussion to [7.5]).

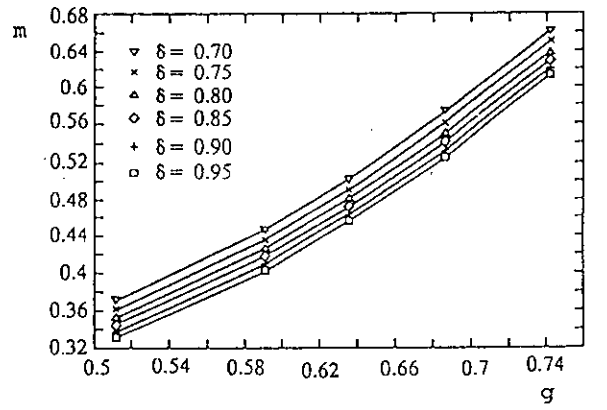

Figure 7.11: Physical approach [7.5]. Dependence of the exponent m of a conductor-tower window gap on g for different values of δ.

7.6 CONCLUSIONS

The influence of air density on the dielectric strength depends on voltage shape and polarity and configuration geometry.

A correction method to take into account limited air density variations ($0.9<\delta<1.1$) has been recently standardized.

The method is not enough accurate when applied to large air density variations: in these cases the methods given in part 7.5 of this report permit to obtain much better accuracy.

7.7 REFERENCES

[7.1] IEC Publication 60-1/1989. "High voltage test techniques.

[7.2] A. Pigini, G. Sartorio, M. Moreno, M. Ramirez, R. Cortina, E. Garbagnati, A. C, Britten, "Influence of air density on the impulse strength of external insulation" IEEE Trans. on Power Apparatus and Systems, Vol. PAS 104-1985.

[7.3] M. Ramirez, M. Moreno, A. Pigini, G. Rizzi, E. Garbagnati, "Air density influence on the strength of external insulation under positive impulse: experimental investigation up to an altitude of 3000m a.s.l.", IEEE paper 89 SM 622-2 PWRD.

[7.4] K. Feser, A. Pigini, "Influence of atmospheric conditions on the dielectric strength of external insulation", ELECTRA 1987.

[7.5] F. A. M. Rizk, "Critical switching impulse strength of long air gaps: modelling air density effect", IEEE paper 91 SM 306-1 PWRD.

[7.6] E. Garbagnati, A. Pigini, G. Sartorio, C. Britten, B. C. Le Roux, "The influence of atmospheric conditions on the dielectric strength of phase to phase insulation when subjected to switching impulses", ISH Dresden 1991.

[7.7] American Meteorological Society, "Compendium of meteorology", Ed. Thomas F. Malone, 1951.

8 INFLUENCE OF AIR HUMIDITY ON THE DIELECTRIC STRENGTH OF EXTERNAL INSULATION

by N. L. ALLEN, J. R. FONSECA, H. J. GELDENHUYS AND J. C. ZHENG.

8.1 GENERAL

Changes of atmospheric humidity have been shown to affect sparkover voltages in non-uniform field gaps. Natural humidity varies, in different parts of the world, between 1 and 30 gm^{-3} and since variations of sparkover voltage of the order of 1 per cent per gm^{-3} have been measured, it is clear that the effects of humidity on the performance of high voltage external insulation are important. In this Chapter, a brief account of the effects of humidity on the physics of discharge processes is followed, in Section 8.3, by a description of the correction procedures recommended by the I.E.C. In the remainder of the Chapter, the variations of sparkover voltages with humidity are discussed for the specific cases of impulse, alternating and direct voltages, with comment also on the case of negative voltage.

8.2 INFLUENCE OF HUMIDITY ON BREAKDOWN PROCESSES

The electrical breakdown of air in non-uniform fields is preceded by three distinct phases, as examined in detail in Chapter 3.

First, a free electron, usually detached from an ambient negative ion, acquires sufficient energy from the electric field to ionize and create an avalanche. Second, if the positive ions in the avalanche so produced have sufficient density to reach a critical size (critical avalanche), the resulting space charge field can initiate further avalanches, so that the positive space charge region extends itself rapidly at the rate of metres per microsecond; this is the formation of a "streamer". In a few cases, especially under direct voltage, after the first avalanche, a glow type corona may occur, only subsequently developing into a streamer. Finally, if voltage is applied for sufficient time, the ions and electrons in the streamer trail can gain energy, so raising the temperature and the level of ionization to form a highly conducting arc-like channel; this is a "leader". The transition from a streamer usually starts near a highly stressed anode and it extends with the comparatively low velocity of a few centimetres per microsecond. When the leader bridges the inter-electrode space, the current rises rapidly and breakdown, or sparkover, is completed.

A change of humidity affects all three processes. It affects the probability that electron detachment occurs, but more importantly, it changes the rate at which ionization and diffusion take place in the electric field and hence, affects the formation of an ion density sufficient for streamer formation to occur.
Since the streamer propagates by further avalanche formation, it follows that humidity changes the conditions for streamer propagation.

The subsequent heating process in the streamer trail is also believed to be affected by humidity change, so that the transition to a leader is facilitated [8.1]. It is an experimental fact that a leader forms more quickly and propagates at higher speed, as humidity increases.

The effects of humidity upon the breakdown process will now be discussed.

8.2.1 Avalanche-type discharge

For relatively small gaps and large electrodes the breakdown occurs as soon as the first critical avalanche is formed. Thus the influence of humidity on the breakdown voltage is the same as on the first critical avalanche formation.

When all humidity-dependent factors are taken into account, it is estimated that an increase of geometric field at the rate of about 0.25 per cent per gm^{-3} is needed to achieve the threshold condition, as humidity

Table 8.1

STREAMER PROPAGATION FIELDS $E_{s_0}^*$ AND HUMIDITY COEFFICIENTS ε

$$E_s^* = E_{s_0}^* \left[1 + \frac{\varepsilon}{100} (h - h_0) \right] \qquad (h_0 = 11\ gm^{-3}).$$

	$E_{s_0}^*$ (kVm^{-1})	ε (% per (gm^{-3}))	Electrode gap details.
Andersson [8.4]	464	2.2	Plane parallel 0.5 - 2.25 cm
Phelps and Griffiths [8.5]	487	1.7	Plane parallel 9 cm
Allen and Boutlendj [8.6]			
(a) pulsed streamer source	490	1.8	Plane parallel 66,47,21 cm
(b) D.C. streamer source	510	2.2	Plane parallel 66 cm
	535	2.5	Plane parallel 47 cm
	542	1.9	Plane parallel 21 cm
Acker and Penney [8.7]	460	-	Non-uniform 3.17 cm
Allen and Dring [8.8]	414	1.0	Non-uniform 60 cm
Geldenhuys [8.9]	464	1.3-1.5	Non-uniform 50 cm
	489	1.3	Non-uniform 50 cm

TABLE 8.2

HUMIDITY COEFFICIENTS, k, UNDER NEGATIVE IMPULSES.

k , percent per gm^{-3}

	k	IMPULSE	GAP GEOMETRY (Rod-plane)
Standring et al, 1963 [8.10]	-0.4	L.I. (1/50 μ s)	1.1 metre
Vlastos, 1966 [8.11]	-0.6	L.I. (1/50 μ s)	0.45 metre
Harada el al, 1971 [8.12]	0	L.I. (2/40 μ s)	0.5 to 2 metre
Allibone et al, 1972 [8.13]	approx - 0.5	L.I. (1/50 μ s)	0.2 to 4 metre
Kucera et al, 1972 [8.14]	0	L.I. (1.2/50 μ s)	$\leq$ 6 metre
Kucera et al, 1970 [8.15]	-0.4 to 0.25	S.I. (200/3200 and 450/4300 μs)	1.5 metre
Harada et al, 1971 [8.12]	0	S.I. (220/2100 μ s)	0.5 to 2.0 metre
Allibone et al, 1972 [8.13]	0	S.I. (80/1000 μ s)	0.2 metre
Feser et al, 1986 [8.16]	0	S.I. (60/2500 μ s)	0.3 metre

is increased [8.2]. This corresponds approximately to the rate of increase of breakdown field, with humidity, that has been observed experimentally in a uniform-field electrode configuration [8.3], where breakdown is governed by avalanche growth alone.

8.2.2 Streamer type discharge

For non uniform field and for impulse voltage the breakdown occurs through the formation of streamers which develop once sufficiently large avalanches are formed. The value of the electric field required for positive streamer propagation is an extremely important parameter in determining the breakdown of air in long gaps. There have been several determinations of the variation with humidity of the streamer propagation field E_s. For the positive streamer it has been found to follow the relation:

$$E_s^+ = E_{s0}^+ \left[1 + \frac{\varepsilon}{100} (h - h_0) \right] \qquad (8.1)$$

where ε is a humidity coefficient. Values of E_{s0}^+ and ε are given in Table 8.1.

These results have been obtained from experiments on the propagation of streamers either in uniform electric fields or in non-uniform fields. The results indicate, on the average, an increase of E_s^+ with humidity of about 1% per gm^{-3}. Data for negative streamer propagation are much more limited. The available data about breakdown voltage in this case where the discharge is governed by negative streamers suggest a limited humidity influence (Table 8.2).

8.2.3 Streamer plus leader discharge type

For non-uniform fields and for relatively slowly rising voltage applications, the breakdown occurs with the formation of streamers and leaders. Leader growth, varies with electrode separation and with rate of voltage rise, as well as with the atmospheric conditions. A simple model is given below.

At the instantaneous sparkover voltage, U_s:

$$U_s = E_l l_l + E_s^+ l_s^+ + E_s^- l_s^- \qquad (8.2)$$

where E_l and E_s^+, E_s^- are the gradients of the leader and positive and negative streamers, of lengths l_l and l_s^+, l_s^- respectively. Equation (8.2) holds when the leader, with the associated streamers at its head, just crosses the electrode gap:

$$l_l + l_s^+ + l_s^- = d \qquad (8.3)$$

Recent measurements [8.17] show a variation in the average value of E_l against l_l. When the leader develops initially from the streamer its propagating field is the same as that of the streamer; as it grows in length, the heating process reduces its resistance and hence its gradient, tending towards the limiting value of 50 kV/m.

$$E_l = 450 \exp\left[- \frac{l_l^{0.55}}{0.751} \right] + 50 \quad \left(\frac{kV}{m}, m\right) \qquad (8.4)$$

Since both E_s^+ and l_l increase with humidity (E_l is assumed independent of humidity), substitution of numerical values shows that the second term in (8.2) tends to increase faster than the first, so that the resulting instantaneous breakdown voltage U_s increases less rapidly with increasing humidity than it would do for a lightning impulse, where streamers only are significant. Thus, the "humidity coefficient" would be reduced. Indeed, equations (8.2) and (8.4) admit the possibility that if l_l is sufficiently large, the value of U_s could be reduced as humidity increases, since E_l also decreases with increasing l_l.

8.3 CORRECTION PROCEDURE

Reference is made to the correction procedure now recommended by IEC.

According to this procedure the 50 per cent breakdown voltage U at any atmospheric condition is related to the value at standard conditions (relative air density $\delta = 1$, absolute humidity $h_0 = 0$ gm^{-3} by the relation

$$U = U_0 k_1 k_2 = U_0 k_t \qquad (8.5)$$

where k_1 is the air density correction factor (which is discussed in Chapter 7) and k_2 is the humidity correction factor which is, in turn expressed by:

$$k_2 = (k)^w \qquad (8.6)$$

Values of k can be obtained from Figure 8.1. One important feature must be noted. In Figure 8.1, k is plotted as a function of h/δ rather than as a function of h alone. This takes into account the fact that absolute humidity corresponds to a constant partial pressure of water vapour, regardless of the changes of air partial pressure which occur with changes of air density. These effects become especially important for measurements at high altitude and have been

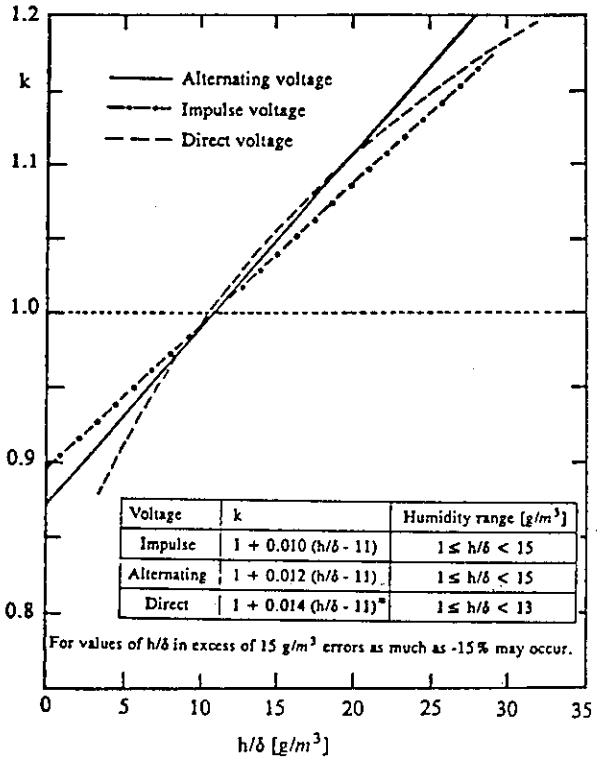

Figure 8.1 k as a function of the ratio of absolute humidity h to the relative air density δ [8.18].
* Linear approximation to curve.

demonstrated by tests performed at different altitudes and in weather chambers as in the example of Figure 8.2.

The exponent w takes into account variations due to electrode geometry and the voltage shape. The value of w is arrived at using a factor g which is defined

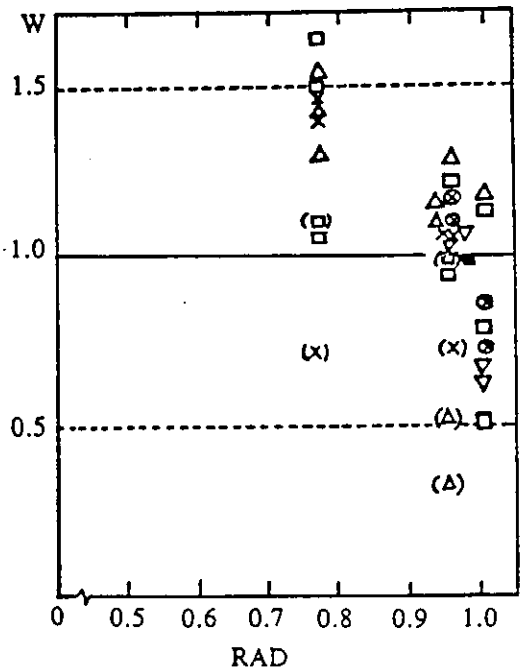

Figure 8.2 Exponent w as a function of relative air density [8.19].

in terms of the streamer propagation gradient E_{so} of 500 kV/m, corrected for the conditions δ and k:

$$g = \frac{U}{500\ \delta k d} \quad (kV,\ m) \qquad (8.7)$$

where d is the length of gap, and U is the 50% breakdown voltage at the actual atmospheric condition for the voltage shape and electrode configuration in question. It has been shown that w is related to g as follows [8.20]:

$$\begin{aligned} w &= g(g - 0.2)/0.8 && g < 1 \\ w &= 1 && 1 < g < 1.2 \\ w &= (2-g)/0.66g && 1.2 < g < 2 \\ w &= 0 && g > 2 \end{aligned} \qquad (8.8)$$

The dependence of w on g has been checked over a wide range of conditions, as shown in Figure 8.3, where experimental values are compared with the curve given by Equations (8.8). The agreement permits the use of these equations in a range of conditions, notably for switching impulses and D.C. where correction was previously difficult.

A comprehensive account of the background to the new procedure is given in reference [8.20]. It must be observed, however, that there still exist a number of exceptional cases, especially when very short and very long gaps or high humidities are involved, which cannot be covered by existing correction procedures. These are discussed later.

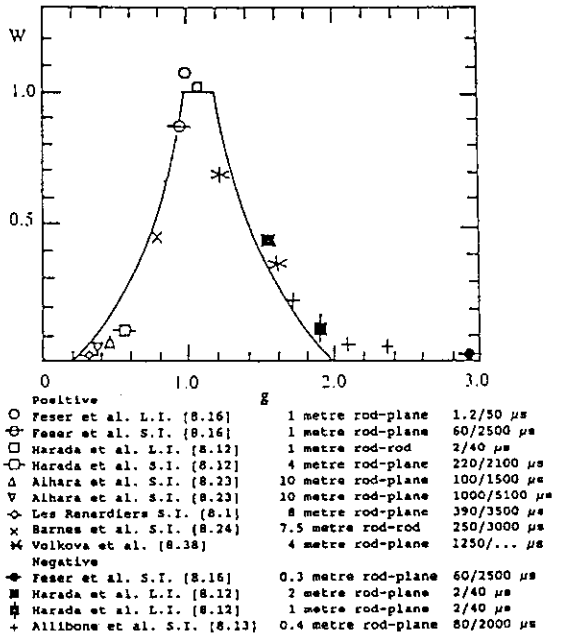

Figure 8.3 Plot of experimental points for w against g and comparison with curve described by equations 8.8.

8.4 APPLICABILITY OF THE CORRECTION PROCEDURE

8.4.1 Air gaps

8.4.1.1 Lightning impulse

Breakdown under positive lightning impulse voltage is less complicated than it is under other voltage forms since the breakdown strength increases linearly with electrode separation, at least in the range of 0.5 to 6 m [8.12] [8.24]. It also increases linearly with humidity, (checked up to d = 4 metres) at approximately the same rate as the variation of streamer propagation field with humidity. A summary of the available information is given in Table 8.3 where experimental w values are given. For rod plane under lightning impulse the w value ranges from 1.0 to 1.26. This

TABLE 8.3

LIGHTNING IMPULSE BREAKDOWN : HUMIDITY EFFECTS IN ROD-PLANE GAP.

	S_0 kVm^{-1}	w	Impulse μ sec	Electrode and gap details
Standring et al. [8.10]	525	1.12	1/50	1.1, 2.0 and 3 m "point"
Harada et al [8.12]	510	1.05	2/40	0.5 m square rod
	505	1.02	2/40	1 m square rod
	525	1.14	2/40	2 m square rod
	533	1.15	2/40	3 m square rod
Allibone and Dring [8.13]	530	1.22	1/50	0.8 m hemisph-ended rod
	540	1.20	1/50	0.6 m hemisph-ended rod
Geldenhuys [8.9]	500	1.00	1.5/52	0.5 m small sphere-ended rod
Feser et al [8.16]	537	1.17	1.2/50	1 m cone-ended rod
Ramirez et al [8.25]	527	1.13	2/48	4 m hemisph-ended rod
Soetjipto et al [8.26]	554	1.26	1/47	0.6 m cone-ended rod
Allen and Boutlendj [8.6]	526	1.12	1/50	1 m hemisph-ended rod
Mean value	526	1.13		

spread may be expected to depend on the spread of experimental values of U and a w value of about 1 may be derived. In general for positive lightning impulses the g value is close to 1 and the proposed correction approach can be considered fully applicable.

Breakdown under negative lightning impulse is more complicated. The breakdown voltage may increase less than linearly with the gap distance, as in the case of the rod plane configuration. The corresponding g value is higher than 1. The influence of humidity is generally smaller than for positive impulses.

In general, evidence of humidity effects show that the proposed procedure can be applied to lightning impulses.

8.4.1.2 Switching impulse

The available information on humidity effects on switching impulse breakdown is less homogeneous than in the case of lightning impulses.

Since 50% breakdown voltages under positive switching impulse are less than those under lightning impulse, $g < 1$ always. A comparison between the experimental w values and those predicted by the correction approach is made in Figure 8.3. Although some scatter exists, the agreement with the curve must be regarded as good, since a small uncertainty in U leads to a large uncertainty in w. Additional information on the humidity exponent w for various positive switching impulses is given in Table 8.4. The proposed correction approach is sufficiently accurate for clearance up to 4 - 5 metres. It is however important to point out that care is needed generally in the application of the I.E.C. procedure to the estimation of sparkover voltages at different humidities when using switching impulses and when large air gaps are considered. The difficulty exists because the minimum of the "U-curve" has been shown to shift to smaller values of time-to-crest with increasing humidity [8.1] [8.27]. The problem is illustrated in Figure 8.4, where notional U-curves for the same gap are shown. For standard humidity h_0, these would, using the IEC procedure, suggest that at humidity h, the sparkover voltage would be of value as indicated at B. However, due to the humidity-induced shift of the U-curve, the actual minimum now occurs at C, which is at a lower voltage then predicted at B.

An example of the humidity influence for very long gaps is given in Figure 8.5, where the influence of the time-to-crest is seen. Where this is relatively short, the U breakdown voltage decreases with increasing humidity, in contrast to behaviour with longer times-to-crest. The correction procedure cannot be applied in this case.

As far as negative SI are concerned, the more limited evidence available shows that experimental points fall close to the w versus g curve in the range $1.2 < g < 2$ (equations 8.8 and Figure 8.3) and that the correction procedure can be applied.

TABLE 8.4

SWITCHING IMPULSE BREAKDOWN : HUMIDITY EFFECTS IN ROD-PLANE GAP.

	S_0 kVm^{-1}	w	Impulse μ sec	Gap
Busch [8.27]	167	.056	700/	14 metres
Andrade et al [8.30]	161	.05	290/2419	13
Busch [8.27]	189	.084	700/	10
Andrade et al [8.30]	205	.11	102/153	10
Aihara et al [8.29]	185	.08	490/	10
Andrade et al [8.30]	223	.14	266/2372	7
Harada et al [8.12]	375	.52	220/2100	2
Allen and Boutlendj [8.28]	405	.64	17/3500	1
Allibone and Dring [8.13]	440	.75	80/1000	0.8
Geldenhuys [8.9]	500	1.0	70/2000	0.5

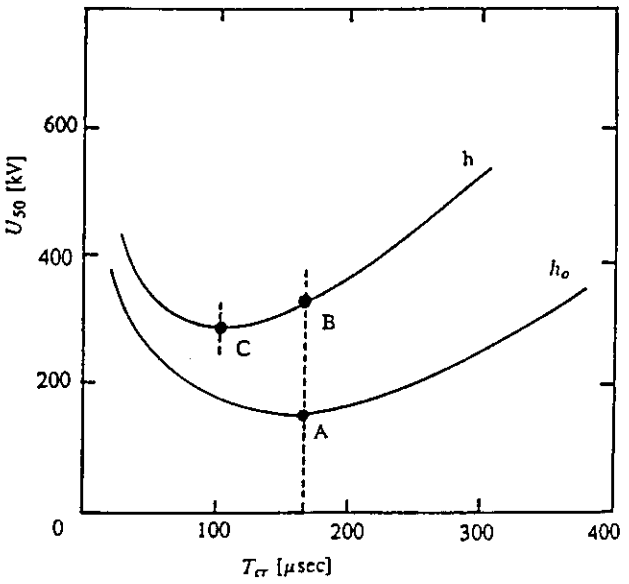

Figure 8.4 Comparison between two U-curves obtained at different humidities.

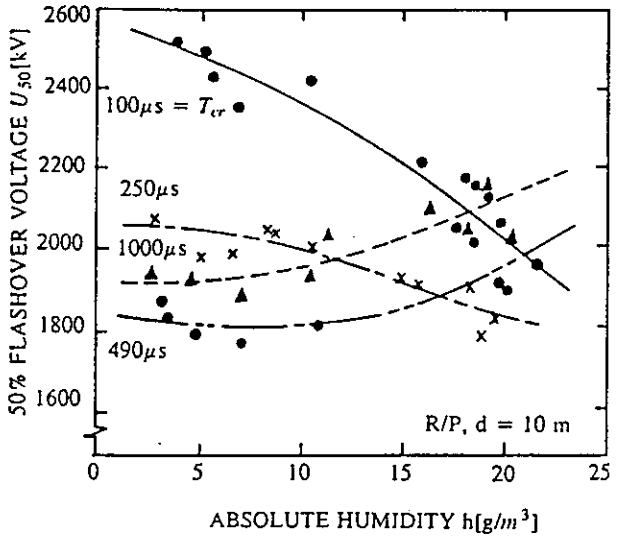

Figure 8.5 S.I. flashover in long gaps with different times to crest [8.29].

8.4.1.3 Direct voltage breakdown

In non-uniform fields, sparkover voltages are determined by glow or streamer pre-discharges, according to the gap length and electrode profile.

As a first approximation the proposed procedure for humidity correction is applicable for gaps larger than 250 mm and smaller than 1500 mm; these conditions are generally characterised by a linear relationship between breakdown voltage and gap distance. When humidity exceeds about 13 gm^3 in longer gaps, there may be significant departures from the linearity between breakdown voltage and gap distance in rod-rod and rod-plane gaps [8.31], [8.32], [8.33]. In this region, breakdown voltages are less than those expected from a linear extrapolation of points at lower humidities; also the departures from linearity are significantly greater than the scatter about individual experimental points (Figure 8.6). In general no correction can be applied in this non-linear region. For small gaps with the discharge governed by glow processes the relationship between

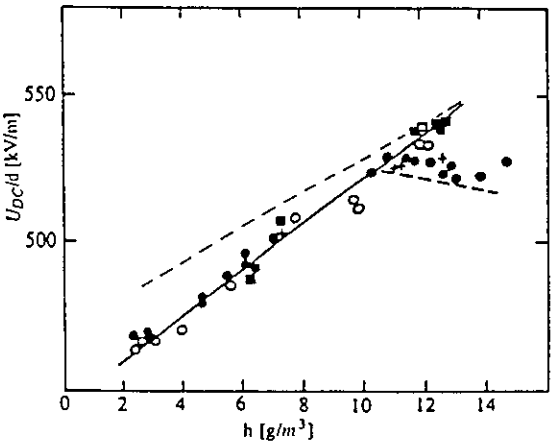

Figure 8.6 D.C. sparkover average stress (kV/m) as a function of humidity, showing departures from linearity at high humidities [8.33]. Full line drawn through points obtained in 1.0 and 1.5 metre gaps. Dashed line for 0.5 metre gap.

breakdown voltage and gap distance is again not linear. Also in this case the humidity correction procedure is not applicable.

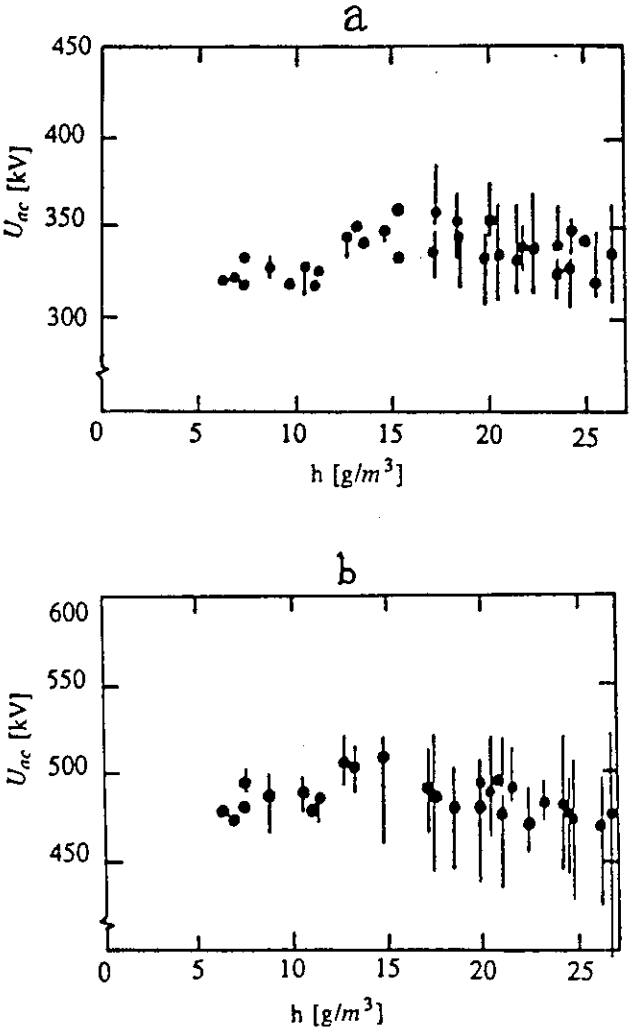

Figure 8.7 A.C. sparkover voltage as a function of humidity [8.36]
(a) 1.0 m gap
(b) 1.5 m gap

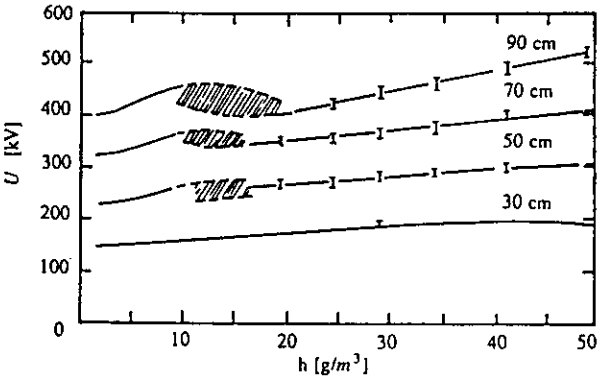

Figure 8.8 A.C. sparkover voltage of rod-plane gaps, as a function of humidity [8.37].

8.4.1.4 Breakdown under alternating voltages

The AC breakdown of air gaps as a function of absolute humidity shows varying tendencies, depending on the gap length, electrode configuration and humidity range. Most of the test data available has been obtained with rod-plane gaps with lengths ranging from 1 m to 6 m, in test chambers or natural weather conditions, indicating that the alternating breakdown voltages vary with humidity in a complicated manner, so that no constant humidity coefficient can be obtained [8.34], [8.35]. In the humidity range below 11 gm^{-3} the breakdown voltages generally increase with humidity, whereas in the higher humidity range, it is practically unchanged or even reduced with increasing humidity, so that the humidity coefficient becomes negative. In addition, much higher jitter in breakdown voltages has been observed in the high humidity range. As a typical case, Figure 8.7 indicates the breakdown voltage versus absolute humidity for rod-plane gaps of 1.0 m and 1.5 m length, [8.36] together with the related scatter limits. Other experimental information is given in Figure 8.8. The changes of slope and sharp increase of scatter can be clearly be identified on these figures [8.37]. The variation with humidity has also been recorded in larger gaps, shown in Figure 8.9, [8.38] where it is compared with long-front S.I. tests.

It is clear from the foregoing that clear systematic trends resulting from humidity change under alternating voltages have not been established for humidities exceeding 11 gm^{-3}. It is suggested, therefore no humidity correction procedure can at present be applied to alternating voltage measurements outside a restricted range of gaps and humidities.

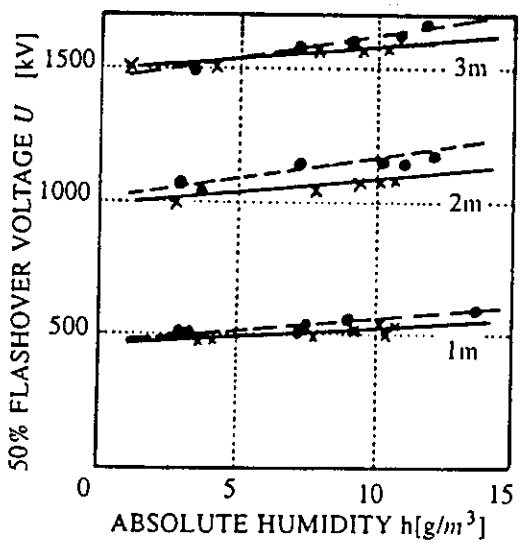

Figure 8.9 Variation of A.C. sparkover in longer gaps [8.38].

8.4.2 Humidity effects in the presence of insulator surfaces

It is important to indicate the influence of humidity on flashover voltages along insulating surfaces, in spite of the fact that there is, as yet, insufficient systematic data to enable standards to be formulated. Surface conditions are critical, but where the discharge develops mainly in air gaps between electrodes without attaching to the surface, no significant difference would be expected between the cases with and without the surface. On the other hand, with insulation structures where the discharge channel adheres to the surface, different effects can be expected. If, in addition condensation occurs, conditions are quite different from those with a clean dry surface in a humid atmosphere, and the term "humidity effects" becomes inapplicable.

Data is available on flashover across insulator strings, post insulators and bushing-type insulators; these show different behaviour when humidity changes.

Figure 8.10 shows the dependence of flashover voltage on absolute humidity for insulator strings containing 10 to 25 units of standard insulators under positive switching impulse [8.12]. Here, the voltage increases with increasing humidity up to 25 gm^{-3}.

Other tests with lightning impulses and with power frequency voltages made on both strings and single cap and pin units (Figure 8.11), show a smaller change in flashover voltage over a similar humidity range [8.39].

Investigations performed in a humidity controlled chamber on post insulators, with a simple cylindrical insulator surface, have shown a linear rise with humidity at the rate of about 1 per cent per gm^{-3}, [8.40] substantially confirming earlier results [8.31] except at the highest humidities. In the same humidity controlled chamber it was found that the

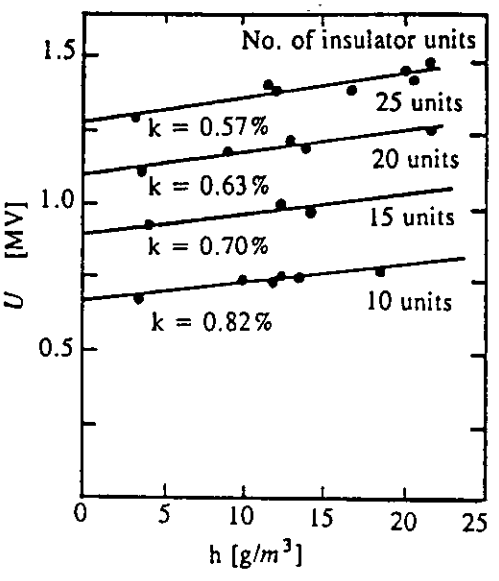

Figure 8.10 S.I. flashover voltage vs absolute humidity for 10-inch suspension insulators, 220/2100 μs impulse corrected to RAD=1 [8.12].

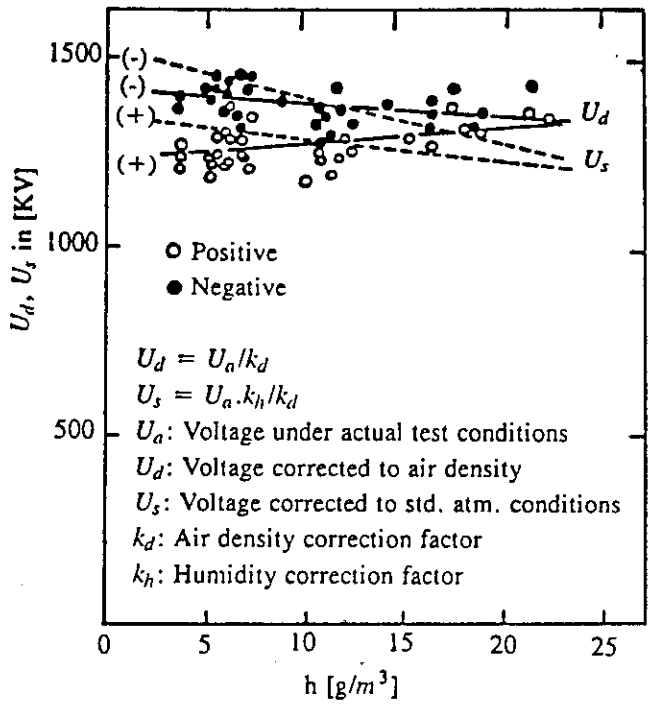

Figure 8.11 LI flashover voltage vs absolute humidity for 250 mm diameter disc insulator [8.39].

flashover voltage of a simulated bushing configuration, under lightning and switching impulses, decreased significantly with increasing humidity; these differences were associated with differing field configurations.

The evidence is thus contradictory, and in general it is recommended not to apply humidity correction when the discharge path directly involves insulators.

8.5 CONCLUSIONS

The new IEC humidity correction procedure is based upon a comparison between the mean stress for sparkover across a non-uniform field gap and the electric gradient required for streamer propagation.

Analysis of the applicability of the procedure has shown that:

1 In the case of lightning impulse voltages, the procedure can be applied for all non-uniform field gaps over a range of humidities up to 20 gm^{-3}.

2 For switching impulses, the procedure can be used, for gaps in the range $0.5 < d < 4$ metres. For longer gaps, there is less precision, with reductions of flashover voltage with increasing humidity in some cases, depending also upon the time to crest. In these cases the correction procedure cannot be applied.

3 With direct voltages, the procedure can be used for large gaps provided the humidity does not exceed about 13 gm^{-3} and the discharge is governed by streamers. Where other modes of predischarge occur (e.g. small gaps, high humidity) the procedure cannot be applied.

4 With alternating voltages anomalous breakdown behaviour in many cases prevents the application of the correction procedure.

5 Insufficient knowledge is available to permit the use of a correction procedure for flashover in the presence of insulator surfaces.

8.6 REFERENCES

[8.1] Les Renardières Group "Positive discharges in long air gaps", 1977 Electra, 53 p 97-162.

[8.2] N. L. Allen "The effect of humidity on avalanche growth and streamer initiation", 1985, J. Phys. D Appl. Phys 18, 47 - 52.

[8.3] D. T. A. Blair, F. M. Bruce and D. J. Tedford 1963 Proc 6th Int. Conf. on Phenomena in Ionised Gases, Paris Vol II, p 321-323.

[8.4] N. E. Andersson "An investigation of the positive point streamer corona, Part II: the field strength necessary for the streamer propagation", 1958 Arkiv for Fysik, 13 441-479.

[8.5] C. T. Phelps and R. F. Griffiths "Dependence of positive streamer propagation on air pressure and water vapour content", 1976, J. Appl. Phys. 47, 2929-2934.

[8.6] N. L. Allen and M. Boutlendj "A study of the electric fields required for streamer propagation in air", 1991, IEE Proc. A138, 37-43.

[8.7] F. E. Acker and G. W. Penney "Some experimental observations of the propagation of streamers in low-field regions of an asymmetrical gap", 1969, J. Appl. Phys. 40, 2397-2400.

[8.8] N. L. Allen and D. Dring "Effect of humidity on the properties of corona in a rod-plane gap under positive impulse voltages", 1984, Proc. Roy. Soc. A396, 285-295.

[8.9] H. J. Geldenhuys (a) "Positive streamer voltage gradient and average breakdown voltage as functions of humidity", 1985, CIGRÉ 33-85 (WG07), 21 IWD (Unpublished). (b) "The breakdown voltage of air in a rod-plane gap over a practical range of air density and humidity", 1987 5th Int. Symp. on High Voltage Engineering, Braunschweig, Paper 14.02.

[8.10] W. G. Standring, D. H. Browning, R. C. Hughes and W. J. Roberts "Effect of humidity on flashover of air gaps and insulators under alternating (50 c/s) and impulse (1/50 μs) voltages", 1963 Proc IEE 110, No.6, 1077 - 1081.

[8.11] A. F. Vlastos "Breakdown of air in the non-homogeneous field", 1966, Proc. IEE, 113, 921-930.

[8.12] T. Harada, Y. Aihara, and Y Aoshima "Influence of humidity on lightning and switching impulse flashover voltages", 1971, IEEE Trans. PAS 90, 1433 - 1441.

[8.13] T. E. Allibone and D. Dring "Influence of humidity on the breakdown of sphere and rod gaps under impulse voltages of short and long wavefronts", 1972, Proc. IEE 119, 1417 - 1422.

[8.14] J. Kucera, T. W. Liao and A. F. Rohlfs "Atmo-

spheric correction factors for high voltage testing", 1972, Electra No 21, 74-84.

[8.15] J. Kucera and V Fiklik "Correction of switching impulse flashover voltages for air humidity", 1970 IEEE Trans. PAS-89 441-445.

[8.16] K. Feser, E Busse and J Schmid "Influence of humidity on air breakdown", CIGRÉ 33-86 (WG 07) 24 IWD.

[8.17] Les Renardières Group "UHV air insulation: physical and engineering research", 1986 Proc IEE 133A, 438-468.

[8.18] I.E.C.-60 1989 "High voltage test techniques", Part I, General definition and test requirements".

[8.19] J.C. Zheng Unpublished.

[8.20] K. Feser and A. Pigini "Influence of atmospheric conditions on the dielectric strength of external insulation", 1987 Electra No 112, 83-95.

[8.21] K. Feser and J. Schmid "Influence of atmospheric conditions on the impulse breakdown of rod-plane gaps", Paper 11.01, 5th Int. Symp. on High Voltage Engineering, Braunschweig, Paper 11.01.

[8.22] G. Carrara "Impulse sparkover voltages of rod gaps", CIGRÉ, Annexe II to Report N328.

[8.23] Y. Aihara, Y. Watanabe and I. Kishizima "Analysis of new phenomenon regarding effects of humidity on flashover characteristics for long air gaps", 1983 IEEE Trans. PAS-102, 3778-3782.

[8.24] H.C. Barnes and D.E. Winters "UHV transmission design requirements - switching surge flashover characteristics of extra long air gaps", 1971, IEEE Trans. PAS-90, 1579-1588.

[8.25] M. Ramirez, A. Villalobos and M. Moreno 1986, CIGRÉ 33-86 (WG07) (Unpublished).

[8.26] S. Soetjipto, G. Riquel and B. Hutzler "Dielectric strength of air gaps at high humidities", 1987, Fifth Int. Symp. on High Voltage Engineering Braunschweig, Paper 11.02.

[8.27] W. Büsch "Air humidity, an important factor for UHV design", IEEE Trans. PAS-91 No. 6 2086-2093.

[8.28] N. L. Allen and M. Boutlendj Unpublished.

[8.29] Y. Aihara, Y. Watanabe and I. Kishizima "Analysis of new phenomenon regarding effects of humidity on flashover characteristics for long air gaps", 1983, IEEE Trans. PAS-102, 3778-3782.

[8.30] V. H. Gomes De Andrade and C. E. Oliveria Coutinho "Dielectric tests on rod-plane gaps at different humidity conditions", 1985, CIGRÉ 33-85 (WG 0T) 26 IWD, unpublished. "The influence of very high humidity in large gaps", 1986, CIGRÉ 33-86 (WG 07) 18 IWD, unpublished.

[8.31] E. Peschke "Effect of humidity on breakdown and flashover at high DC voltages in air", ETZ-A 90, No. 1.

[8.32] T. Harada, Y. Aihara, M. Honda, T. Watanabe, Y. Kamata, K. Yoshida, Y. Maruyama "DC flashover tests of rod-rod gaps in Japan", 5th Int. Symp. on High Voltage Engineering, Braunschweig, August 1987, Paper 11.07.

[8.33] K. Feser and R. C. Hughes "Measurement of direct voltages by rod-rod gap", 1988, Electra 117.

[8.34] A. Fischer "The influence of humidity on DC and AC breakdown voltage of air gaps", 1970, Electra No. 10 65-77.

[8.35] G. N. Aleksandrov, V. M. Rudakova "Influence of air humidity on long air gaps", 1969, Electriceski Stancil No. 8.

[8.36] J. C. Zheng and Y. M. Yang "Influence of humidity on the dielectric strength of large air gaps under A. C. Voltages", 1989, 6th ISH, New Orleans.

[8.37] K. Feser "Influence of humidity on the breakdown characteristics under A.C. voltage", 1970, E.T.Z. A Bd. 91, No.10.

[8.38] O. V. Volkova, A. S. Rejngold, V. J. Cernysev "Influence of humidity on flashover voltages of long air gaps" 1968 Elektricestovo No. 3 49-53.

[8.39] K. Taketani and K. Naito "Influence of humidity on flashover voltage of insulators", 1991, CIGRÉ 33.91 (Coll.) (Leningrad), 4.1 IWD.

[8.40] J. C. Zheng and Y. Liu "Influence of humidity on the impulse flashover voltages of air in the presence of insulating surfaces", 1991, CIGRÉ 33.91 (Coll.) (Leningrad), 4.2 IWD.

9 PERFORMANCE OF CONTAMINATED INSULATORS UNDER TRANSIENT OVERVOLTAGES. SURVEY OF EXPERIMENTAL DATA

by E. LEMKE, A. FRACCHIA, E. GARBAGNATI, A. PIGINI

9.1 INTRODUCTION

External insulation may be subjected, in service, to various transient stresses, of internal and external origin, which can be represented in laboratory by lightning impulses, LI, switching impulses, SI, and by short duration AC application, TO. Depending on the line condition, the transient overvoltages may be superimposed on the permanent AC or DC voltage. That condition can be represented in laboratory by composite voltages (eg. LI, SI, TO, superimposed on AC or DC stresses).

The above transients may occur in various environmental conditions and may affect insulators characterized by various degrees of contamination. In particular a critical condition may arise when there is simultaneous presence of pollution and wetting on the insulator surface. The simulation of the above condition may require various pollution test procedures, according to the peculiarity of the environment considered.

Many tests were performed to investigate the pollution influence on the withstand characteristics of insulator configurations under transient overvoltages, ([9.1] to [9.15]).

The available experimental information indicates that the presence of a wetted pollution layer may remarkably affect the strength not only at operating voltage but also under transient voltages.

In the following the performance of external insulation under transient overvoltage will be reviewed with the aim to obtain indications about the strength reduction which is important for the insulator design.

In the appendix a short summary of the knowledge available about the discharge process under transient overvoltages and polluted conditions is also given .

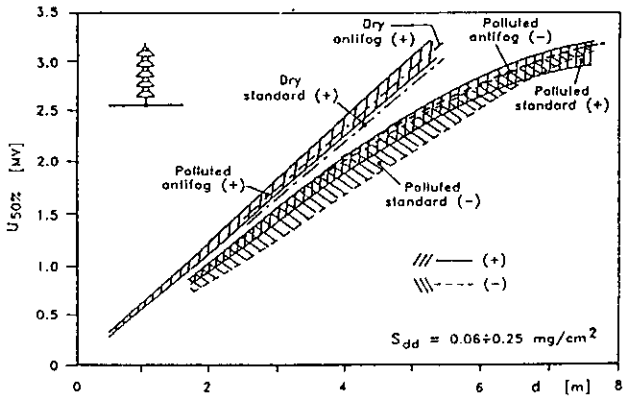

Figure 9.1: LI flashover voltage of cap and pin standard and antifog insulators strings. Solid layer method, wet contaminant. Comparison with data in dry condition [9.5].

9.2 GENERAL TRENDS ABOUT THE PERFORMANCE OF CONTAMINATED INSULATORS UNDER TRANSIENT VOLTAGES

A summary of published data relevant to the performance of contaminated insulators (suspension and post type) under transient overvoltages is presented in the following. Results obtained with different test procedures (salt fog and solid layer) have been analyzed for the following transient voltages:

1a) Lightning impulse (LI) alone
1b) LI superimposed on AC voltages

2a) Switching impulse (SI) alone
2b) SI preceded by AC energization
2c) SI superimposed on AC voltage
2d) SI superimposed on DC voltage

3a) Temporary overvoltage (TO) alone
3b) TO with AC pre-stress

9.2.1 LI PERFORMANCE

a) LI alone

The available data generally refer to the standard LI (1.2/50 μs).

In Figure 9.1, the 50 % flashover voltage of cap and pin insulator strings is given as a function of the insulator length d. The results were obtained by the solid layer method (wet contaminant) with a salt deposit density, Sdd ranging from 0.06 to 0.25 mg/cm². For comparison purpose the strength under dry condition with positive LI is also reported. The figure indicates a remarkable strength reduction in presence of pollution with reference to the dry condition. The reduction tends to increase with the increase of the insulator length leading to non linear characteristics. The strength saturation makes it difficult to keep the LI withstand voltage of insulator strings higher than 3000 kV, particularly for standard units. The strength of standard type insulators is reduced for both polarities, resulting in close values. For antifog insulators the decrease is larger for negative polarity, which therefore represents the most critical one.

The influence of the pollution severity Sdd on the strength reduction is shown in Figure 9.2, which reports the specific flashover voltage as a function of Sdd of the contaminated layer. The performance of standard and antifog cap and pin insulators and smooth cylinder insulator have been considered. The data indicate that the reduction is practically constant above a Sdd of 0.1 mg/cm² for both positive and negative polarities. Further, the results indicate once again the importance of the insulator profile. Strengths as low as 200 kV/m were measured on an insulator model without sheds (smooth glass cylinder).

b) LI superimposed on AC

Results given in [9.4] indicate that dry bands on the surfaces of polluted insulators result in the most significant lowering of impulse strength for heavily

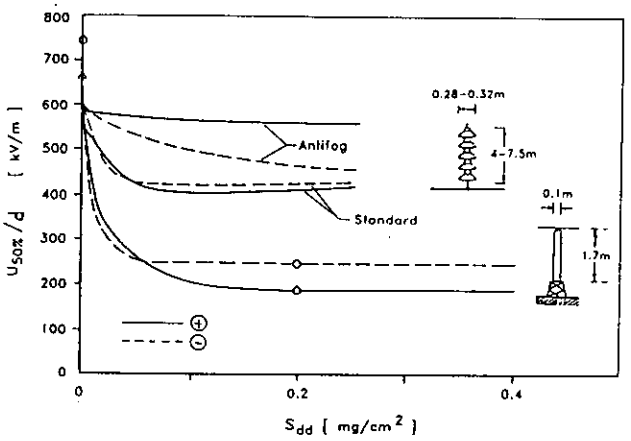

Figure 9.2: LI flashover voltage of cap and pin insulators strings and of a post insulator model as a function of pollution severity. Solid layer method (wet contaminant) [9.5].

polluted insulators. This reduction is about 30-40 % with reference to the strength obtained with LI only. Without dry bands the strength reduction is about 10-20 %.

9.2.2 SI PERFORMANCE

a) SI alone

As for air gaps, the influence of the impulse shape is to be expected also for contaminated insulators. Unfortunately few data are available in this respect [9.6], [9.7], and they refer to rather short insulator lengths (1 to 2 m), thus not allowing very quantitative indications. However, as a general trend, the strength tends to be lower with the longer impulse duration.

Most of the investigations were carried out with impulses close to the standard one (250/2500 μs) and of positive polarity, which is also the most critical voltage polarity under contaminated conditions. Consequently, in the following major attention will be paid to standard impulse shapes of positive polarity.

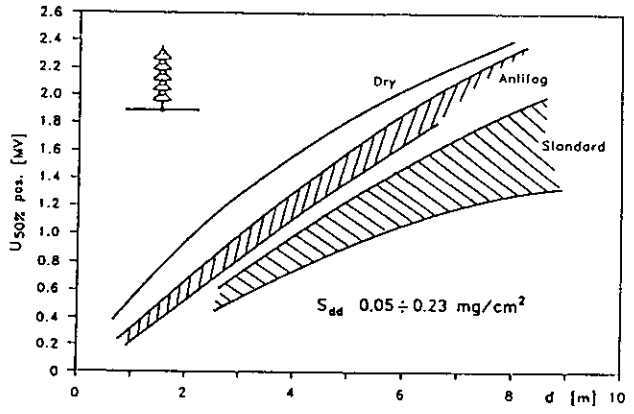

Figure 9.3: SI flashover voltage of cap and pin insulators strings as a function of insulators length. Solid layer method, wet contaminant [9.3], [9.7].

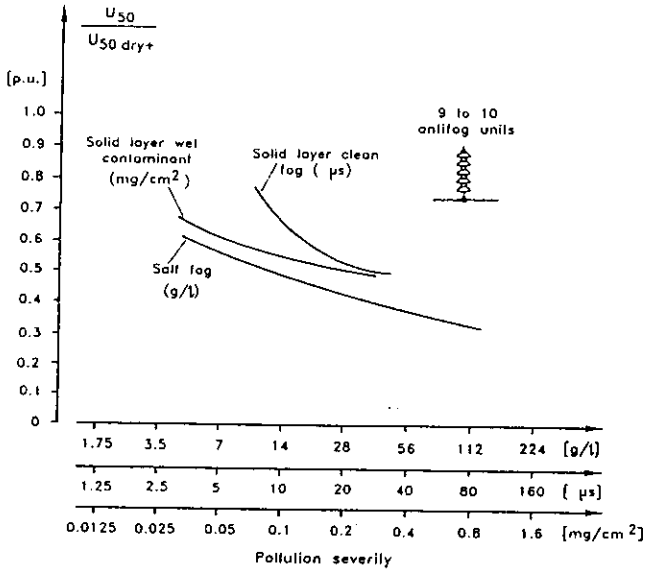

Figure 9.4: SI flashover voltage of cap and pin insulators strings in per unit of the flashover voltage in dry condition as a function of pollution severity. Solid layer and salt fog methods [9.1], [9.7].

The presence of pollution and wetting can cause a heavy strength reduction with respect to dry condition, as shown by the set of data of Figure 9.3, which reports the strength of cap and pin insulator strings as a function of the string length (data derived from [9.3], [9.7], obtained with the solid layer method and referring to a Sdd range from 0.05 to 0.23 mg/cm^2). Again the insulator profile plays a major role: the reduction with standard type insulators is much larger than with antifog one.

The strength reduction depends largely on pollution severity, as evident from Figure 9.4 (data derived from [9.1] and [9.7], obtained with salt fog and solid layer methods, respectively).

The data in Figure 9.4 show that the strength tends to decrease when the pollution severity is increased, even for high pollution severity.

b) SI preceded by AC energization

Results, obtained with standard and antifog cap and pin insulators, standard and antifog long rod insulators and post type insulators, are summarized in Figure 9.5. The pollution tests considered have been performed using the salt fog method with test severities ranging from 2.5 to 225 g/l. The figure shows the ratio $U_{50}/U_{50\ dry}$ versus test severity (g/l) for both polarities. For comparison purposes corresponding data obtained with SI alone are also given.

It is evident that the AC pre-stress produces a reduction in the SI strength, which is more pronounced with negative polarity.

c) SI superimposed on AC voltage

Results, relevant to standard and antifog cap and pin insulators and standard long rod insulators, are summarized in Figure 9.6. The data, obtained by salt fog method, indicate a strength reduction similar to that obtained in the case of SI preceded by AC energization.

d) SI superimposed on DC voltage

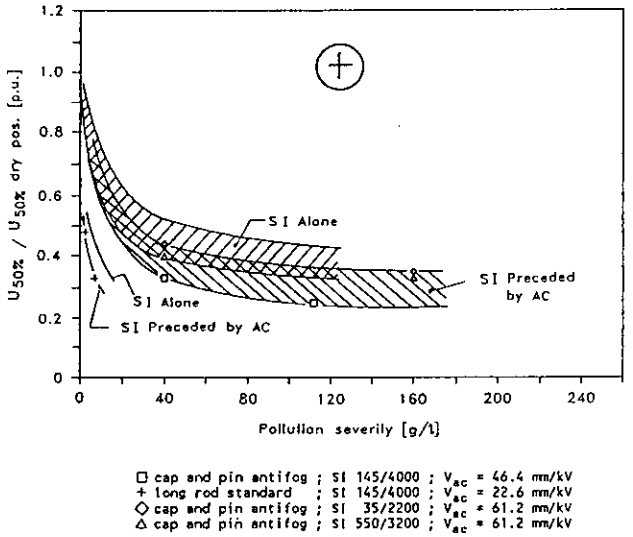

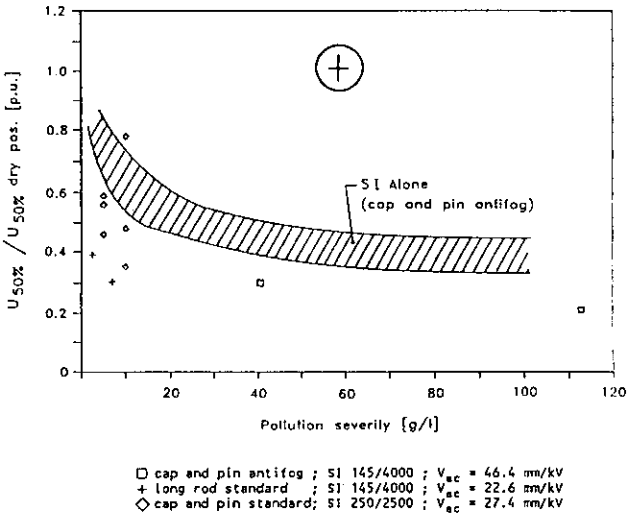

Figure 9.6: Pollution tests (salt fog method) with SI superimposed on AC on cap and pin and long rod insulators. Comparison with data relevant to SI alone [9.1], [9.11].

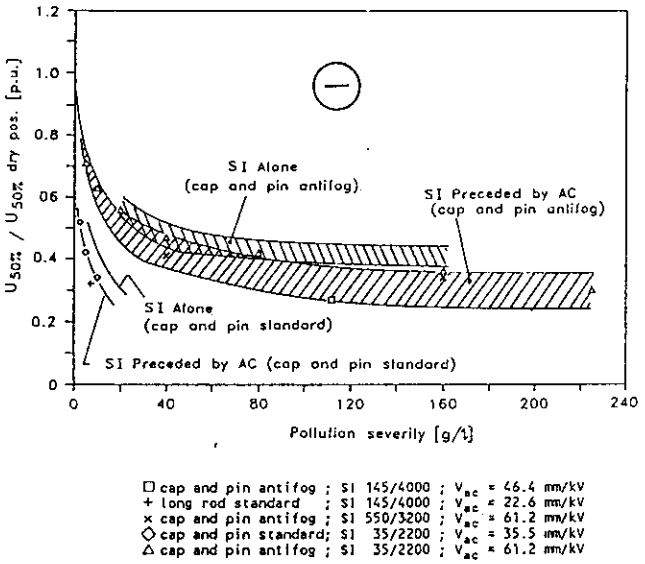

Figure 9.5: Pollution tests (salt fog method) with SI preceded by AC on cap and pin and long rod insulators. Comparison with data relevant to SI alone [9.1],[9.2].

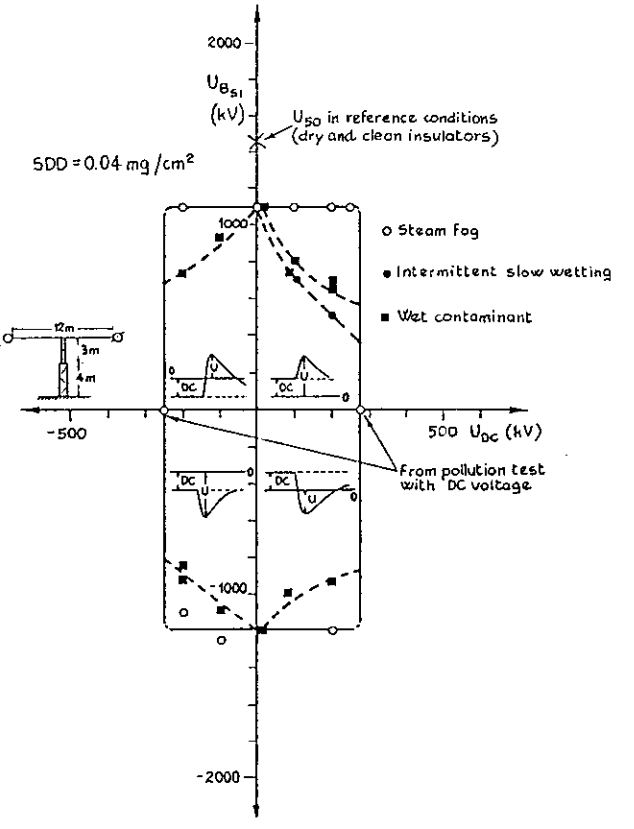

Figure 9.7: Pollution tests (solid layer method) on insulators columns with SI superimposed on DC [9.11].

Figure 9.7 shows the SI flashover voltages as a function of the DC pre-stress, varying both amplitude and polarity. The results were obtained by the solid layer method (wet contaminant) with a fixed test severity (Sdd = 0.04 mg/cm²).
Again, the data point out that the pre-stress may have a remarkable influence on the strength.
It is evident that the strength reduction is strongly influenced by increasing the amplitude of the pre-stress voltage.

e) Influence of dry bands on the SI strength

As suggested in [9.11], the additional strength reduction found with composite voltages may be attributed to the dry bands formed by the applied pre-stress. Tests made without pre-stress but with non uniform pollution distribution (dry bands simulation) gave results similar to those obtained with pre-stress applied to uniformly contaminated insulators, as shown in the example of Figure 9.8.

9.2.3 PERFORMANCE UNDER TRANSIENT OVERVOLTAGE

As long as the overvoltage duration increases, the flashover process becomes closer and closer to that under permanent AC voltage.

Figure 9.9 shows examples of results obtained with various pollution procedures [9.15] on porcelain

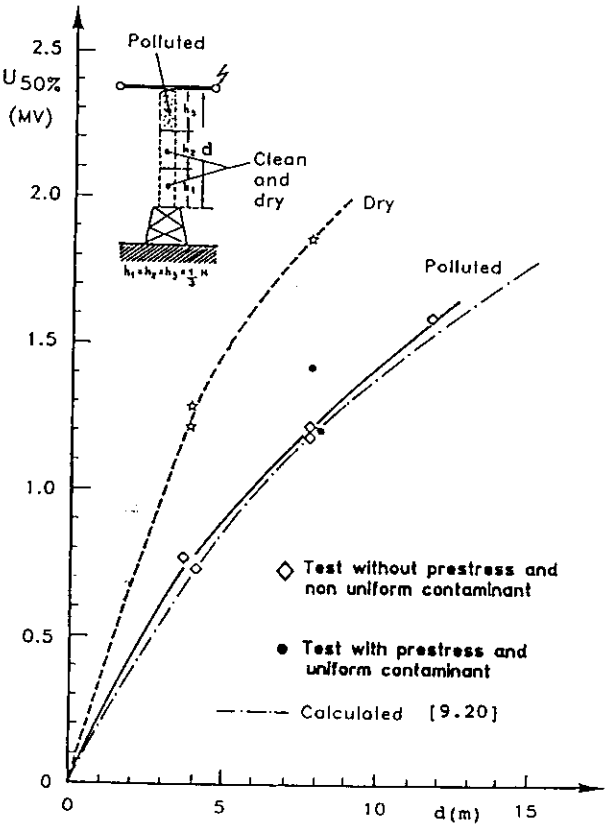

Figure 9.8 Tests on insulator column [9.10]. Comparison of the results:
- in dry condition under positive SI
- contaminating uniformly the column and applying a positive SI preceded by AC
- contaminating non uniformly the column and applying a positive SI alone (solid layer method, wet contaminant, Sdd=0.04 mg/cm²)

housing (longitudinal insulation of circuit breaker). In the figure the flashover voltage obtained with TO is given in p.u. of the strength measured with permanent voltage, with the same pollution method, and is reported as a function of the TO application time. It is clear from the figure that the flashover voltage tends to come towards permanent voltage and with a relatively short duration overvoltage. However the curves show different trends which may be related to the test procedure and test object characteristics.

The pre-stress affects also the strength with TO [9.12], [9.15]. Examples of results obtained with pre-

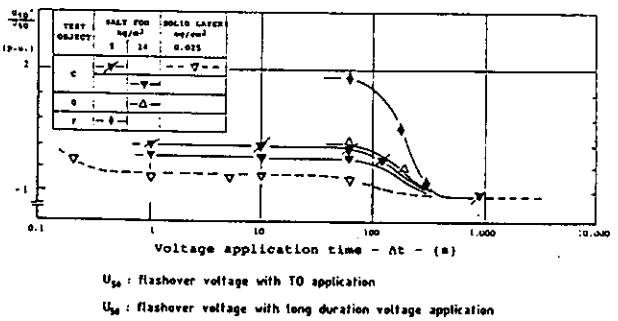

Figure 9.9: Pollution tests on longitudinal circuit breaker insulation with TO. Flashover voltage vs. overvoltage application duration.

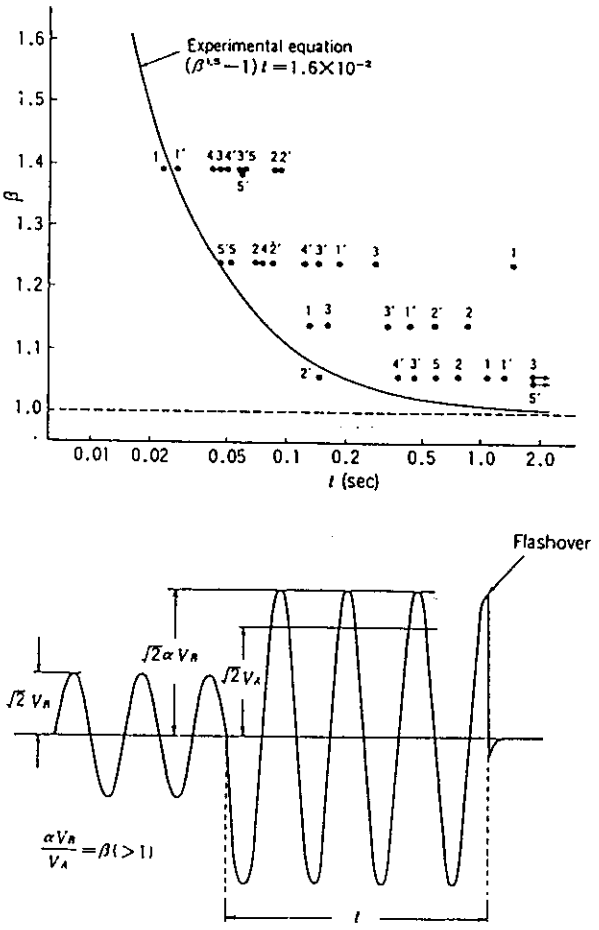

VA : Withstand voltage of an insulator string derived from the continuous energization methods : the Wet Contaminant Method or the Fog Withstand Method
VB : Base voltage simulating the normal operating condition.
t : Time to flashover.
α : Overvoltage factor.
β = αVB/VA : Ratio of overvoltage to withstand voltage.

Figure 9.10: Pollution test on suspension type insulators with TO preceded by AC energization. Flashover voltage vs. overvoltage application duration.

stress are shown in Figure 9.10 [9.12]. With pre-stress the strength becomes very close to that under permanent voltage for voltage application durations in the second range.

9.3 IMPORTANCE OF THE EXAMINED STRESS CONDITIONS FOR INSULATOR DESIGN PURPOSES

The analysis of the available information has shown that the strength of insulators under transient overvoltages and contaminated conditions may be much lower than that in dry condition. This reduction becomes even higher in the presence of dry bands, i.e. when an overvoltage occurs on a polluted insulator, being already energized.

A preliminary indication of the impact of transient overvoltages under pollution conditions on the design may be obtained by comparing the strength with the stress expected under the overvoltages considered. In this respect it is convenient to compare the transient overvoltage strength of contaminated insulators with that required by the same insulator under permanent AC voltage, when subjected to the same contamination condition.

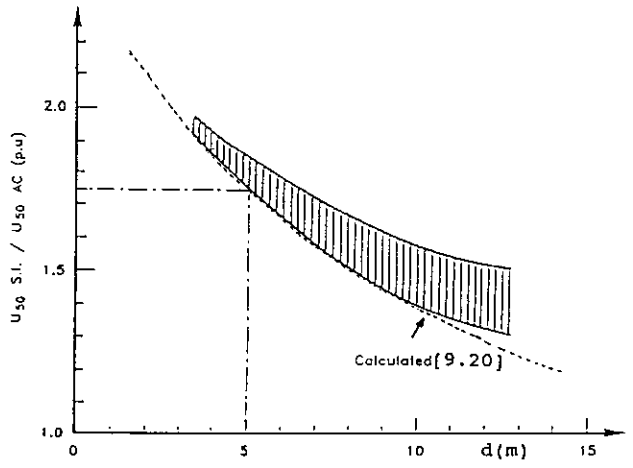

Figure 9.11: Ratio between the positive SI strength and the AC strength as a function of the insulator length. Solid layer method, wet contaminant, Sdd = 0.04 mg/cm^2 .

Starting from the data in Figure 9.1 it can be easily derived that the LI strength under contaminated conditions is 4-5 times that under AC.

The SI strength becomes closer to that under AC.
As an example Figure 9.11 reports the ratio between SI and AC strength as a function of the insulator length (data from [9.10], obtained with solid layer method).
The figure indicates that, at least for the configuration considered, the ratio decreases with insulator length reaching values as low as 1.3 - 1.5 p.u. for very long insulators. When comparing the strength with possible switching overvoltage stresses (usually higher than 1.5 p.u.) the importance of the examined condition for design purpose appears evident.

The strength under TO can be very close to that under AC (see Figure 9.9 and 9.10).

9.4 CONCLUSIONS

Contamination may significantly reduce the strength of insulators under transients overvoltages with respect to the reference dry condition.

A more precise indication about the criticality of the transients should be based on a statistical analysis, taking into account the probability of the simultaneous occurrence of high values of the overvoltages and of critical contamination conditions [9.15].

REFERENCES

[9.1] G. Carrara, M. Sforzini, "Analysis of pollution test methods", IEEE CP 68-CP-163, 1968.

[9.2] Ely, Roberts, "Switching impulse flashover of air gaps and insulation in an artificially contaminated atmosphere", Proc. IEE, Vol. 115, N.11, 1968.

[9.3] Okada, Koga, "Switching surge flashover characteristics of long disk insulator strings under polluted conditions", IEEE PAS 89, N.3, March 1970.

[9.4] Lushnikoff, Parnell, "The effects of pollution and surface discharges on the impulse strength of line insulation", IEEE PAS 90, N.4, 1971.

[9.5] Okada, Kimoto, Koga, "Lightning impulse flashover characteristics of long disk insulator strings under polluted conditions", IEEE Paper, 71-CP 114-PWR, 1971.

[9.6] Macchiaroli, Turner, "Switching surge performance of contaminated insulators", IEEE Paper 71 TP-141-PWR, 1971.

[9.7] Hiroshe, Seta, Ichiara, Anjo, Okada, "Switching surge insulation characteristics of insulators under polluted condition", CIGRE Report 33-83 (WG 04).

[9.8] Kizewetter, Lebedev, Merkhalev, Ostapenko, "characteristics of EHV insulation in contaminated and moist conditions", CIGRE Session 19.. 33-16.

[9.9] Kucera, Plechanova, "A probabilistic choice of insulators for alternating voltage and electric strength at switching impulses in the areas with pollution", CIGRE Session 1982, 33-04.

[9.10] Garbagnati, Marrone, Porrino, Perin, Pigini, "Switching impulse performance of post insulators in polluted conditions", 5th ISH, Braunschweig 1987.

[9.11] Cortina, Marrone, Pigini, Thione, Petrusch, Verma, "Study of the dielectric strength of external insulation of HVDC systems and application to design and testing", CIGRE 1984 Session, 33-1.

[9.12] Itabashi, Osada, Seta, Naito, "A study of short-time AC flashover voltage of contaminated insulators and a consideration of its application to transmission line design", IEEE PAS 95, 1976.

[9.13] Macchiaroli, Turner, "Comparison of insulator types by the wet contaminant and clean fog test method", IEEE PAS 89, Feb. 1970.

[9.14] Kimoto, Fujimura, Naito "Performance of heavy duty UHV disk insulators under polluted condition", IEEE Paper No 71 TP 649-PWR.

[9.15] Bargigia, Marrone, Mazza, Perin, Pigini, "Longitudinal insulation performance of HV circuit breakers under the joint effect of pollution and temporary overvoltages", CIGRE 1990.

[9.16] Erler F., "Neue Erkenntnisse über die Vorlichtbogenverlängerung während des Kriechüberschlages dicker Isolatoren bei Impuls- und Wechselspannung", Doctoral Thesis 1970. Dresden University of Technology.

[9.17] MOSCH W, LEMKE E., "Switching surge flashover of insulators under pollution condition", IIT MADRAS 1981.

[9.18] Toepler M., "Zur Kenntnis der Gesetze der Gleitfunkenbildung", Annalen der Physik 21 (1906) 193-222.

[9.19] Lemke E., "Durchschlagmechanismus und Schlagweite-Durchschlagspannungs-Kennlinien von inhomogenen Luftfunkenstrecken bei Schaltspannungen", Doctoral Thesis (1967) Dresden University of Technology.

[9.20] Lemke E., Zhrih M., "SI flashover model for long insulators under contaminated condition", 7th ISH Dresden (1991) paper 43.22.

[9.21] Obenaus F., "Der Einfluss von Oberflächenbelag (Tau - Nebel - Salz - Schmutz) auf die Überschlagspannung von Isolatoren", Hescho-Mitteilungen (1933) H. 70, 2203-2239.

[9.22] Hampton B. F., "Flashover mechanism of polluted insulation", Proc. IEE 11 (1964) 5, 985-990.

[9.23] Rizk F., "Mathematical models for pollution flashover", ELECTRA 78 (1981) 71-103.

APPENDIX

EVALUATION OF THE DISCHARGE PROCESS UNDER TRANSIENT OVERVOLTAGES

Let us consider an impulse voltage with a time to crest (t_s) much smaller than the time to half value (t_h). The main influence on the leakage flashover is given by t_h [9.16], [9.17] (see Figure A1). At very short times to half value (t_h smaller than 200 μs) no pre-arc will occur and mainly streamer discharges could develop. Then the flashover voltage is determined by the requirement of voltage for streamer discharges and may attain a value close to dry conditions.

At very long times to half value, i.e. longer than 3000 μs, a long pre-arc could be formed. In this case, the specific leakage flashover voltage will be determined by the pre-arc only and reaches values of approximately 0.7 kV/cm.

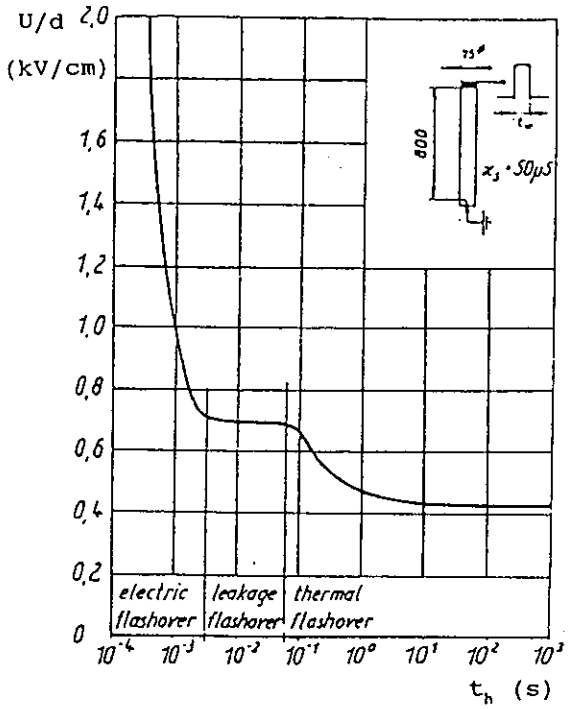

Figure A1: Flashover strength versus the voltage time duration for a cylindrical model insulator under pollution conditions [9.17].

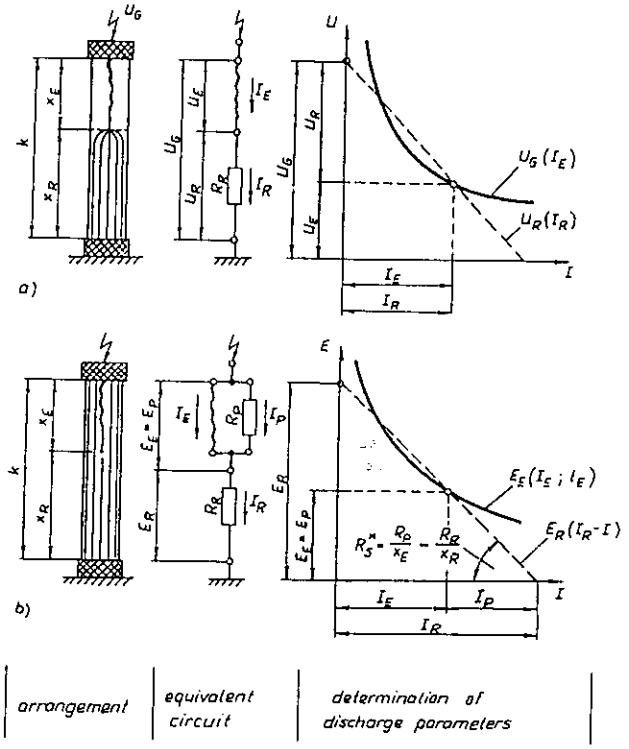

Figure A2: Flashover models for AC/DC (a) and SI (b) [9.20].

With virtual impulse duration longer than 100 ms, a further decrease of the flashover voltage will be observed. This is not caused by a new flashover mechanism but due to the fact that the pollution layer will be heated up by the current flowing for a longer time duration, and the surface conductivity will be increased.

In the range between 200 and 3000 μs of t_h (SI range) the performance is more complicated, as analyzed in the following.

EVALUATION OF THE DISCHARGE PROCESS UNDER SWITCHING OVERVOLTAGES

Discharge without dry bands (application of SI only)

Based on the analysis of experimental data as well as on simplified assumptions for the very complex flashover mechanism specially for a leader discharge [9.18], [9.19] a flashover model was developed [9.20]. Whereas the AC/DC flashover is governed by the pre-arc [9.21]to [9.23], it is not the case with the SI stress where the leader discharge becomes more important. Because of its comparatively short life time and low energy dissipation the leader may not produce any dry bands, as in the case of an existing pre-arc. Furthermore, the main leader gradient is much higher than the gradient in the pre-arc, i.e. the current absorbed by the bridged layer can not be neglected, as in the case of AC / DC stresses. From this follows that, instead of the usual voltage (U) - current (I) characteristic for AC / DC, for SI only the strength (E) -current (I) characteristic is applicable [9.20], in order to evaluate the instantaneous discharge parameters (Figure A2).

Analogous to the AC / DC flashover criterion, a critical condition for the SI flashover arises, if the dotted straight line in Figure A 2b, which represents the negative slope of the layer resistivity per unit length, becomes a tangent of the E-I leader characteristic, given by the full curve in Figure A 2b.

Discharge with dry bands (application of SI with pre-stress)

As reported in [9.10], the SI strength may essentially be reduced in the presence of dry bands. If the flashover strength is drawn versus the dry band length, typical U-curves are obtained.

In the presence of a short dry band, having a length a_T (Figure A3), the flashover under positive SI first occurs along this dry band in a very short time (air breakdown in the μs range), followed by the flashover along the contaminated layer of the length a_B during a much longer time period (creepage flashover in the ms range).

For dry band lengths smaller than 1 m, the strength of the air gap corresponds to the positive streamer gradient, i.e. 450 kV/m. For longer dry band lengths the mean breakdown strength corresponds to the minimum possible breakdown voltage per unit length of long air gaps under positive SI, i.e. it can be expressed by the well known SI strength of the rod-plane gap in air.

In order to check if the developed approach works, even for insulators of practical interest, results of calculation are compared with available experimental data. Because non-uniform contamination is to be regarded as the worst case, only the presence of dry bands of critical lengths shall be considered in the following.

As an example, Figure 9.8 shows the results obtained

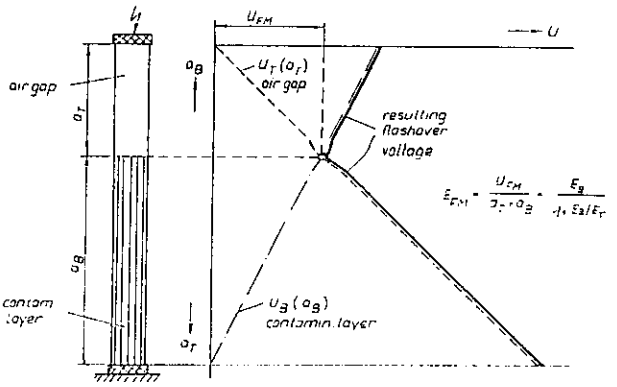

Figure A3: Approach for the evaluation of the minimum flashover strength in the presence of dry bands [9.20].

for a post insulator, where experimental data of [9.10] are used. As evident from the dotted curve, the calculation meets the measurements quite well up to the longest investigated insulator length of 12 m.

Another example is reported in Figure 9.11. Here, the calculated minimum curve is also in satisfactory agreement with experimental data from [9.10] for practical insulators up to 12 m length.

10 INFLUENCE OF ICE AND SNOW

by T. KAWAMURA, K. NAITO

10.1 INTRODUCTION

In some cold areas, heavy snow and/or freezing rain are encountered and the insulators are sometimes covered with snow or ice. When snow or ice are not melted, they do not exhibit low resistivity. In the process of melting, however they exhibit lower resistivity, partially or in considerable portion along the surface of the insulators. Observation of the dynamic leakage current and resistivity with time was observed by many researchers [10.1]. Such phenomena may cause partial drying, sparking, etc. on the surface along the insulators which is similar to that observed on polluted and wetted insulators. Thus, there is a considerable reduction of the flashover voltage of the insulators after they are covered with snow or ice and when the snow or ice is melting.

10.2 CRITICAL CONDITIONS AND MAIN INFLUENCING PARAMETERS

There are many publications on understanding the degradation of surface insulation by snow or ice, but there are only few on actual insulator string assemblies covered with snow [10.2 to 10.7] or ice [10.2], [10.7 to 10.10]. This is because of the difficulty in carrying out the impulse voltage tests on insulators covered with snow or ice. Typically, the worst condition of snow-covered insulators is found on tension insulator string assemblies. Typical worst conditions of ice-covered insulator are found on suspension insulator string assemblies because ice cycles do not tend to bridge individual sheds of horizontally mounted insulators. Thus, all the test results published were on insulators assuming the above situations.

It is very difficult to make flashover tests with natural snow or ice on insulators; in the tests reported so far snow or ice seems to have been artificially formed. Namely, in the case of a snow test natural snow from the ground was moved and piled on the insulators in some way by the laboratory technicians. The resistivity of the water melted from the snow was 20 - 150 kΩ cm. In the case of ice tests, water in cold weather was sprayed by using suitable hoses on insulators, and then froze on the insulators. The resistivity of the water used was 70 - 300 kΩ cm. Table I gives the summary of all the resistivity values from the References.

TABLE I: Summary of resistivity of water melted from snow or that used for producing ice.

Ref.	RESISTIVITY (kΩ cm) Snow	Ice
10.1	-	-
10.2	-	30
10.3	40-60	-
10.4	20-100	-
10.5	20-30	-
10.6	20-100	-
10.7	25-150	15
10.8	-	15
10.9	-	15
10.10	-	7
10.11	-	-

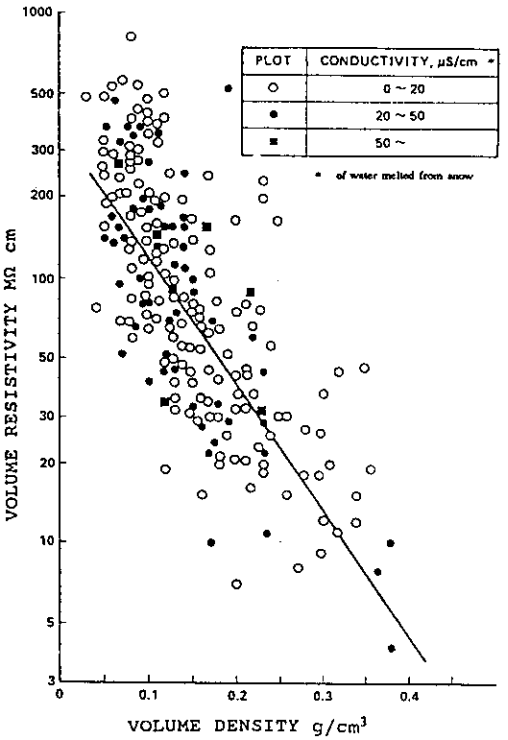

Figure 10.1: Relation between volume density and apparent resistivity of snow as it was [10.11].

Impulse flashover voltage characteristics of snow or ice covered insulator assemblies have been usually obtained by applying the impulse voltage without superimposing the AC operating voltage before tests. On an actual line, however, switching or lightning surge attacks the insulator assemblies covered with snow. But the snow condition is critical due to the melting of the snow by leakage currents and/or partial discharges under the AC operating voltage. In view of this, a few tests have been made on snow or ice covered insulator string assemblies, while simulating the effect of the superposition of impulse voltage on the AC operating voltage.

Since the performance of a snow or ice covered insulator is influenced by the resistivity of the snow or ice, the obtained data appear to be well characterized by the resistivity of water melted from snow or ice [10.3], [10.11]. Also, because the good correlation between volume density and volume resistivity of the snow [10.11] as shown in Figure 10.1, some flashover data are characterized by the volume density of snow [10.6]

10.3 GENERAL TRENDS ABOUT THE DIELECTRIC PERFORMANCE OF SNOW OR ICE COVERED INSULATORS

Linearity was found between the switching impulse flashover voltage and the insulator length, for line insulators when they were covered with snow [10.2], [10.3], [10.5]. An example of the data is shown in Figure 10.2 [10.5].

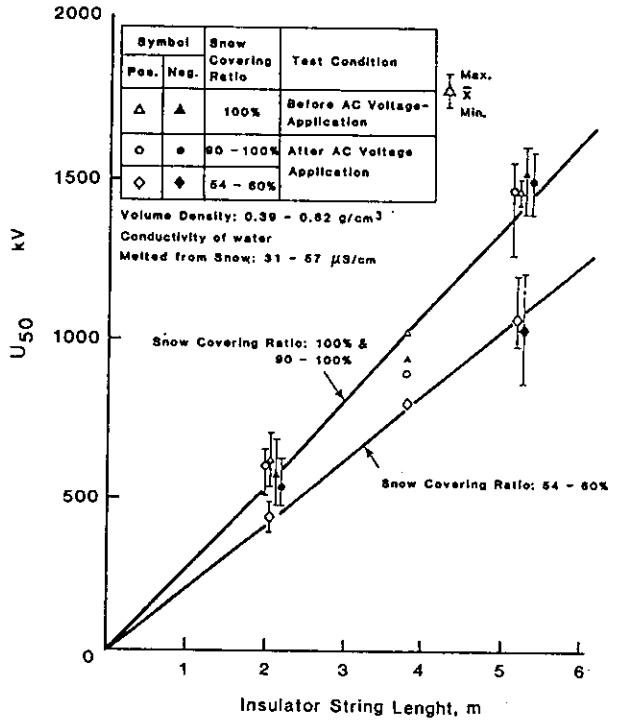

Figure 10.2: Relationship between U_{50} under SI and insulator string length [10.5].

The relationship between the length of longitudinal snow coverage on the insulator string and the switching impulse flashover voltage results in a U-shaped curve [10.2 to 10.7]. Minimum flashover voltage lies at 60 to 80 % of the snow covering ratio. Typical examples are shown in Figure 10.3 [10.5]. Figure 10.4 shows the relationship between the switching impulse flashover voltage of snow covered insulator assembly and the volume density of the snow. Flashover voltage decreases as the volume density increases but there is no reduction of flashover voltage for volume density greater than 0.6 g/m³ [10.6].

As shown in Figure 10.5, linearity was also found in the relationship between the lightning impulse flashover voltage of the snow covered insulator assembly and the gap spacing between the arcing horns [10.4]. A drastic reduction of 35 - 50 % in the

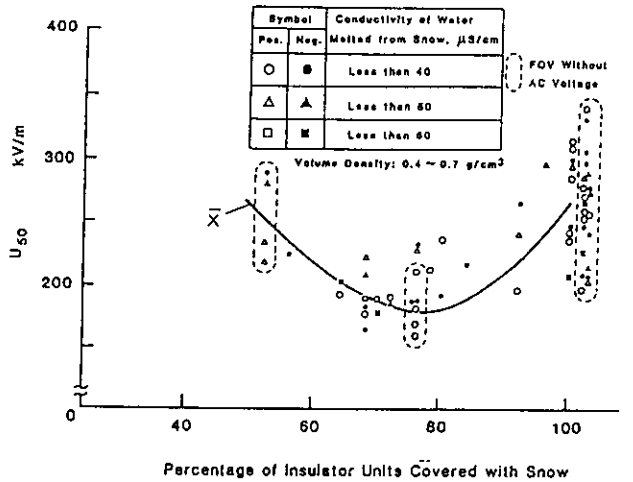

Figure 10.3: Relationship between U_{50} under SI and the percentage of insulators units covered with snow [10.5].

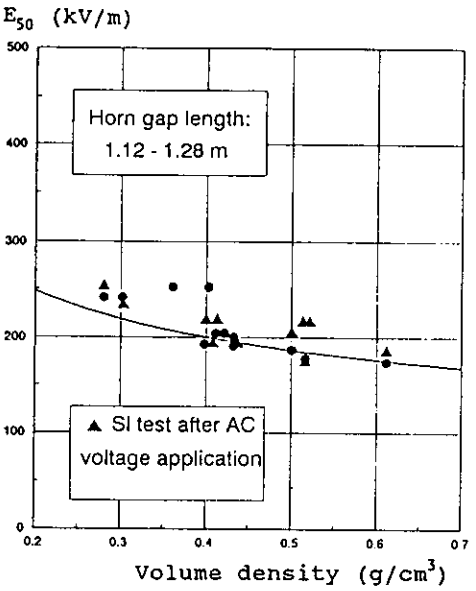

Figure 10.4: Relationship between SI flashover voltage and volume density of the snow [10.6].

flashover voltage compared with the case without snow on the insulator assembly is seen in this Figure. No special tendency in the relationship between the flashover voltage of snow covered insulator assemblies and the snow covering ratio has been confirmed. Minimum flashover voltage was however obtained at the snow covering ratio of 100 % (complete coverage).

No clear relationship has been reported between the switching impulse flashover voltage and insulator length when insulators were covered with ice. However, the flashover voltage of suspension insulator string [10.6 to 10.10] and station post insulators stack [10.8] is said to have fallen to 50 % or so of that under clean and dry condition. Figure 10.6 shows an example of published data [10.9].

10.4 CRITERIA FOR INSULATION DESIGN

The AC withstand voltage characteristics of a tension insulator string covered with snow is shown in Figure

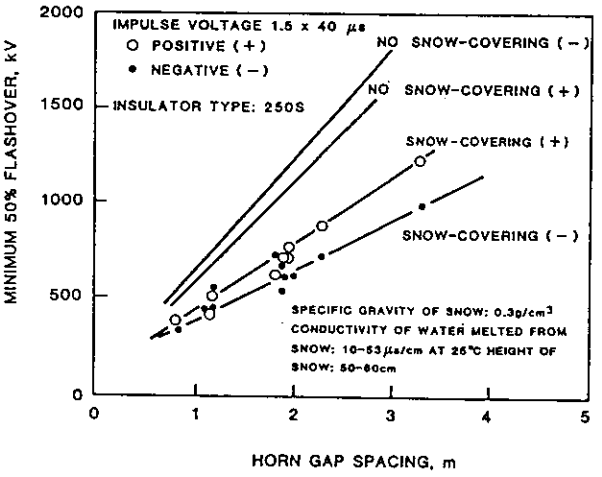

Figure 10.5: Lightning impulse. 50% flashover voltage of snow covered assembly [10.4].

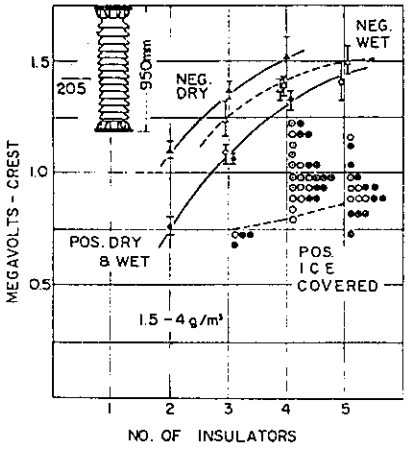

Hollow marks show wet condition. Marks ⊙, ● and--- show flashover voltages of stacks covered with ice for positive switching surge.

⊙ ; five flashover data

● ; five withstand data

Figure 10.6: Positive and negative flashover characteristics of solid-core cylindrical post insulator stacks for switching impulse voltage with a virtual front time of 120 to 140 μs.

10.7 [10.7]. Similar AC withstand voltage characteristics are indicated for various insulators covered with ice in [10.3]. There is additional literature showing similar AC characteristics, but there is no literature which indicates DC withstand voltage characteristic except [10.2]. Referring to these, consideration on the application criteria to insulation design may be made.

Design criteria for withstand voltage of insulators covered with snow or ice is indicated as 75 kV/m for AC and DC voltages and 200 kV/m for switching impulse voltages [10.2]. Thus, the design for AC and DC

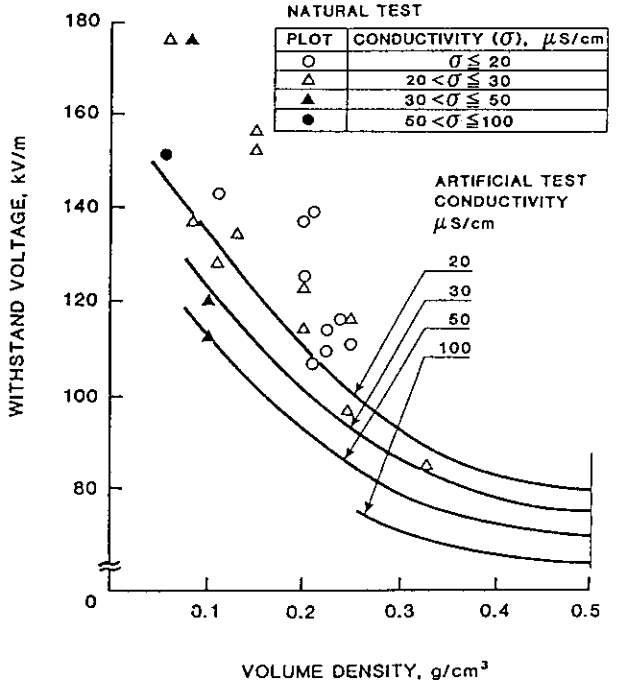

Figure 10.7: Withstand voltage as a function of volume density of the snow [10.7].

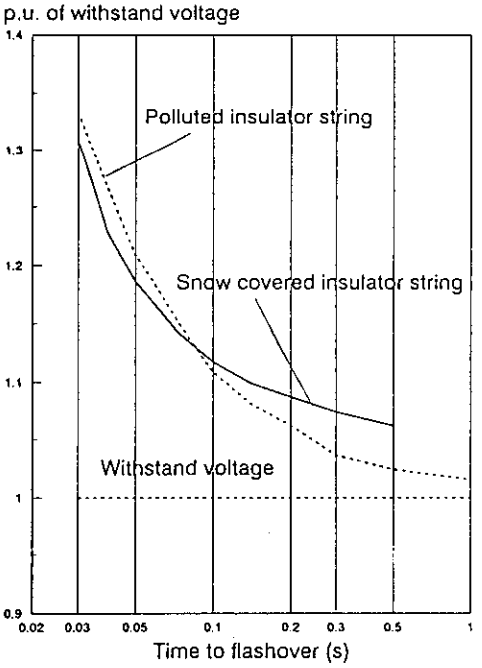

Figure 10.8: Time to flashover voltage characteristics of snow covered insulator string compared with a polluted insulator string [10.12].

operating voltage can be considered conservative for switching surges of less than about 1.9 p.u. [10.2]. But switching impulse voltage characteristics can be critical for a system of larger surge magnitude. For snow or ice of low conductivity, insulator length may be critical, and the resulting lower withstand voltage characteristics should be considered.

Lightning impulse flashover voltage is also reduced to 50 % or so of that under dry conditions. Whether an insulation design should take into account this characteristic or not, shall be determined considering the amount of accumulation of snow or ice, probability of simultaneous occurrence of lightning, and also lightning performance of the concerned systems [10.3].

There are only a few reports on the performance of AC withstand characteristics against simulated temporary AC overvoltage [10.4], [10.12]. Figure 10.8 shows a summary from [10.12] which indicates that a curve for snow covered insulators is almost the same as that for polluted insulators. Thus, a design criteria similar to that for pollution may be employed.

10.5 CONCLUSIONS

After evaluating the performance of insulation system under snow and ice situations, the following guideline evolve:

- Insulation design of a transmission line is generally determined by the insulator contamination design for AC operating voltage.
- Snow or ice, depending upon the resistivity of water melted, can be more serious than ordinary pollution.
- Switching or lightning impulse flashover voltage can be reduced by 50 % or so. Thus, switching or lightning surge may be critical to the external insulation.
- An insulation design should be determined taking in to account the amount of accumulation

of snow or ice.

- The probability of a simultaneous occurrence of lightning and a magnitude of switching and lightning surges that may result in insulation failure, should be evaluated.

- For an AC temporary overvoltage, the design criteria similar to that for pollution may be employed.

10.6 REFERENCES

[10.1] H. M. Khalifa, R. M. Morris,"Performance of line insulators under rain ice", IEEE Trans. on PAS, Vol. PAS-86, No. 6, 1967.

[10.2] Y. Watanabe, "Flashover tests of insulators covered with ice or snow", IEEE Trans. on PAS, Vol. PAS-97, No. 5, Sept./Oct. 1978.

[10.3] T. Fujimura, K. Naito, Y. Hasegawa, T. Kawaguchi,"Performance of insulators covered with snow or ice", IEEE Trans. on PAS, Vol. PAS-98, No. 5, Sept./Oct. 1979.

[10.4] H. Matsuda, H. Komuro, K. Takasu, "Withstand voltage characteristics of insulators strings covered with snow or ice", IEEE PES Summer Meeting Paper No. 90 SM 355-8 PWRD, 1990.

[10.5] M. Yasui, T. Iwama, Y. Sumiya, K. Naito, R. Matsuoka, M. Nishikawa, "Investigation of switching impulse flashover voltage performance of UHV class tension insulator assembly covered with snow", IWAIS-90 Paper No. B4-5-(1), 1990.

[10.6] K. Takasu, H. Matsuda, H. Ogawa, "Withstand voltage characteristics of insulator strings covered with snow", CRIEPI Research Report No. T88026, December 1988 (in japanese).

[10.7] T. Udo, "Switching surge sparkover characteristics of air gaps and insulator strings under practical conditions", IEEE Trans. on PAS, Vol. PAS-85, No. 8, pp. 859-864, 1966.

[10.8] T. Udo, T. Tada, Y. Watanabe, "Switching surge sparkover characteristics of air gaps and insulator strings under the non-standard conditions", IEEE Trans. on PAS, Vol. PAS-87, No. 7, pp. 361-367, 1967.

[10.9] T. Udo, Y. Watanabe, K. Mayumi, G. Ikeda, T. Okada, "Switching surge flashover characteristics of long insulator strings and stacks", CIGRE Paper, 25-04, 1968.

[10.10] J. E. Brown, C. L. Nellis, L. Y. Lee, "Switching impulse and 60 Hz performance of iced 500 kV insulators strings", Bonneville Power Administration, Technical Report, No. ERJ-75-9, January 16, 1975.

[10.11] M. Yasui, K. Naito, Y. Hasegawa, "AC withstand voltage characteristics of insulator string covered with snow", IEEE Trans. on PD, Vol. 3, No. 2, April, 1988.

[10.12] M. Yasui, "Insulation design of UHV AC transmission line", Trans. of IEE of Japan, Vol. 107-B, No. 5, pp. 244-250, 1987 (in japanese).

11 INFLUENCE OF HIGH TEMPERATURE AND COMBUSTION PARTICLES (PRESENCE OF FIRES)

by J. FONSECA, K. SADURSKY, A. BRITTEN, M. MORENO, J. VAN NAME

11.1 INTRODUCTION

Fire has been reported as responsible for power systems outages in many countries [11.1].

Types of fires which cause outages include: burning sugar cane fields, forest fires, grass fires, refuse burnings, oil fires, natural gas fires, etc.

The flashover voltage of air insulation at high temperatures, as under fire conditions, is drastically reduced when compared with values at ambient temperature.

The dielectric strength is dependent on the type of voltage stress (AC, DC, impulse) and also on the proportion of the gap covered by flames.

At high temperatures the flashover voltage of an electrode configuration is reduced due to the main following principal changes within the gap:

Decrease of the relative air density

For constant pressure the relative air density decreases with increasing temperature according to the expression:

$$\delta = \frac{0.289\ p}{273+t} \qquad (11.1)$$

where p is in mbar and t in °C.

Field measurements have shown that in the flames, temperature values of 900 °C can be reached, thus δ can be reduced to 0.25.
The reduction for air density may be evaluated according to the procedures given in chapter 7.

Generation of combustion particles in the gap

In the presence of fires a great number of floating particles are generated within the gap. The quantity of generated particles varies with the fire source being, for example, greater for grass or sugar cane fires than for alcohol or gasoline fires. These particles produced by burning are responsible for the greatest reduction on the breakdown voltage under fire.

Other phenomena, such as thermoionic emission from electrodes, [11.2] can occur at high temperatures but these are not usually encountered on the fires of interest here.

These phenomena may affect the strength under laboratory conditions, specially in short gaps under fire, where such levels of temperature could eventually be reached.

11.2 DIELECTRIC STRENGTH

As shown in the previous chapters for other environmental conditions the dielectric strength may depend on the type of voltage stress. Unfortunately most of the available data has been obtained only under permanent (mainly AC) voltages.

11.2.1 Power frequency voltage

Table I shows the flashover voltage of a 3 m conductor-plane configuration under various temperatures originating from different fire sources [11.3].

Table I: Dielectric strength at power frequency voltage of a 3 m conductor-plane configuration.

Gap conditions	Flashover voltage kV/m (rms)
Without fire, t=15 °C	250
Without fire, t=100 °C	190
Without fire, t=120 °C	170
Fire with gasoline	100
Fire with alcohol	80
Fire with sugar canes leaves [1]	50

[1] Discharge gap taken from conductor to the tip of the cane.

The results indicate that the flashover voltage depends on the combustion material and is a minimum when the gap is bridged by flames of sugar cane leaves. The largest reduction of the strength in this case is believed to be caused by a much higher density of burning particles generated in the gap by the sugar cane fire rather than by the alcohol and gasoline fires.

Tests under sugar cane fire were performed in Brazil [11.6], in a 1 m conductor-conductor and conductor-plane (conductor-tip of the cane) configuration (Table II).

Table II: Dielectric strength of a 1 m gap, under sugar cane fire.

Configuration	Withstand voltage kV/m (rms)
conductor-plane	35
conductor-conductor	35

The lower strength values obtained in these tests can be attributed to the test procedure used (withstand test). In case of the flashover test (Table I) the voltage was continuously increased up to flashover. As the fire of sugar cane leaves was very fast and had a random behaviour it probably happened that lower voltages were not simultaneously applied with the worst fire conditions giving, for this reason, an indication of higher flashover voltage.
The results also indicate that the breakdown voltage

was independent of the configuration considered. The research was completed with observations of programmable sugar cane fires under 138 kV AC transmission lines [11.6] which substantially confirmed the above findings.

Simulation of a transmission line flashover was also made in a 76 m long, 2 phase test line energized to 495 kV phase-to-phase [11.1].
Five identical wood structures (3x3x4.9 m) were built as fuel supplies and placed midpoint on the ground between phases.
The first two fires failed to produce flashover. The addition of nine automobile tyres in the other two fires caused flashovers between the 7.6 m phase to phase spacing and the 5.8 m to the wood structure.
The gradient values in these cases were:

-phase-to-phase: 65 kV/m
-phase-to-structure: 49.3 kV/m

The strength reduction can be attributed to the use of different burning materials as shown in table I. However, as the voltage, distance between phases and distance to ground were fixed, no information about the critical gradient could be obtained from these tests, which is estimated to be much lower than the quoted values for the case of an automobile tyres fire.

Finally tests performed on short clearances under laboratory conditions [11.4],[1.5] with simulation of floating particles have indicated a reduction of the breakdown gradient to 7 kV/m. Possibly the reduction was caused by an unidentified factor, present in the laboratory and not present in the field conditions actual or simulated.

11.2.2 DC VOLTAGE

Most of the results available refer to short gaps [11.2], [11.7], and can hardly be extrapolated to large gaps.

Tests were carried out with a bipolar experimental line (± 450 kV) under a fire in vertically standing spruce trees (Figure 11.1) with a clearance to ground of 13.7 m and a clearance to the trees of 6.7 m. The rating operating voltage during the test was +450 kV for one pole and -450 kV for the other pole. When the trees were burning a large number of flashovers were obtained [11.8].

11.3 CONCLUSIONS

The flashover gradient of an air gap covered by fire is independent of the electrode shape and gap length and is drastically reduced by the presence of combustion particles in the gap.

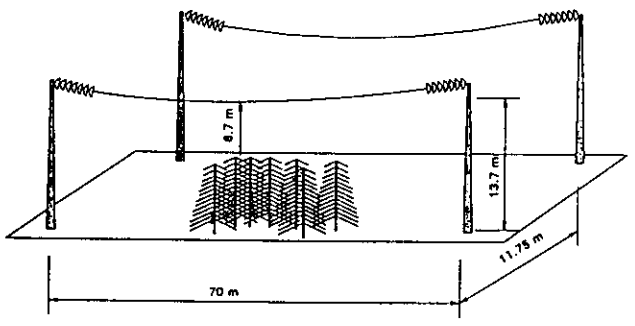

Figure 11.1 Test line configuration [11.8]

Field tests and laboratory simulation of field conditions have indicated that the average flashover gradient can be reduced to about 35 kV/m under power frequency (rms value).

While these values may be taken provisionally for reference for design purpose, tests are to be encouraged to improve knowledge, taking into consideration that lower strength values were obtained in laboratory conditions.

Information about the strength under overvoltages and in presence of fire would also be of interest.

11.4 REFERENCES

[11.1] H. J. West, D. W. Mc Mullam, "Fire induced flashovers of EGV transmission lines", IEEE PES Winter Meeting, New York, Paper A73047-2, February, 1978.

[11.2] H. Jahn,"Einfluß der Temperatur auf die Durchschlgspannung einer Inhomogenen Funkenstrecke in Luft", Elektrie, Berlin, November 1969.

[11.3] M. Moreno, "Performance of external insulation in presence of flames due to sugar cane burning", CIGRE WG 33.07/10 IWD, 1985.

[11.4] K. J. Sadurski, "Results of initial laboratory study into the effects of fire under power lines", CIGRE WG 33.07/11 IWD, 1985.

[11.5] K. J. Sadurski, J. P. Reynders, "High voltage AC breakdown in presence of fires", Sixth International Symposium on High Voltage Engineering, New Orleans, September 1989.

[11.6] J. R. Fonseca, A. L. Tan, V. Monassi, et all, "Effects of agricultural fires on the performance of overhead transmission lines, IEEE-PES Summer Meeting, Paper 89 SM 791-5 PWRD, July 1989.

[11.7] K. J. Sadurski, A. C. Britten, "Flame induced breakdown under DC conditions", CIGRE WG 33.07/9 IWD, 1989.

[11.8] R. Lanoie, H. P. Mercure, "Influence of forest fires on power line insulation", Sixth International Symposium on High Voltage Engineering, New Orleans, September 1989.

12 CONCLUSIONS

by W.G. 33.07

The state of the art about the dielectric strength of external insulation has been reviewed in the previous chapters aiming to give up dated information for insulation design. The following conclusions and indications for future research can be derived from the analysis of present state of knowledge.

- Knowledge about the dielectric strength under transient overvoltages is now becoming well established. However many aspects still deserve further consideration.

- Many models of the discharge process have been proposed: they are very useful tools for rationalising the results, understanding the effects of the various influencing parameters and extrapolating the results. The models may also permit development of better criteria for the estimation of the dielectric strength with reference to very low discharge probabilities, which can not be easily explored by usual experimental procedures.
  Most of the models are however semi-empirical and deeper development of the basic physics of the discharge process may permit big improvements. In particular, understanding of discharge phenomena in complex conditions is necessary, such as discharge on insulator surface, under rain, under humidity and pollution.

- The methods for the evaluation of the dielectric strength under standard atmospheric conditions and under standard rain are generally sufficiently accurate for design purposes. In a few cases, when the insulators significantly affect the discharge, the accuracy of the evaluation may be not sufficient, thus suggesting specific investigation.

- The methods proposed for the estimation of the influence of air density, including influence of altitude, and the influence of air humidity are generally sufficiently accurate. Studies to improve the accuracy of the methods are however of interest for a few cases, again when insulator surfaces are involved in the discharge, in the case of small gaps and for very large gaps.

- General methods to evaluate the strength in non standard environmental conditions (e.g. in presence of contamination, snow, ice, fires) are not available. Further experimental research and modelling is necessary to improve knowledge of the dielectric strength in these conditions.
  The research have also to consider aspects of emerging importance, such as the dielectric performance of insulators under acid rain, leading to high surface conductivity.

- Finally, there are some areas that still require investigation by the Working Group to enhance the usefulness of these Guidelines to the electric power transmission, distribution and utilisation industry, and these areas form the bases of the continuing activity of the Working Group.
  When coordinating the information in these Guidelines with the documents being prepared by IEC TC 78, Tools for Live Working, it has become apparent that the understanding of specific issues still need to be advanced. These include the applicable values of gap factors, minimum approach distances, critical wave shape(s) for evaluation of sparkover, the effect of the complexity of line and station electrical equipment configurations, movement of a conductive "object" into and through the air gap, and new work techniques. This issues impinge upon the work practices, and also on the use of various items of tooling and equipment (e.g. helicopters, conductor carts, robots, portable gaps for transient overvoltage controls) during energized work.

Le CIGRÉ a apporté le plus grand soin à la réalisation de cette brochure thématique numérique afin de vous fournir une information complète et fiable.

Cependant, le CIGRÉ ne pourra en aucun cas être tenu responsable des préjudices ou dommages de quelque nature que ce soit pouvant résulter d'une mauvaise utilisation des informations contenues dans cette brochure.

Publié par le CIGRÉ
21, rue d'Artois
FR-75 008 PARIS
Tél. : +33 1 53 89 12 90
Fax : +33 1 53 89 12 99

The greatest care has been taken by CIGRE to produce this digital technical brochure so as to provide you with full and reliable information.

However, CIGRE could in any case be held responsible for any damage resulting from any misuse of the information contained therein.

Published by CIGRE
21, rue d'Artois
FR-75 008 PARIS
Tel : +33 1 53 89 12 90
Fax : +33 1 53 89 12 99